

**LEVEL II**

**(13)**

DOT/FAA/RD-81/72

Systems Research &  
Development Service  
Washington, D.C. 20590

# Considerations for the Design of Ground Clutter Cancelers for Weather Radar

Dusan S. Zrnic'  
Said Hamidi

National Severe Storms Laboratory  
National Oceanic and Atmospheric Administration  
1313 Halley Circle  
Norman, OK 73069

**AD A109624**

**(12) 85**

**DTIC  
COPY  
JAN 15 1982  
H**

February 1981

Interim Report

This document is available to the U.S. public  
through the National Technical Information  
Service, Springfield, Virginia 22161

**DTIC FILE COPY**

**(8)**



U.S. Department of Transportation  
Federal Aviation Administration

**244670**

**82 01 11 157**

**Best  
Available  
Copy**

NOTICE

This document is disseminated under the sponsorship of the Department of Transportation in the interest of information exchange. The United States Government assumes no liability for its contents or use thereof.

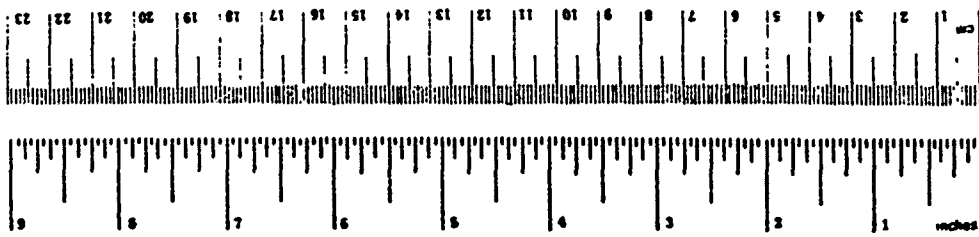
Accession For	
NTIS GFAAI	<input checked="" type="checkbox"/>
DTIC TAB	<input type="checkbox"/>
Unannounced Justification	
By _____	
Distribution _____	
Announcement _____	Codes
Dict _____	OR
<b>A</b>	

Technical Report Documentation Page

1. Report No. DOT/FAA/RD-81/72		2. Government Accession No. AD-A109624		3. Recipient's Catalog No.	
4. Title and Subtitle CONSIDERATIONS FOR THE DESIGN OF GROUND CLUTTER CANCELERS FOR WEATHER RADAR				5. Report Date February 1981	
				6. Performing Organization Code	
7. Author(s) Dusan S. Zrnic <sup>1</sup> and Said Hamidi				8. Performing Organization Report No.	
9. Performing Organization Name and Address National Severe Storms Laboratory 1313 Halley Circle Norman, OK 73069				10. Work Unit No. (TRAIS)	
				11. Contract or Grant No. IAA DTFA01-80-Y-10524	
12. Sponsoring Agency Name and Address Department of Transportation Federal Aviation Administration Systems Research and Development Service Washington D.C. 20590				13. Type of Report and Period Covered Interim Report April 80 - February 81	
				14. Sponsoring Agency Code ARD-231	
15. Supplementary Notes T <sub>u</sub> sub c					
16. Abstract Study of the ground clutter problem at the Norman site indicates that clutter cross sections of 40 to 50 dB below 1 <sup>sq. m</sup> are typical. Doppler spectrum width, $\sigma_d$ , of the clutter signal is between 0.1 and 1 m/s with the mean value of 0.25 m/s at an antenna rotation rate of 10 <sup>1/s</sup> . The design of clutter filters is very much dependent on this width and for proper cancellation the passband cutoff velocity $v_p$ must be larger or equal to 4.8 $\sigma_d$ . Several canceling schemes are investigated, and the most efficient one is with a third order recursive filter. This filter achieves a 50 dB rejection in the stop band with total annihilation of DC. One dB ripple is in the passband, and the ratio of passband cutoff $v_p$ to stop band cutoff $v_s$ is about 3.5. The filter operates best in steady state, but it can also be made to operate in transient by properly initializing its memory elements. Performance on 64 simulated and real time samples show that no more than 10 dB loss in effective canceling over steady state occurs if the filter is initialized. To minimize weather signal loss, canceling is recommended only in regions that contain clutter. Therefore, the range extent over which canceling is performed should vary with elevation. Also the antenna rotation at the two lowest angles should be slower.					
17. Key Words Ground clutter canceler Doppler weather radar			18. Distribution Statement Document is available to the U.S. public through the National Technical Information Service, Springfield, Virginia 22161		
19. Security Classif. (of this report) Unclassified		20. Security Classif. (of this page) Unclassified		21. No. of Pages 77	22. Price

## METRIC CONVERSION FACTORS

Approximate Conversions to Metric Measures		Approximate Conversions from Metric Measures		
Symbol	When You Know	Multiply by	To Find	Symbol
<b>LENGTH</b>				
in	inches	2.5	centimeters	mm
ft	feet	30	centimeters	cm
yd	yards	0.9	meters	m
mi	miles	1.6	kilometers	km
<b>AREA</b>				
in <sup>2</sup>	square inches	6.5	square centimeters	cm <sup>2</sup>
ft <sup>2</sup>	square feet	0.09	square meters	m <sup>2</sup>
yd <sup>2</sup>	square yards	0.8	square meters	m <sup>2</sup>
mi <sup>2</sup>	square miles	2.6	square kilometers	km <sup>2</sup>
	acres	0.4	hectares	ha
<b>MASS (weight)</b>				
oz	ounces	28	grams	g
lb	pounds	0.45	kilograms	kg
	short tons (2000 lb)	0.9	tonnes	t
<b>VOLUME</b>				
teaspoons	teaspoons	5	milliliters	ml
fluid ounces	fluid ounces	30	milliliters	ml
cups	cups	0.24	liters	l
pints	pints	0.47	liters	l
quarts	quarts	0.96	liters	l
gallons	gallons	3.8	liters	l
cubic feet	cubic feet	0.03	cubic meters	m <sup>3</sup>
yd <sup>3</sup>	cubic yards	0.76	cubic meters	m <sup>3</sup>
<b>TEMPERATURE (exact)</b>				
°F	Fahrenheit temperature	5/9 (after subtracting 32)	Celsius temperature	°C
<b>TEMPERATURE (exact)</b>				
°C	Celsius temperature	9/5 (then add 32)	Fahrenheit temperature	°F



\* 1 in. = 2.54 exactly. For other exact conversions and more detailed tables, see NIST Mon. Publ. 284, Units of Weights and Measures, Part 2, N. S. D. Catalog No. C1310296.

## TABLE OF CONTENTS

	Page
List of Figures	iv
List of Tables	vi
1. Ground Clutter Properties	1
1.1 Ground Clutter Reflectivity	1
1.2 Doppler Spectrum Width of Ground Clutter	6
2. Transmitted Waveforms, Scanning Strategy and Clutter Canceling	16
3. Ground Clutter Filter	19
3.1 Recursive Filter-Contiguous Pulse Train	19
3.2 Recursive Filter, Stepped Input and Initialization	28
3.3 Other Techniques	39
4. Conclusions	42
APPENDICES	
A. Errors in Pulse Pair Derived Velocity and Spectrum Width Due to Anomalous Signal	44
B. Finite Impulse Response - FIR Filter	49
C. Clutter Rejection in the Autocovariance Domain	56
D. Antenna Speed, Apparent Pattern, and Dwell Time	61
E. Program Flow Charts	64

## LIST OF FIGURES

	Page
Fig. 1.1 Survey from Norman Doppler.	1
Fig. 1.2 Ground clutter map @ 0° elevation.	3
Fig. 1.3 Same as 1.2 except the elevation angle is 0.4°.	4
Fig. 1.4 Same as 1.2 but the elevation angle is 0.8°.	5
Fig. 1.5 Histograms of ground clutter power.	7
Fig. 1.6 Clutter spectrum widths due to antenna rotation and wind speed.	8
Fig. 1.7 Plot of clutter power spectra.	9
Fig. 1.8 Bias of the width estimate.	10
Fig. 1.9 Histograms of clutter spectrum width from the Oklahoma City area.	11
Fig. 1.10 Same as 1.9 but returns are from the prairie.	12
Fig. 1.11 Same as 1.9 but returns are from the wooded area.	13
Fig. 1.12 Scattergram of clutter spectrum widths.	14
Fig. 1.13 Idealized frequency response of the high pass filter.	15
Fig. 2.1 Interlaced pulse train.	17
Fig. 2.2 Standard deviation of velocity estimates.	18
Fig. 2.3 Standard deviation of spectrum width estimates.	18
Fig. 3.1 Block diagram of the third order high pass elliptic filter.	19
Fig. 3.2 Frequency response characteristic of the recursive filter 1.	20
Fig. 3.3 Block diagram of data flow.	20
Fig. 3.4 Power spectrum of time series containing ground clutter and weather signal.	22
Fig. 3.5 Power estimate after the recursive filter.	23
Fig. 3.6 Estimated mean velocity from time series data filtered by the recursive filter 1.	24
Fig. 3.7 Same as 3.6 but filter 2 is used.	25
Fig. 3.8 Same as 3.6 but filter 3 is used.	26
Fig. 3.9 Same as 3.8 but the C/S ratios are larger.	27
Fig. 3.10 Estimated mean velocity when the true velocity is in the notch of filter 3.	29
Fig. 3.11 Same as 3.10 but filter 1 is used.	29
Fig. 3.12 Estimated mean signal spectrum width from time series data filtered with filter 1.	30
Fig. 3.13 Same as 3.12 but filter 2 is used.	31
Fig. 3.14 Same as 3.13 but filter 3 is used.	32
Fig. 3.15 Same as 3.14 but the C/S ratios are larger.	33
Fig. 3.16a Same as 3.15 but the mean velocity increases in steps of 1 ms <sup>-1</sup> .	34

	Page
Fig. 3.16b Same as 3.16a but filter 1 is used.	34
Fig. 3.17 Step response of the recursive filter.	35
Fig. 3.18 Mean velocity and spectrum width estimates without initialization.	37
Fig. 3.19 Same as 3.18 but initialization is applied.	38
Fig. 3.20 Doppler spectra of a weather signal and clutter.	40
Fig. 3.21 Spectrum plot of weather and clutter when the time series is a) not filtered b) filtered c) filtered and properly initialized d) under steady state conditions.	41
Fig. A.1 Magnitude of the normalized velocity error versus the magnitude of the normalized velocity difference.	46
Fig. A.2 The ratio of signal and clutter correlation coefficients for Gaussian shaped spectra.	47
Fig. A.3 Biased spectrum width when signal and clutter are present.	47
Fig. A.4 Same as A.3 but S/C=15 dB.	48
Fig. B.1 Amplitude and magnitude response for high pass FIR filter.	49
Fig. B.2 Number of sample points for various passband cutoff widths.	51
Fig. B.3 Power spectra of ground clutter at antenna rotation rates of $1^\circ\text{s}^{-1}$ and $10^\circ\text{s}^{-1}$ . Number of samples is 32.	53
Fig. B.4 Same as B.3 but the number of samples is 64.	54
Fig. B.5 Spectral window corresponding to the Von Hann data window.	55
Fig. B.6 Spectral window corresponding to Hamming data window.	55
Fig. C.1 Logarithm of estimated mean power with no filtering and with autocovariance filtering technique.	59
Fig. C.2 Plot of estimated mean velocity with no filtering and with auto- covariance filtering technique.	59
Fig. C.3 Plot of estimated mean width with no filtering and with auto- covariance filtering.	60
Fig. D.1 Apparent beamwidth normalized to the 3 dB beamwidth versus the normalized rotation rate.	62
Fig. D.2 Standard deviation of pulse pair derived mean velocity estimates and spectrum width estimates.	63

LIST OF TABLES

		Page
Table 1.1	Ground clutter cross section per unit area.	6
Table 2.1	Typical range of pulse repetition times $T_p$ .	16
Table 2.2	Antenna scanning strategy that allows ground clutter cancellation and fast updates.	17
Table 3.1	Coefficients of the high pass elliptic filter.	19
Table B.1	The number of sample points needed for various passband and stopband cutoff frequencies.	50

## 1. GROUND CLUTTER PROPERTIES

This section examines some important properties of ground clutter that influence the design of a canceler. Measurements and data are for the Norman Doppler radar which has a medium to small clutter problem as compared to airports in the vicinity of major cities.

### 1.1 Ground Clutter Reflectivity

Surrounding ground influences radar observations in two ways. Returns from the ground through the mainlobe or sidelobes create strong spectral power around zero velocity which contaminates the spectral moment estimates of weather echoes. Also, tall objects interfering with the radar beam act as blockages which may totally prevent the illumination of weather beyond.

Figure 1.1 illustrates the blockage surrounding the Norman Doppler. Note that there are not many significant blockages above  $0.5^\circ$  in elevation, and that most of the blockages extend to less than  $0.2^\circ$ . Thus, we have chosen  $0^\circ$ ,  $0.4^\circ$  and  $0.8^\circ$  in elevation to be the angles for data collection.

Three different terrains characterize the area around the Norman site: urban Oklahoma City to the north, forests to the east, and prairies to the southwest. Clutter characteristics from these three areas are separately analyzed.

The map of the Norman ground clutter for the three elevation angles is shown on Figures 1.2, 1.3, and 1.4. These displays are in terms of equivalent reflectivity factor (dBZ) and only reflectivities above a threshold (indicated with the cursor) are depicted. Total areas of clutter above a fixed reflectivity for this data set are plotted on Fig. 1.5.

One can use Figures 1.2 through 1.5 to roughly assess the performance of a ground clutter canceler, which is explained in following paragraphs. Let us model the ground clutter and the weather signal with Gaussian spectra and corresponding autocorrelation functions.

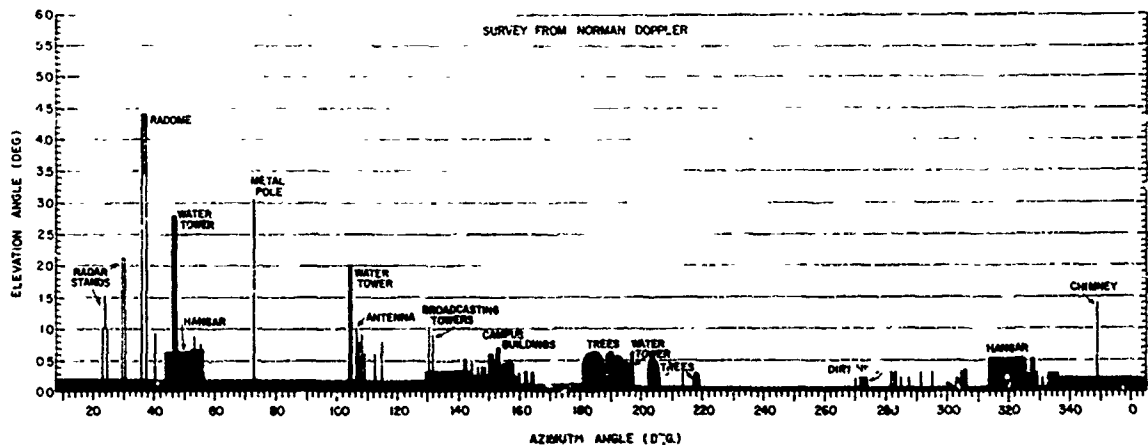


Figure 1.1 Survey from Norman Doppler. Very few objects exceed  $0.5^\circ$  in elevation.

Clutter spectrum:

$$\frac{C}{\sqrt{2\pi} \sigma_c} e^{-v^2/2\sigma_c^2} = F \left[ C e^{-\frac{\pi^2 \sigma_c^2}{2v_a^2} n^2} \right] \quad (1.1)$$

Signal spectrum:

$$\frac{S}{\sqrt{2\pi} \sigma_v} e^{-(v-\bar{v})^2/2\sigma_v^2} = F \left[ S e^{-\frac{\pi^2 \sigma_v^2}{2v_a^2} n^2 + j\pi\bar{v}/v_a} \right] \quad (1.2)$$

where  $C$  is the clutter power at a certain range,  $\sigma_c$  the width of the clutter Doppler spectrum, and  $S$  is signal power and  $\sigma_v$  spectrum width at the same range.  $v_a$  is the unambiguous velocity,  $n$  the lag number while  $F$  indicates the Fourier transform. Even though the Gaussian model is a simplification, it allows a wide range of clutter spectra to be easily modeled. Moreover, superposition of Gaussian spectra can produce more complicated clutter for which still the strongest one is dominant and must be filtered.

Throughout this study we will assume that either a Fourier transform or a pulse pair algorithm is used to estimate the mean Doppler and the Doppler spectrum width. If the Fourier transform is used, then the filtering would be done by properly weighting the time series data (inphase and quadrature components) prior to the transform. For the pulse pair algorithm, the most natural filter would be a recursive one, although a Fourier transform could be used twice (once forward to obtain and reject the coefficients near zero and then back to regenerate the time series).

In Appendix A, it is shown that when pulse pair processing is used the ratio

$$\beta = \frac{S\rho_s}{C\rho_c}$$

where

$$\rho_s = e^{-\pi^2 \sigma_v^2 / 2v_a^2} \quad (1.3)$$

$$\rho_c = e^{-\pi^2 \sigma_c^2 / 2v_a^2}$$

must be larger than 10 dB in order to maintain the mean velocity error below  $1 \text{ m}\cdot\text{s}^{-1}$  for any velocity.

From Figures 1.2, 1.3, and 1.4 we see that ground clutter larger than 40-45 dBZ is sparse enough so that weather signals of similar magnitudes should be discernible. If weather echoes are 50-55 dBZ, then meaningful estimates of mean velocity (see Appendix A) should be possible and due to the spacial continuity of weather (gust fronts, etc.) observation throughout the whole PPI could be made. But gust fronts have low reflectivities and in order to measure their velocities, one needs to cancel the ground clutter. For accurate mean velocity estimation via the pulse pair processor, one needs a 10 dB ratio of signal to clutter residue and 15 dB ratio if spectrum width is estimated (Appendix A). Thus the canceler must reduce the residue at least 10 dB below signal power. Therefore, a 50 dB canceler would allow moment estimation up to about 40 dB of C/S ratio.

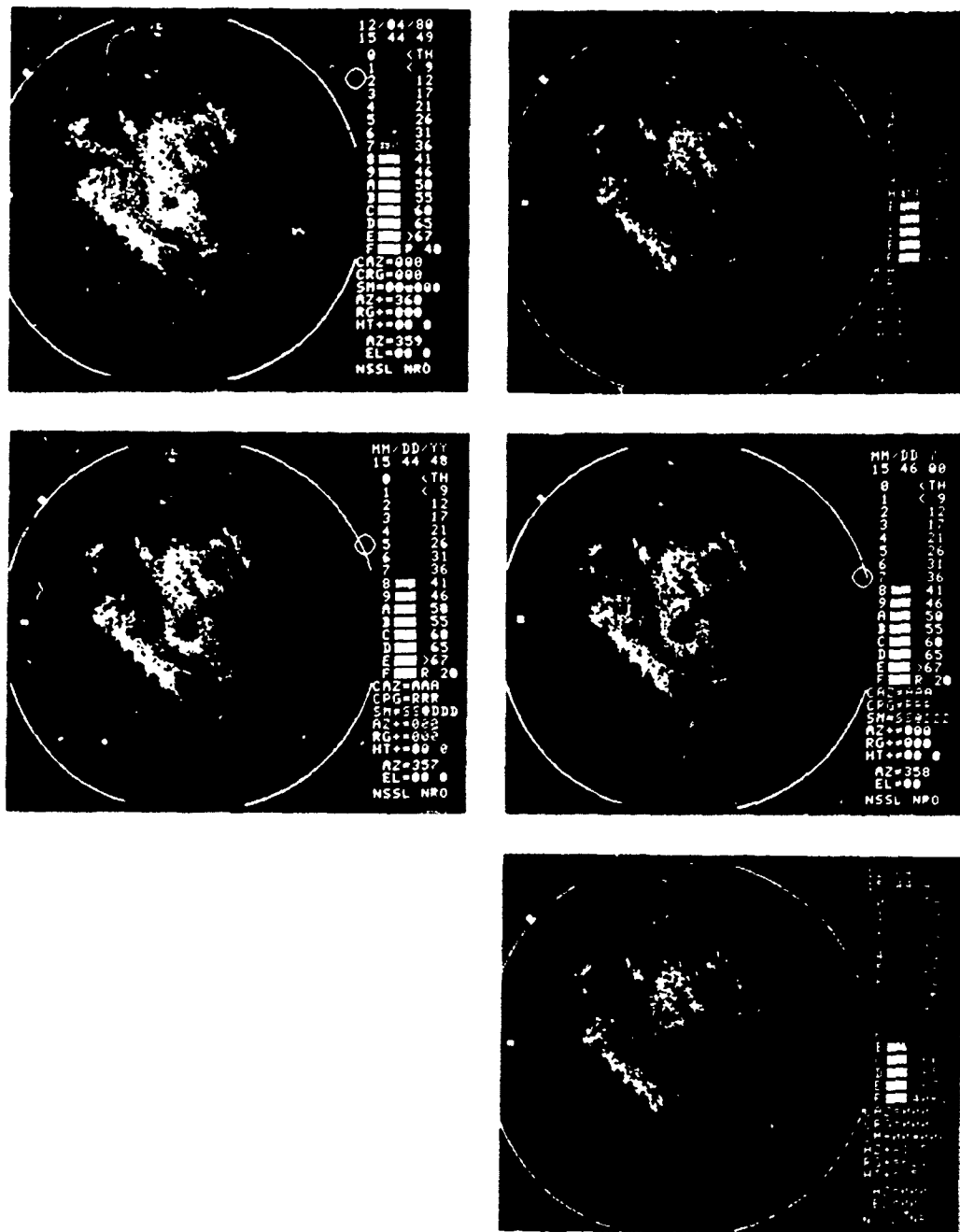


Figure 1.2. Ground clutter map at  $0^\circ$  elevation. Equivalent reflectivity factor (dBZ) above some threshold is displayed. Range mark is at 40 km. The thresholds are indicated with the cursor's position. Categories of displayed reflectivity in dBZ are from 9 to over 67. Note a false indication of uniform reflectivity (about 8 km in diameter) centered at the radar, that decreases in circular steps. This is due to receiver saturation which creates a constant power at the digital, integrator input. When that constant power is multiplied with the range squared,  $r^2$ , to obtain reflectivity, a monotonic decrease occurs as  $r$  gets smaller. Therefore, at this elevation angle the radar is totally blind to 4 km in range. Peak transmitter power was 200 kW.

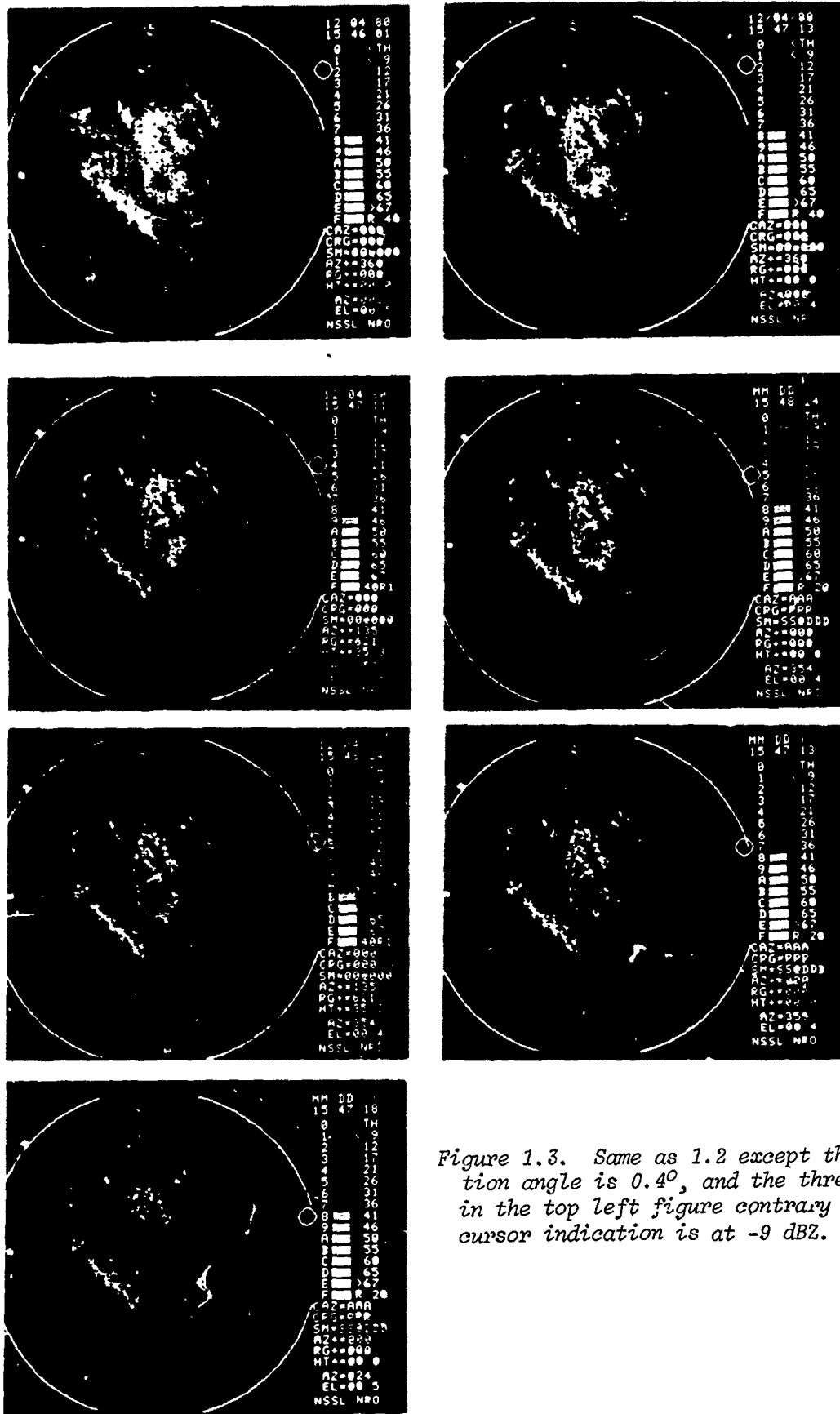
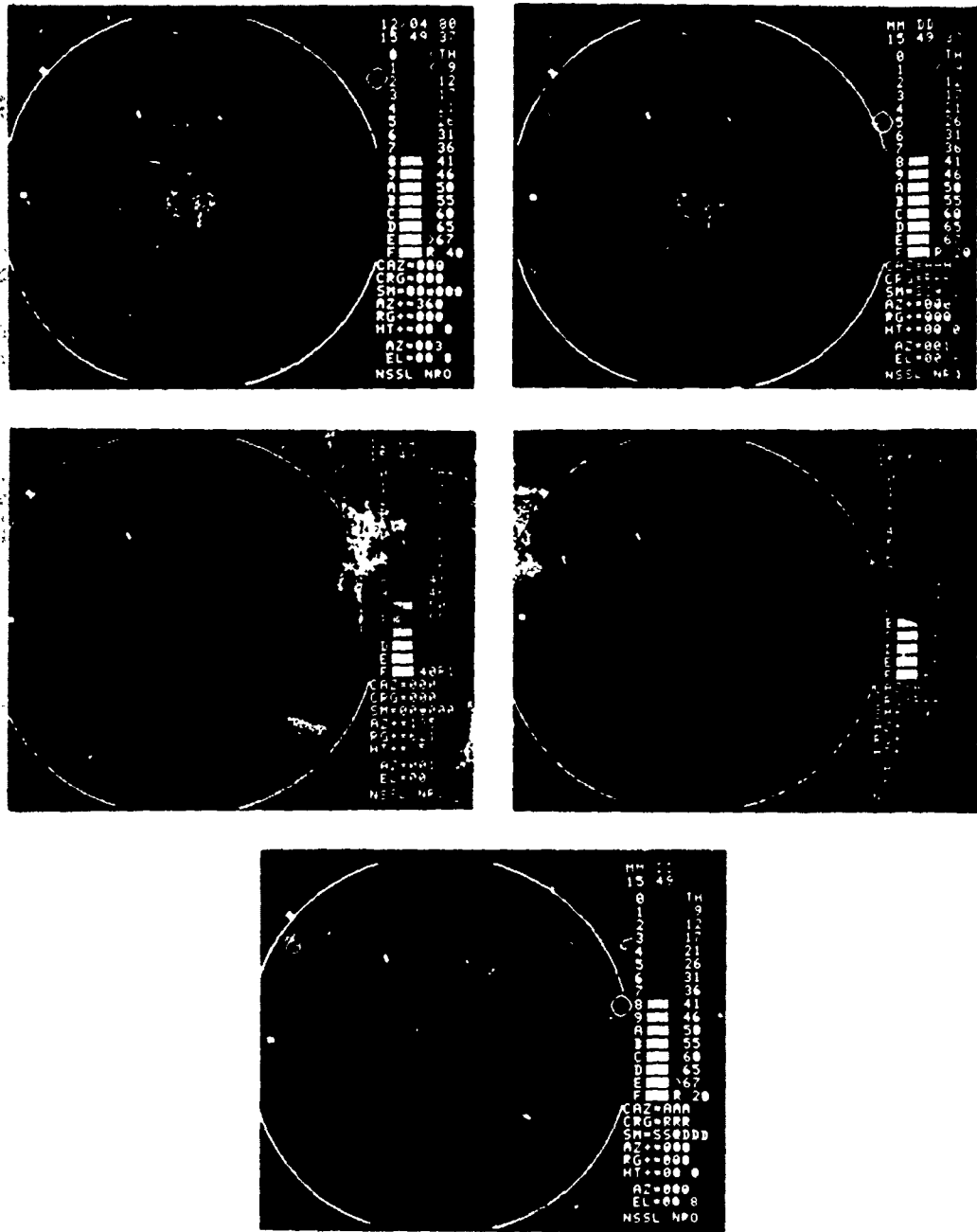


Figure 1.3. Same as 1.2 except the elevation angle is  $0.4^\circ$ , and the threshold in the top left figure contrary to cursor indication is at  $-9$  dBZ.



This margin is also needed between the spectrum peak and its sidelobes if the Fourier method of eliminating clutter is employed. This is so because clutter spectrum widths are typically about  $0.2 \text{ m}\cdot\text{s}^{-1}$  so that the spectrum peak ratio from (1.1) and (1.2) is

$$\frac{C\sigma_v}{S\sigma_c} \approx \frac{10C}{S} \quad (1.4)$$

for a  $\sigma_v$  of  $2 \text{ m}\cdot\text{s}^{-1}$ , and we note that 50 dB of clutter spectrum cancellation would allow signals with powers 40 dB below clutter powers  $C$  to be seen.

Cumulative areas of ground clutter obtained for the three elevation angles (Figures 1.2, 1.3, and 1.4) are shown on Figure 1.5. We note that the area of ground clutter with reflectivity larger than 30 dBZ is  $400 \text{ km}^2$  at  $0^\circ$ ,  $300 \text{ km}^2$  at  $0.4^\circ$  and  $50 \text{ km}^2$  at  $0.8^\circ$ . For the Norman radar gust front echoes with -10 dBZ equivalent reflectivity factor are above noise up to 30 km which is also the range of ground clutter extent. Therefore, a 50 dB canceler would enable us to see such weak echoes through most of the PPI except in the above mentioned areas.

Measurement of ground clutter cross section per unit area yielded values about 40 dB below  $1 \text{ m}^2/\text{m}^2$  with a typical example in Table 1.1. Note that these data are about 10 dB lower than the ones found in Nathanson (1969), which is not unusual considering the variability of clutter characteristics.

Table 1.1

Range (km)	Average clutter cross section (dB below $1 \text{ m}^2/\text{m}^2$ )
8.3 - 11.9	-39.96
13.1 - 16.7	-51.84
17.9 - 21.5	-40.01
22.6 - 26.3	-68.26

## 1.2 Doppler Spectrum Width of Ground Clutter

Two mechanisms produce broadening of the ground clutter spectrum. These are movement of trees under the influence of wind and the rotation of the antenna while data are being collected. Groginsky and Glover (1980) have fitted the data of Nathanson for the width due to wind with the following regression line:

$$\sigma_{CW} = 8 \cdot 10^{-3} v_w^{1.2} (\text{m}\cdot\text{s}^{-1}) \quad (1.5)$$

where the wind velocity  $v_w$  is in  $\text{m}\cdot\text{s}^{-1}$ .

Antenna rotation at a rate  $\alpha$  contributes (Nathanson 1969)

$$\sigma_{C\alpha}^2 = \left( \frac{\alpha \lambda \cos \theta_e}{2\pi\theta_l} \right)^2 \ln 2 \quad (1.6)$$

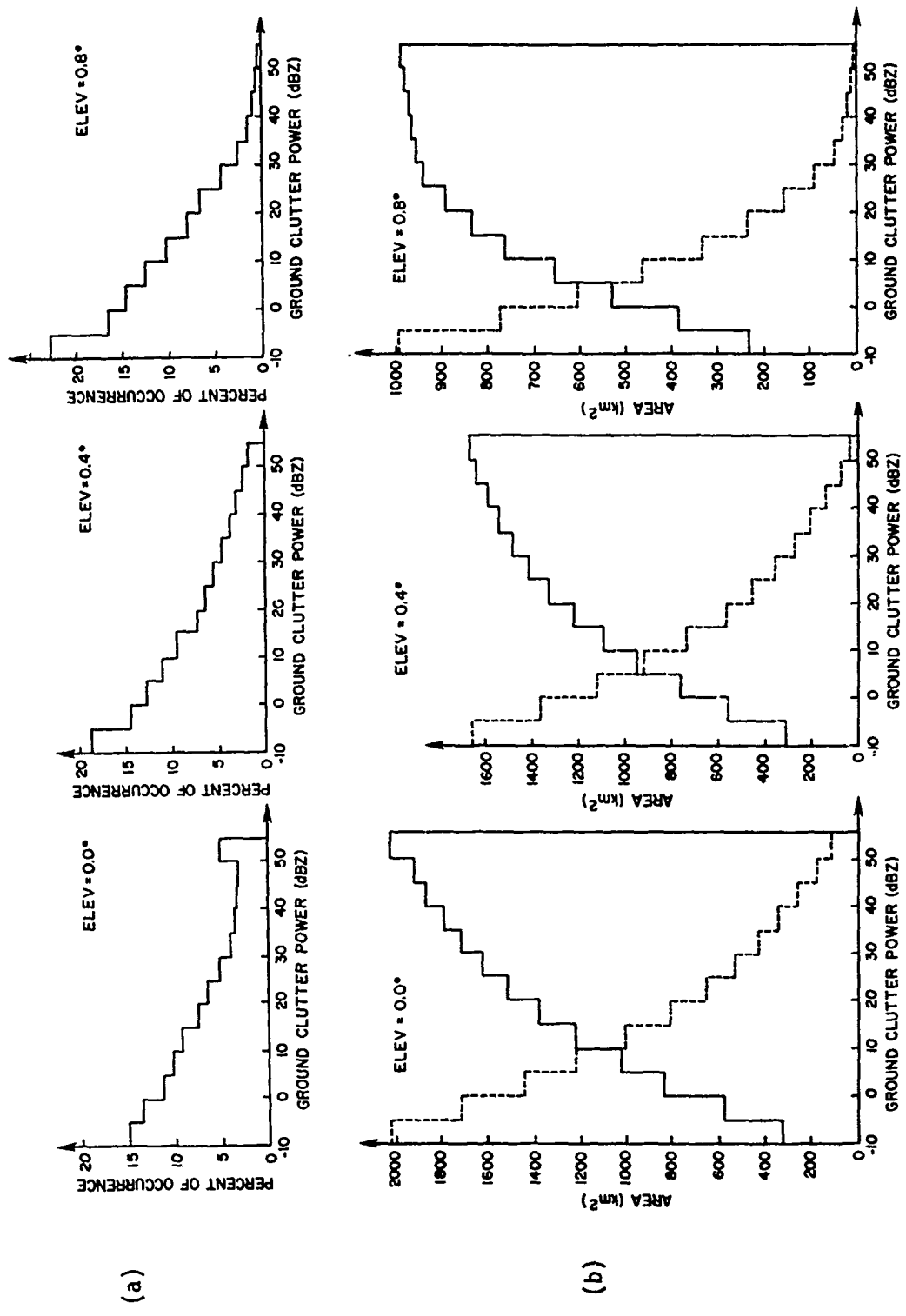


Figure 1.5. a) Histograms of ground clutter power for three elevation angles (Figs. 1.2, 1.3, and 1.4) of the Norman site. The total with respect to which percentages are taken represents all returns larger than -10 dBZ. The last category contains values larger than 50 dBZ. During data collection, there were no noticeable echoes from clear air or insects. b) Cumulative areas of ground clutter for the three elevation angles. Dashed line is for clutter power equal or larger than the abscissa. Solid line is for powers less or

where  $\theta_1$  is the one-way half-power beamwidth,  $\theta_e$  the elevation angle and  $\lambda$  the wavelength. The curves for  $\sigma_{cw}$  and  $\sigma_{ca}$  are plotted on Figure 1.6 on which one can observe that a  $1^\circ$  beamwidth antenna rotating at 3 rpm produces a width of  $.23 \text{ m}\cdot\text{s}^{-1}$ . At wind speeds of  $10 \text{ m}\cdot\text{s}^{-1}$  (20 knots), the width is broadened by  $.12 \text{ m}\cdot\text{s}^{-1}$ . Thus the total rms clutter width would be

$$\sigma_c = \sqrt{\sigma_{cw}^2 + \sigma_{ca}^2} = .25 \text{ m}\cdot\text{s}^{-1}$$

Spectral analysis of time series data collected with the Norman radar confirms this finding. Some typical spectra (Figure 1.7) show what is to be expected at Norman with rotation rate  $1^\circ \text{ s}^{-1}$  and  $10^\circ \text{ s}^{-1}$ . The differences in widths at these two rates are difficult to measure because noise and sixty cycle harmonics mask the weak spectrum skirts. Still, we note that the third spectral points both side of zero are higher at the  $10^\circ \text{ s}^{-1}$  rotation rate due to more broadening. If 5 spectral coefficients about zero were eliminated (i.e.,  $-1.06$  to  $1.06 \text{ m}\cdot\text{s}^{-1}$ ), about 50 dB of canceling would be achieved.

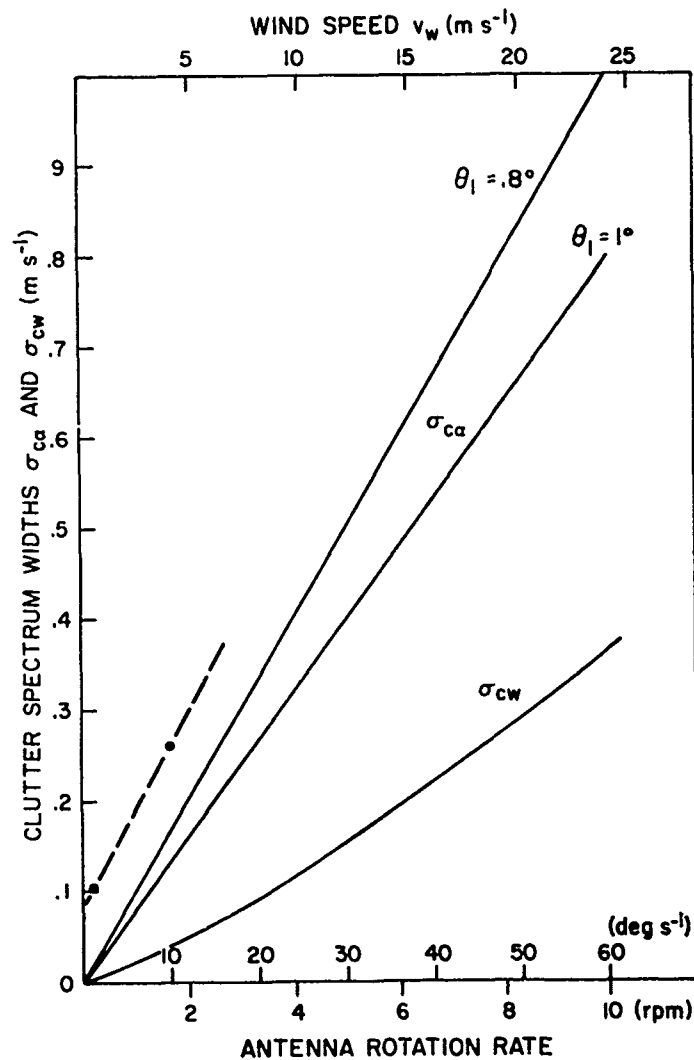


Figure 1.6. Clutter spectrum widths  $\sigma_{ca}$  due to antenna rotation (scale on lower axis) and  $\sigma_{cw}$  due to wind speed (upper axis). Dashed line is through two estimated data points (see text).

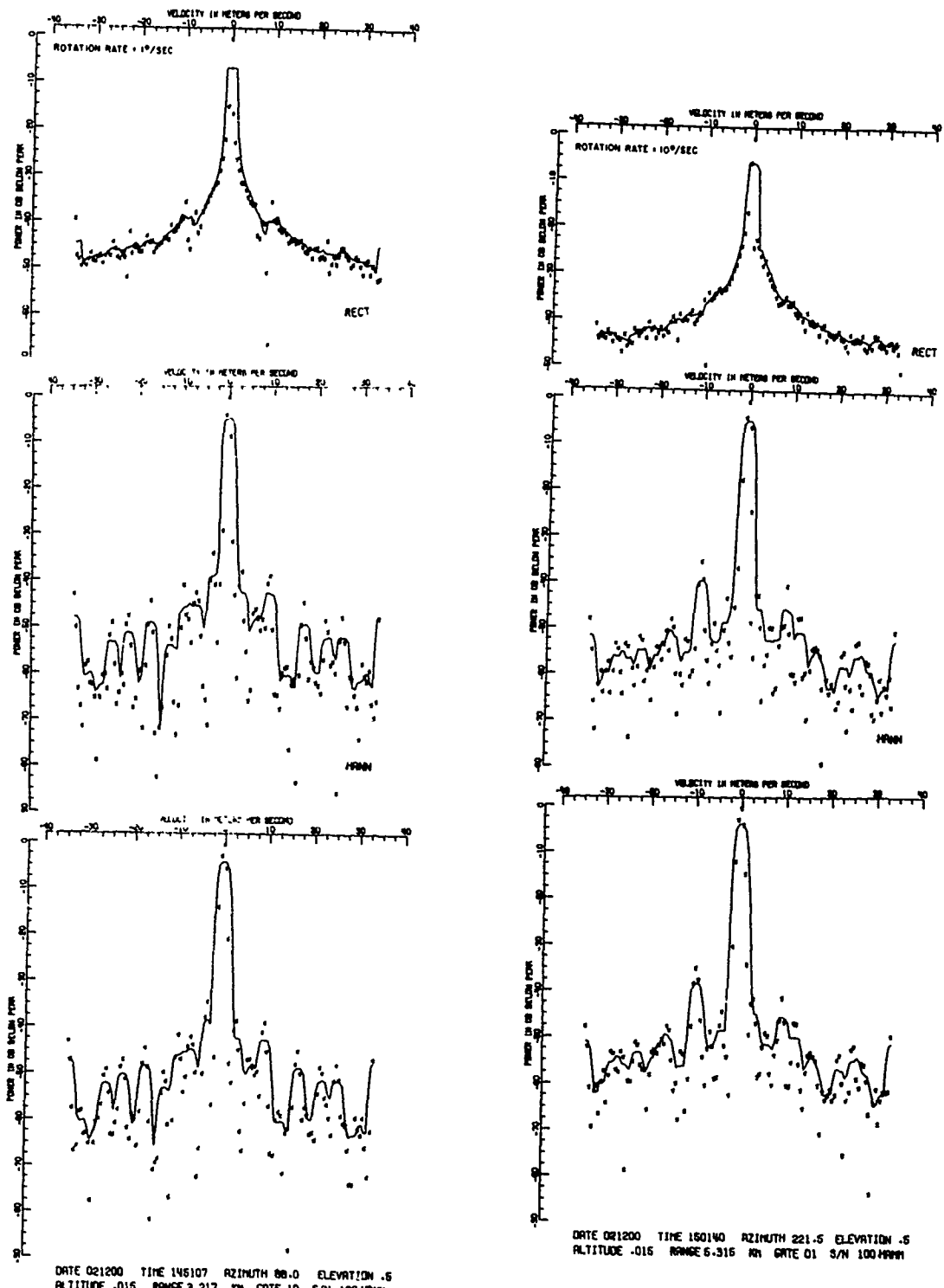


Figure 1.7. Plot of clutter power spectra (128 points) in dB below peak versus velocity in  $m \cdot s^{-1}$  using from top to bottom rectangular, von Hann and Hamming windows. The antenna is rotating at the rate of  $1.0^\circ s^{-1}$  and  $10.0^\circ s^{-1}$ . Spectral powers are marked with X's and a five point running average is drawn for visual clarity. The peaks at  $\pm 10 m \cdot s^{-1}$  are third harmonics of 60 Hz picked up by the video channel prior to the A/D converter.

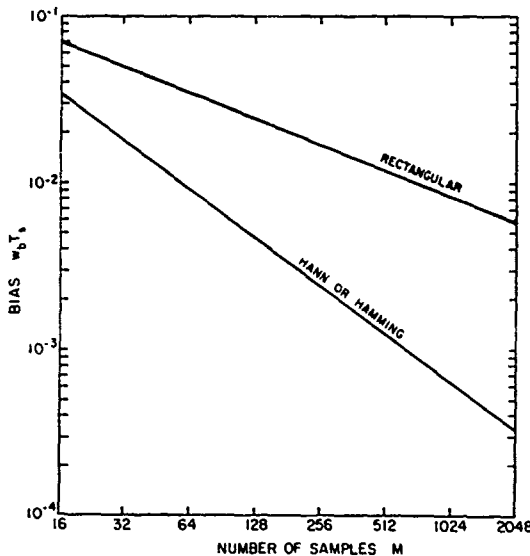


Figure 1.8 Bias of the width estimate due to the finite time window associated with Fourier spectral processing. To obtain the bias in  $m \cdot s^{-1}$ , multiply the ordinate values with the Nyquist interval ( $68 m \cdot s^{-1}$  for the Norman Doppler radar).

Estimation of narrow spectrum widths is complicated because the bias effect due to finite data lengths may be much larger than the width to be measured. For instance, the von Hann window with 128 samples contributes on the average  $0.3 m \cdot s^{-1}$  of bias to the measured width, while with 1024 points the bias is  $.04 m \cdot s^{-1}$ . (See Figure 1.8.) For practical reasons histograms of spectrum width were computed utilizing a 128 point discrete Fourier transform. To eliminate the effects of noise and 60 Hz harmonics only ten spectral lines around zero were considered. Our results (Figures 1.9-1.11) have very little terrain dependence probably because the winds were light ( $4.63 m \cdot s^{-1}$ ). At a rotation rate of  $10^\circ s^{-1}$  the mean widths are about four times larger than at  $1^\circ s^{-1}$ , rather than 10 times as suggested by (1.6). We thus must conclude that biases are significant. Roughly the unbiased mean width at  $10^\circ s^{-1}$  would be about

$$\sqrt{.4^2 - .3^2} \approx .26 m \cdot s^{-1}$$

which is plotted on Figure 1.6. The formula (1.6) predicts  $.17 m \cdot s^{-1}$  for broadening due to antenna rotation and the higher measured value can be attributed to wind effects and other broadening mechanisms not included. An independent check of the bias in the measured widths was made from the scattergram of the widths obtained with the 128 point transform versus 1024 point transform (Figure 1.12). To a  $.4 m \cdot s^{-1}$  width (from the 128 point FFT) corresponds  $.28 m \cdot s^{-1}$  from the 1024 point FFT, which is quite close to the  $.26 m \cdot s^{-1}$  obtained from the theoretical bias curves.

A sensible unbiasing of the width at  $10^\circ s^{-1}$  rotation is difficult because the predicted window bias is often larger than the total measured width. Thus, we accept the measured value of  $.1 m \cdot s^{-1}$ . In summary, the Doppler spectrum width is between  $.1$  and  $.5 m \cdot s^{-1}$  with the mean at  $10^\circ s^{-1}$  of about  $.25 m \cdot s^{-1}$ . The relationship of two measured points to the theoretical curves is shown on Figure 1.6, and we note that the slope of the measured curve is close to the theoretical prediction.

Now let us assume that L dB of clutter cancellation (in the spectrum domain) is desirable with the filter having a passband velocity  $v_p$ . Then for an idealized characteristic as on Figure (1.13), we can find an approximate relationship between  $v_p$  and the clutter spectrum width  $\sigma_c$  by requiring that

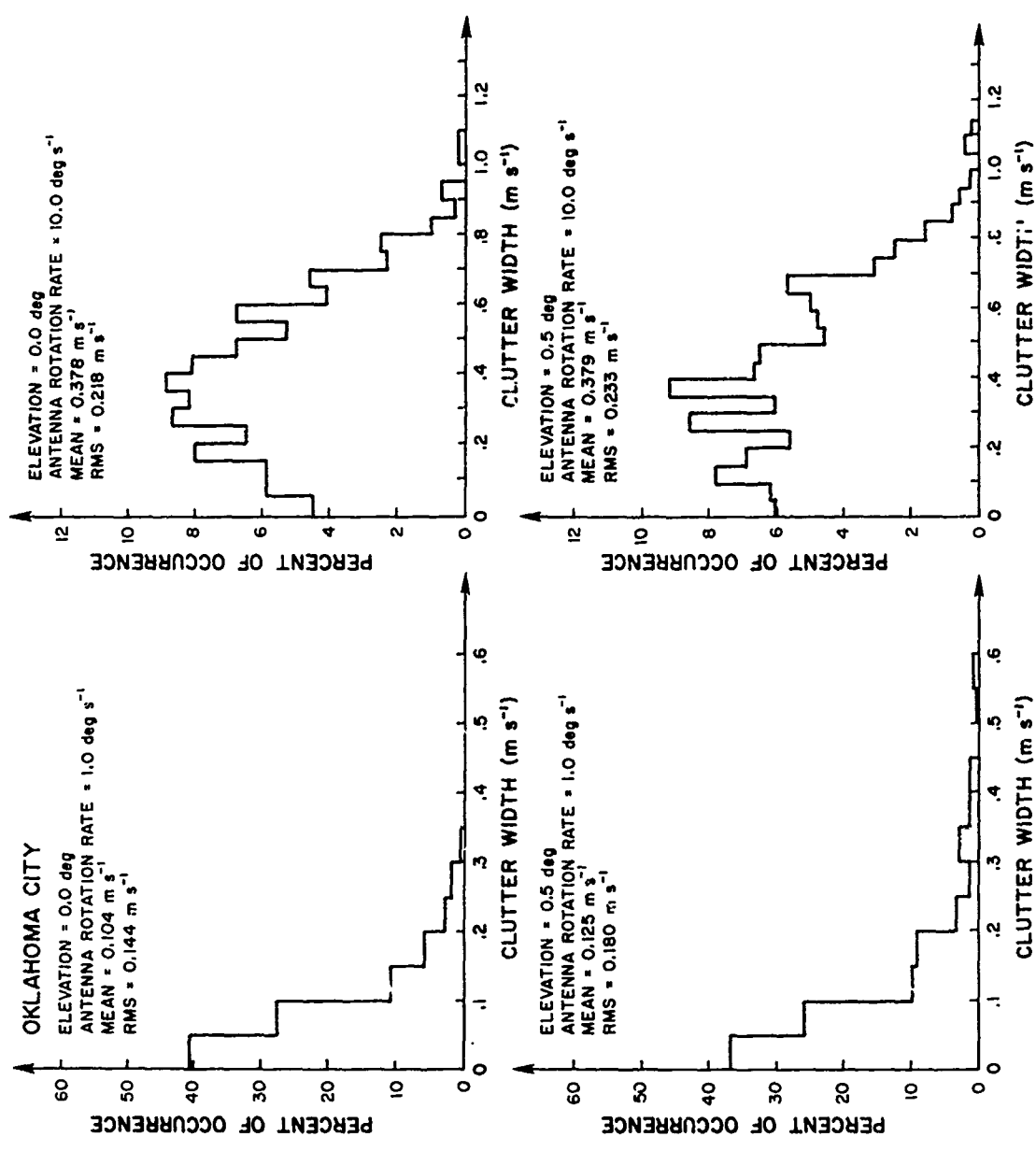


Figure 1.9. Histograms of clutter spectrum width for two elevation angles 0° and .5° and two antenna rotation rates. The mean and rms values for each histogram are indicated and returns are from the Oklahoma City area to the north of radar. The spectrum window bias has not been removed.

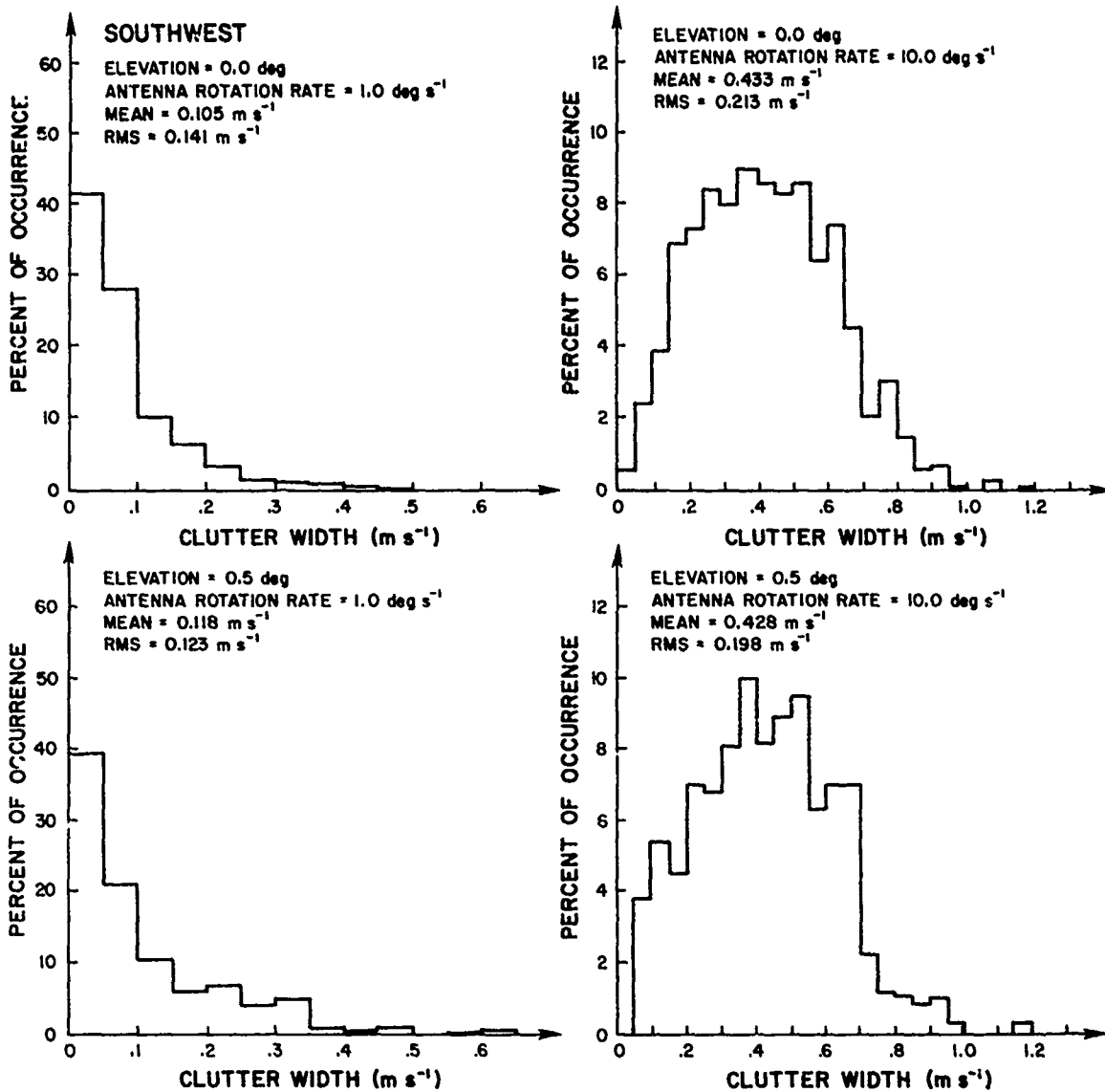


Figure 1.10. Same as 1.9 but returns are from the prairies southwest of the radar.

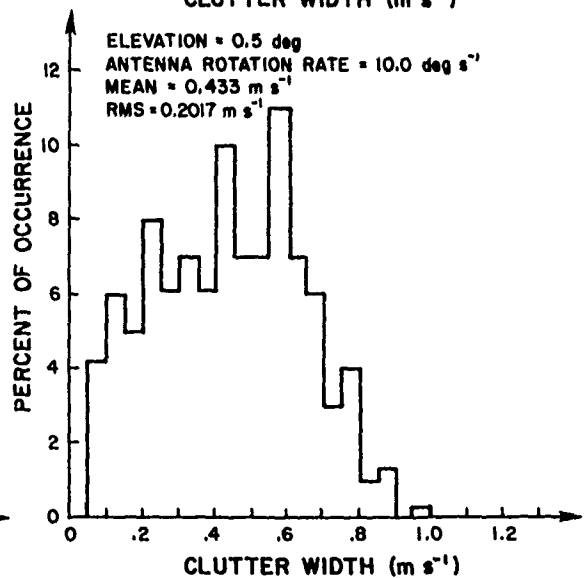
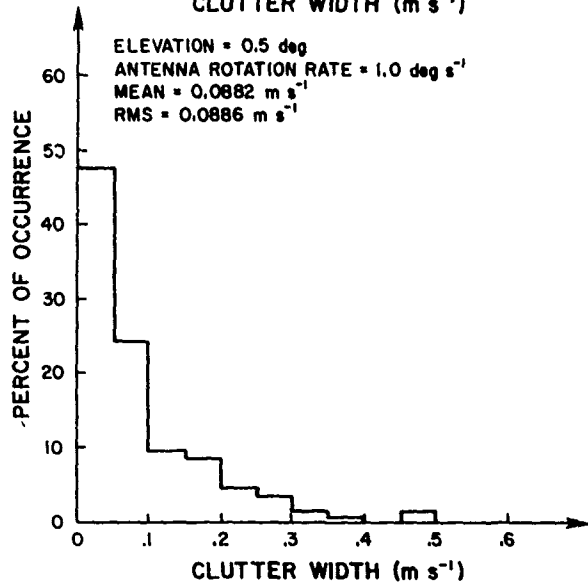
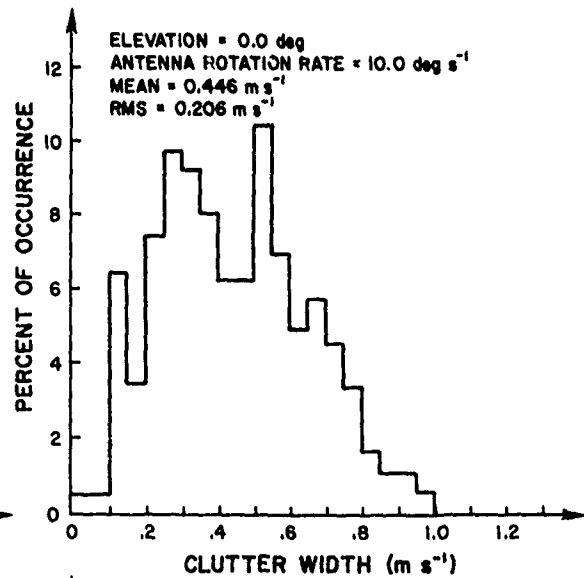
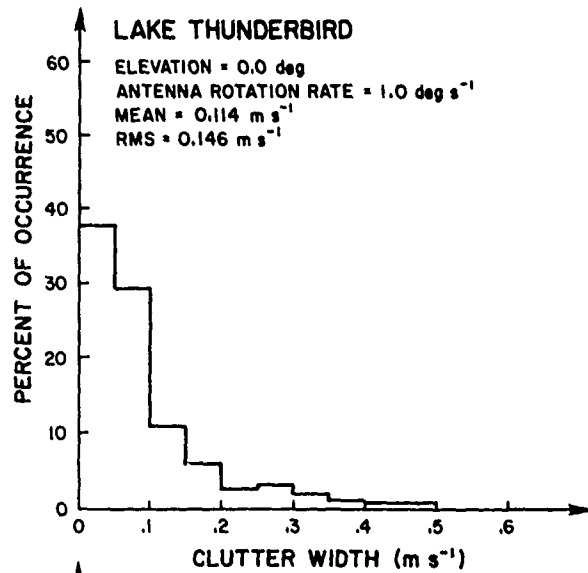


Figure 1.11. Same as 1.9 but the returns are from the wooded area around Lake Thunderbird east of the radar.

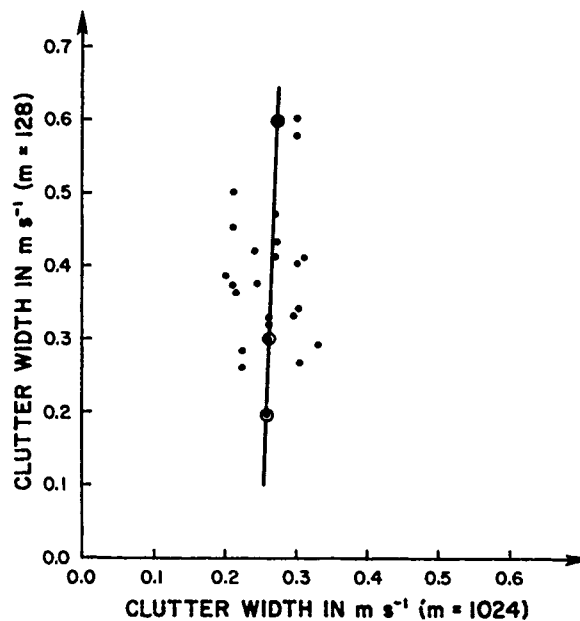
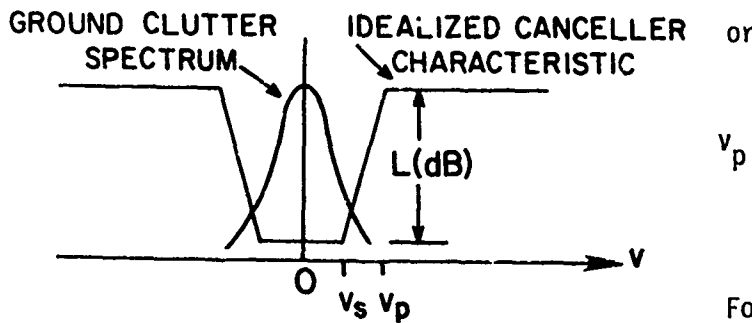


Figure 1.12. Scattergram of clutter spectrum widths obtained from a 128 point Fourier transform versus width values from a 1024 point transform. Both sequences were weighted with the von Hann data window. The solid line represents a least squares fit.

$$10 \log e^{-\frac{v_p^2}{2\sigma_c^2}} = -L \quad (1.7)$$



$$v_p = \sigma_c \sqrt{\frac{L}{5 \log e}} \quad (1.8)$$

For instance 50 dB rejection requires:

$$v_p = 4.8 \sigma_c \quad (1.9)$$

Figure 1.13. Idealized frequency (velocity) response of the high pass filter. The stopband width is  $2 v_s$  and passband cut-off width is  $2 v_p$ .

which is about  $1 \text{ m}\cdot\text{s}^{-1}$  at  $\sigma_c = .2 \text{ m}\cdot\text{s}^{-1}$ . However, for widths from  $.1$  to  $.5 \text{ m}\cdot\text{s}^{-1}$ , the  $v_p$  should span  $.48$  to  $2.4 \text{ m}\cdot\text{s}^{-1}$ . This indicates that the clutter filter should have a notch of variable width dictated by the antenna rotation.

Both the recursive filter and the FIR filter require certain time to achieve clutter cancellation. For a FIR filter the time needed is  $MT_c$  which is also the duration of its transient response. We define this time to be also the settling time of a recursive filter with the same specification as the nonrecursive filter. Even though longer dwell times are needed for a filter with sharper characteristics, it is not the filter dwell time that dictates the radar update rates. These are determined by the desired accuracy of moment estimates. For instance, with a continuous pulse train one may use more or less than  $M$  samples ( $M$  is the FIR filter length or length of an equivalent FIR when the recursive filter is used) in the autocovariance processor, and the velocity or spectrum width estimates after filtering may be updated more frequently than every  $M$  pulses. Thus one can always match the update times to the antenna rotation rate (see Appendix D). With a change in rotation rate the spectrum width of ground clutter changes and to maintain proper filtering the notch must be adjusted according to (1.9). For instance at 6 rpm the passband cut-off velocity should be  $v_p = 2.5 - 3 \text{ m}\cdot\text{s}^{-1}$ . The filter with  $v_p = 3 \text{ m}\cdot\text{s}^{-1}$  is discussed thoroughly in a later section where it is labeled as filter number 2.

## 2. TRANSMITTED WAVEFORMS, SCANNING STRATEGY AND CLUTTER CANCELING

Methods for canceling clutter are intimately tied to the signal design and processing schemes of the weather radar. For brevity, we consider only techniques that are economically feasible and intuitively satisfying. Thus, at the onset we will assume that an 8 or more bit A/D converter is available so that its saturation would be unlikely. If a pulse to pulse automatic gain control circuit (AGC) is used, it should have a large time constant so as to smooth variations presented to the filter. Thus, we will ignore the effects of AGC since these in principle can be either accounted for or avoided.

For precise moment estimation, a recursive filter (infinite impulse response IIR) or a finite impulse response filter (FIR) are feasible. Delay line cancelers cannot be employed in conjunction with the pulse pair processor (see Groginsky and Glover, 1980) and our attempt to do filtering on the composite autocovariance of signal plus clutter had meager success (see Appendix C).

We consider a 50 dB rejection in the stopband and a 1 dB ripple in the pass-band reasonable goals to achieve since a recursive filter with such characteristics in steady state has already been designed by Raytheon engineers (Groginsky and Glover, 1980). Incidentally, no more than 50 dB of cancellation is possible if an 8-bit A/D converter is used because when the clutter spans the full 8-bit range, its quantization noise is 50 dB below its average power. The performance of this recursive filter on a contiguous pulse train is shown in the next section while the FIR filter and the number of pulses needed to achieve the desired characteristics is discussed in Appendix B.

The type of transmitted signal has a tremendous bearing on which of the two filters would yield better results. To take full advantage of the recursive filter, the transmitted sequence must be uniform and uninterrupted. This would then require two frequencies--one for velocity measurements and the other for reflectivity. The performance of a dual frequency radar in clutter can be exactly predicted from the knowledge of the filter type. Also the required update rates to achieve tolerable errors in estimates can be obtained from published curves (Zrnic', 1979). We will not dwell on this; rather, in the next few paragraphs, we discuss an interlaced pulse scheme and a corresponding scanning strategy that allows considerable clutter cancelling at low elevation angles where it counts.

Let us assume that the PRT,  $T_s$ , of the radar would be variable and somewhere between the limits as in Table 2.1.

Table 2.1

PRT	$T_s$	.781 ms	1.2 ms
Unambiguous velocity	$v_a$	$32 \text{ m}\cdot\text{s}^{-1}$	$20.8 \text{ m}\cdot\text{s}^{-1}$
Unambiguous range $r_a$ for velocity measurements		117 km	180 km

Operation with the longest PRT produces maximum dwell time, and if we do not allow more than 50 percent degradation in the apparent antenna pattern due to

rotation during acquisition, we find the relationship between rotation rate  $\alpha$  ( $^{\circ}\text{s}^{-1}$ ),  $T_s$  and the number of samples  $M$  for a  $1^{\circ}$  antenna beamwidth (see Appendix D)

$$\alpha M T_s = 1 \quad (2.1)$$

Both the FIR filter and IIR require about 64 samples for good clutter canceling (i.e., notch width  $2 v_p \approx 4 \text{ m}\cdot\text{s}^{-1}$ , and 40 to 50 dB cancelation, see Fig. B.6). Let's accept  $M=64$  and let us add another 8 PRT's for reflectivity estimation as in Fig. 2.1.



Figure 2.1 Interlaced pulse train for separate velocity and reflectivity estimation. At low elevation angles about 64 pulses are needed to achieve good clutter canceling, while at higher elevation angles  $M$  could be 16. To estimate reflectivity with acceptable accuracy, a broadband pulse must be employed in conjunction with some range averaging (Krehbiel and Brook, 1979).

The pulse for reflectivity would need to be a broadband signal (perhaps 5 to 10 MHz) to reduce statistical fluctuations of reflectivity estimates (Krehbiel and Brook, 1979). From (2.1) we find the rotation rate  $\alpha=12^{\circ}\text{s}^{-1}$  (or 2 rpm). Such a slow rotation rate need not be maintained throughout the whole scan. Only the two lowest elevation angles ( $.5^{\circ}$  and  $1^{\circ}$ ) would definitely require that much canceling. At higher elevations, the canceler can be bypassed and the rotation rate increased. For instance, 16 contiguous pulses with some averaging in range are sufficient to provide adequate accuracy (Figs. 2.2 and 2.3). With 8 more PRT's for reflectivity we find  $M'=24$  (where  $M'$  is the number of system periods,  $T_s$ , needed for both reflectivity and velocity) and  $\alpha\approx 36^{\circ}\text{s}^{-1}$  or 6 rpm. A possible scanning strategy employing the above principle is listed in Table 2.2.

Table 2.2

Elevation angle	$M'$	Rotation rate	Time
$.5^{\circ}, 1^{\circ}$	72	2 rpm	1 min
$2^{\circ}, 3^{\circ}, \dots, 13^{\circ}$	24	6 rpm	2 min
$15^{\circ}, 17^{\circ}, 19^{\circ}, \dots, 25^{\circ}$	24	6 rpm	1 min

While this may not be an optimum strategy, it illustrates that 4-minute update times are realistic with significant ground clutter canceling capability at the two lowest elevation angles.

If a notch width  $2 v_p$  of  $8 \text{ m}\cdot\text{s}^{-1}$  is acceptable, then a 32 point weighted Fourier transform may be adequate (see Appendix B), in which case the rotation rate at the lowest elevation angles would increase by a factor of two. This would then allow canceling at two additional elevation angles ( $2^{\circ}$  and  $3^{\circ}$ ). Also use of initialization on a recursive filter could further reduce the number of needed contiguous pulses. This is an area requiring more research.

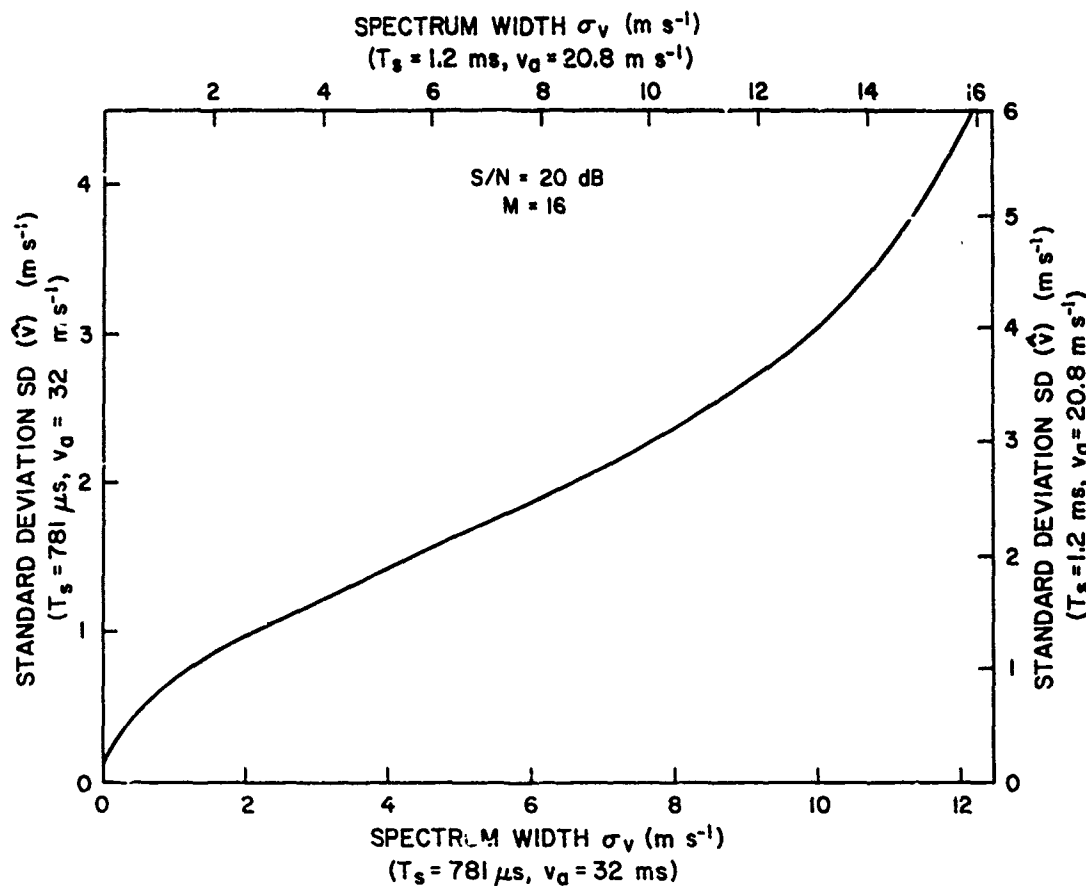


Figure 2.2 Standard deviation of velocity estimates from the pulse pair algorithm with 16 pulses (i.e., 15 pairs). The upper and right scales are for  $T_s = 1.2 \text{ ms}$ ; the lower and left scales are for  $T_s = 781 \mu\text{s}$ .

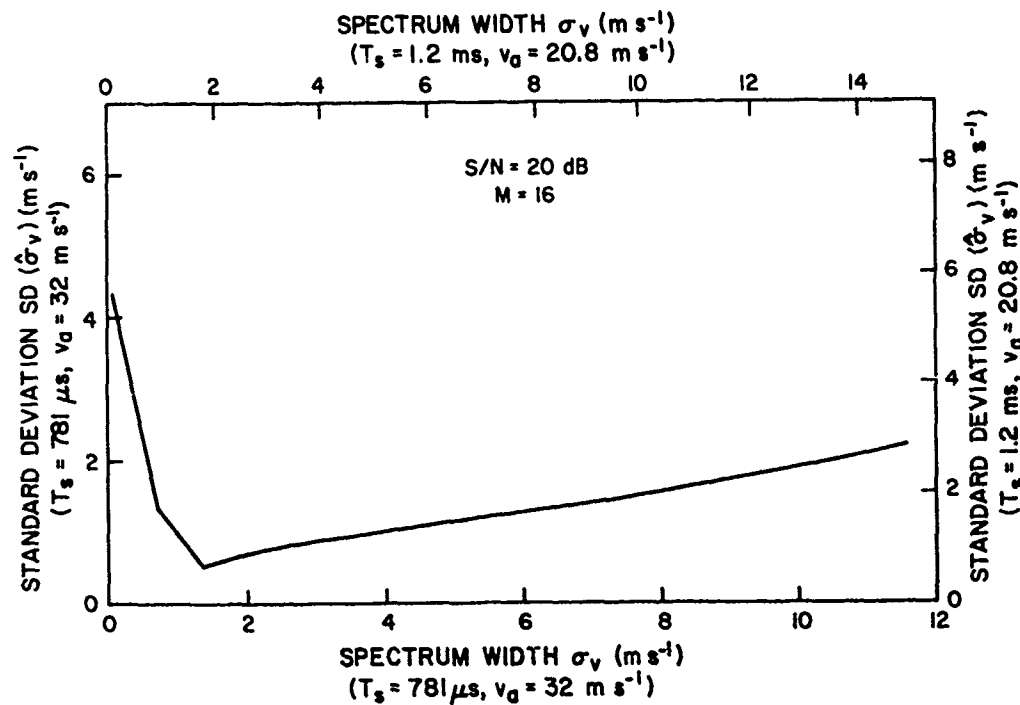


Figure 2.3 Standard deviation of spectrum width estimates from the pulse pair algorithm with 16 pulses.

### 3. GROUND CLUTTER FILTER

This section examines practical cancelers that could function in conjunction with the pulse pair processor. A recursive filter that operates on contiguous pulse pairs is examined first.

#### 3.1 Recursive Filter-Contiguous Pulse Train

The recursive filter we consider is a three pole elliptic filter with a 50 dB rejection in the cutoff band and a transmission zero at DC, a 1 dB ripple in the passband and a variable notch width. This type of a filter has been built by Raytheon for the AFGL (Groginsky and Glover, 1980). In Table 3.1 are listed three filters that we have designed and analyzed. Figure 3.1 is the appropriate flow chart that defines the K coefficients.

Table 3.1. Coefficients for the high pass elliptic filter.

Filter number	$f_p$	$v_p$	$f_s$	$v_s$	$K_1$	$K_2$	$K_3$	$K_4$
	Hz	(m/s)	Hz	(m/s)				
1	16	0.8	4.5	0.225	1.999621	1.959927	0.965686	0.858737
2	60	3.0	17.0	0.85	1.994598	1.809719	0.895496	0.455619
3	80	4.0	22.6	1.13	1.990548	1.715192	0.863963	0.339933

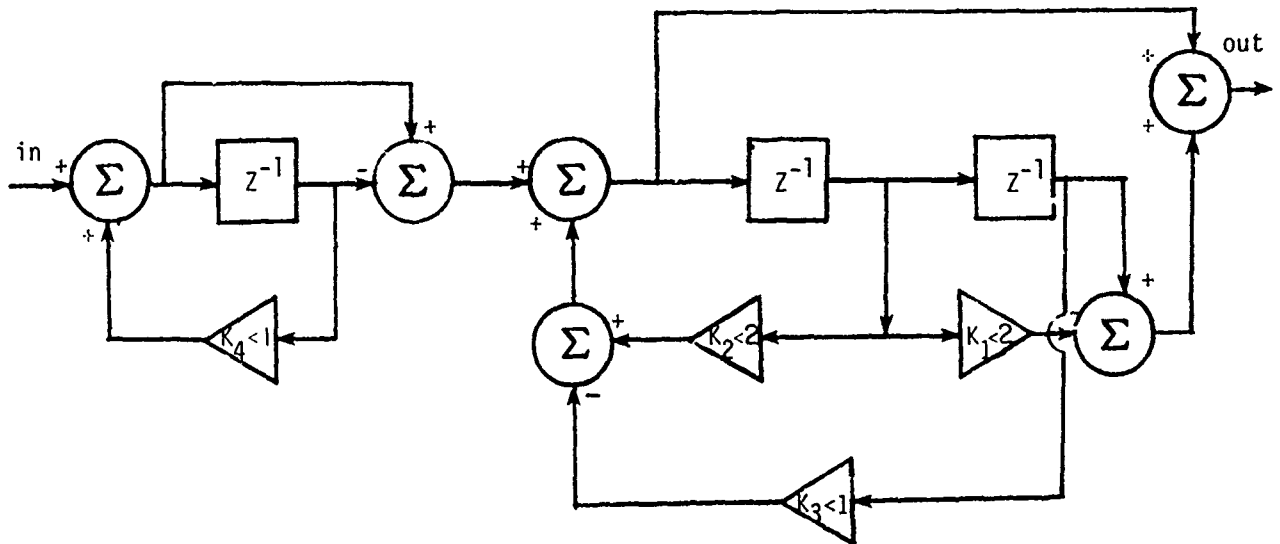


Figure 3.1. Block diagram of the third order high pass elliptic filter.

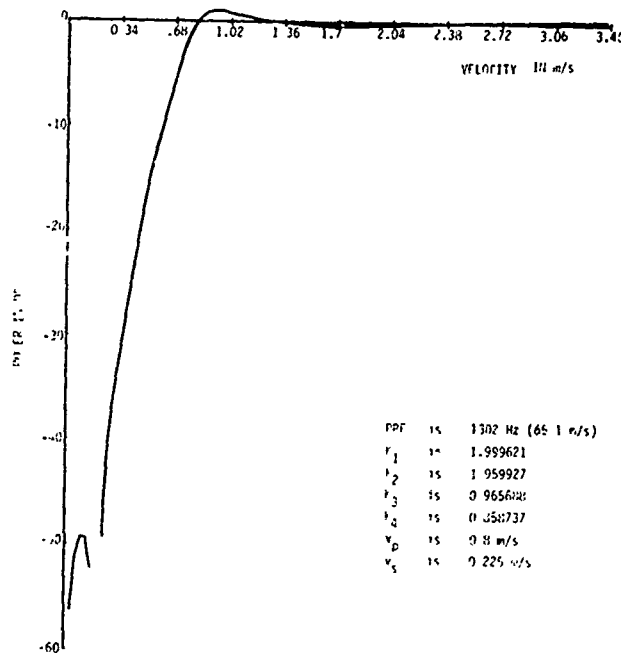


Figure 3.2. Frequency (Doppler velocity) response characteristic of the recursive Filter 1. The Nyquist interval is  $65.1 \text{ m}\cdot\text{s}^{-1}$ ; in subsequent simulations it is slightly reduced to  $64 \text{ m}\cdot\text{s}^{-1}$ .

For illustration, the transfer characteristic of the Filter 1 is shown on Fig. 3.2, which demonstrates that the specifications have been met. The other two filters have very similar characteristics but with a wider notch.

The recursive filter operates on the I, Q digital video samples before the pulse pair processor. (Fig. 3.3).

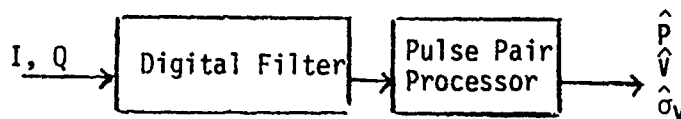


Figure 3.3 Block diagram of data flow. I and Q are the digitized video signals that must be filtered prior to pulse pair processing.

In addition to the mean velocity  $\hat{v}$  and spectrum width  $\hat{\sigma}_v$  estimates, the processor provides an estimate of echo power  $\hat{p}$ .

To illustrate the performance of the tandem filter-pulse pair processor, simulations on synthetic time series data and on some real data were conducted.

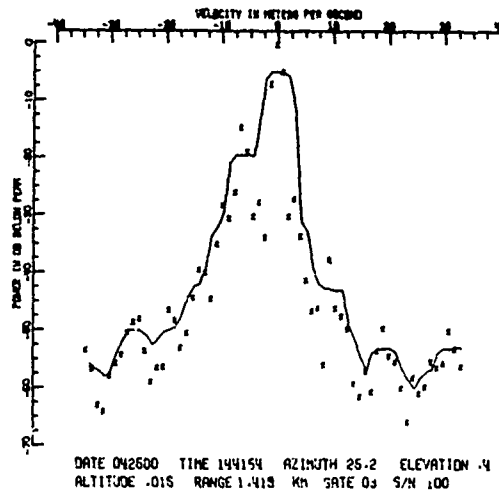
Roundoff effects on coefficients and finite word lengths of data were not considered. Groginsky and Glover (1980) show that coefficients with 12 to 16-bit word lengths (depending on radar PRT) do not degrade the filter performance. Also, data with 8 or more bits would have ground clutter quantization noise more than 50 dB below the ground clutter power when it spans the whole A/D range.

On Fig. 3.4a, b are the spectra obtained from real time series data before and after the recursive Filter #2. To reduce transient effects, the first 40 points of 128 time series data were tapered with the raised cosine. The power spectrum of the last 64 points is taken. In either case prior to taking the spectrum, data were multiplied with the von Hann window. It is evident from the comparison of 3.4a and b that a 50 dB notch was achieved and that the weather peak (at  $-7 \text{ m}\cdot\text{s}^{-1}$ ) that was 15 dB below clutter would, after filtering, produce a viable mean velocity and width estimates. Note also that if the DC line and one spectral power either side of it are removed from the von Hann weighed periodogram (Fig. 3.4a), the weather echo would stick 12.5 dB above the clutter peak. After the recursive filter, the weather peak is 22 dB above the highest clutter residual which means that at least 37 dB of clutter power has been canceled. This filter's stopband cutoff is between  $-.85 \text{ m}\cdot\text{s}^{-1}$  and  $.85 \text{ m}\cdot\text{s}^{-1}$  where we see over 50 dB of cancellation was achieved (Fig. 3.4b). Passband cutoff is between  $-3 \text{ m}\cdot\text{s}^{-1}$  and  $3 \text{ m}\cdot\text{s}^{-1}$  and the residual's peak is at  $4 \text{ m}\cdot\text{s}^{-1}$  where the slight overshoot of this filter's frequency response occurs.

Digital computer simulation of the block diagram on Fig. 3.3 was done to test the quality of the output after filtering. The input time series data were synthesized such that they contained a clutter and weather signal of Gaussian spectral shapes and had a Gaussian statistics (see Zrnic', 1975, for details and Appendix E for program flow charts). Unambiguous velocity,  $v_a$ , was set to  $32 \text{ m}\cdot\text{s}^{-1}$ . In the results that follow, the filter was allowed to reach steady state before 64 points were processed with the pulse pair estimator to obtain  $\hat{P}$ ,  $\hat{v}$ , and  $\hat{\sigma}_v$ . Seventy of the estimates were averaged to obtain the mean curves that are shown on Figs. 3.5 through 3.16. Graphs on Fig. 3.5 suggest that filters with wider notch (numbers 2 and 3) overall create less bias in the power estimate  $\hat{P}$  than the narrowest filter, except near the zeroth velocity. Also evident is the need for a very good match between the notch width and the width of the clutter spectrum. It seems that filter 1 would be better matched to a clutter width of  $.1 \text{ m}\cdot\text{s}^{-1}$  rather than the  $.2 \text{ m}\cdot\text{s}^{-1}$  used as example here. We point out that estimation of power from the coherent data (I, Q) would be attempted only if no echoes are overlaid. Otherwise, the power should be estimated from the reflectivity channel. Modest canceling of ground clutter in the reflectivity channel is possible (see Preprints of the 19th Radar Meteorology Conference) but will not be discussed here.

Graphs of the estimated mean velocity versus true mean velocity for the 3 filters are shown in Figs. 3.6, 3.7, and 3.8. These (and other figures not shown) suggest that the formula (1.9) for the notch width is essentially correct. This formula states that the canceler will perform well if clutter widths are less than  $v_a/4.8$ . For instance, Filter 1 is matched to the clutter width of  $\sigma_c = .16 \text{ m}\cdot\text{s}^{-1}$ ; for this width (see figures) and smaller widths (not shown) it performs well but we see that at  $\sigma_c = .2 \text{ m}\cdot\text{s}^{-1}$  the estimate is good only up to 20 dB of C/S ratio. Filter 2 is matched to  $\sigma_c = .63 \text{ m}\cdot\text{s}^{-1}$  and we note that the performance is good for  $\sigma_c = .2$  and  $.5 \text{ m}\cdot\text{s}^{-1}$  and is very degraded at  $\sigma_c = 1 \text{ m}\cdot\text{s}^{-1}$  as it should be. Filter 3 is matched to  $\sigma_c = .83 \text{ m}\cdot\text{s}^{-1}$ , and we note beginning of degradation at  $\sigma_c = 1 \text{ m}\cdot\text{s}^{-1}$ . An overbiased estimate (by  $2 \text{ m}\cdot\text{s}^{-1}$  or less) occurs at large signal widths ( $8 \text{ m}\cdot\text{s}^{-1}$ ) and good C/S ratios (Fig. 3.8) due to canceling of low velocity components in the weather spectrum.

(a)



(b)

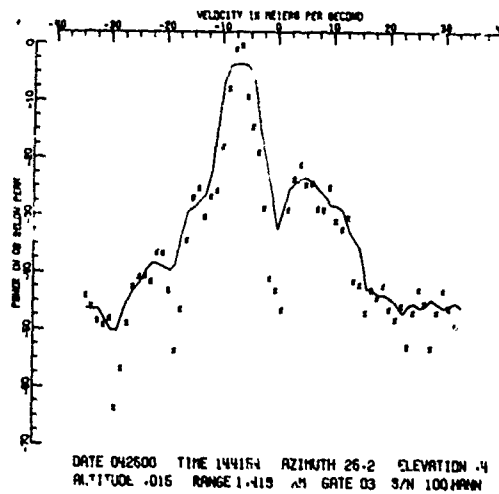


Figure 3.4. a) Power spectrum of time series containing ground clutter and weather signal. Logarithms of powers with respect to the peak are plotted (X's) and the solid curve is a five-point running average for visual clarity. b) Same as a) but time series data were filtered with the elliptic recursive Filter #2.

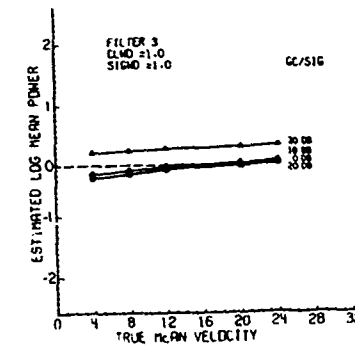
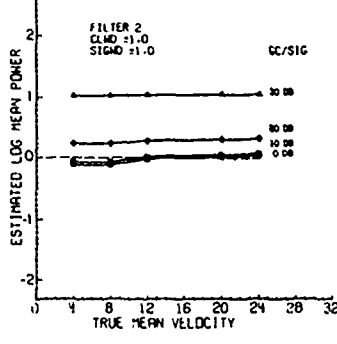
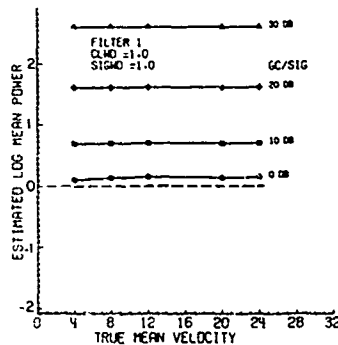
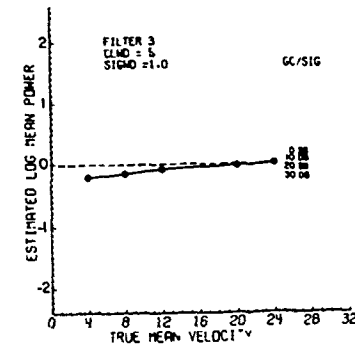
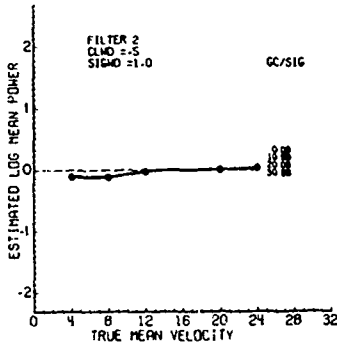
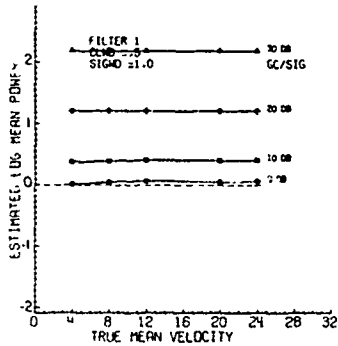
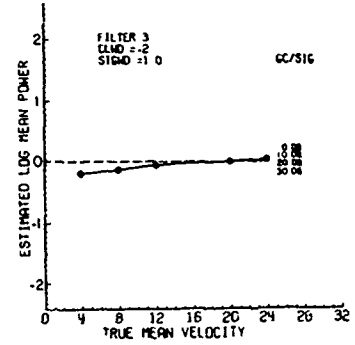
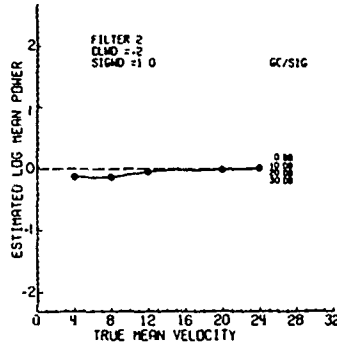
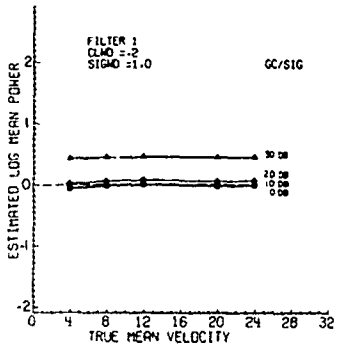
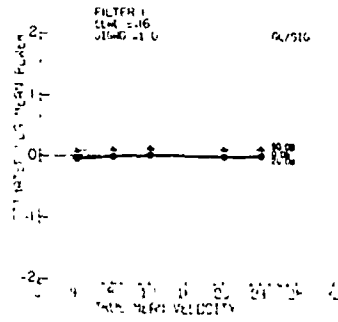


Figure 3.5. Power estimate after the recursive filter. On the ordinate are logarithms of  $\hat{P}/\bar{P}$  where  $\bar{P}$  is the true mean power. The sequence from left to right corresponds to filters 1, 2, and 3 (see Table 3.1). Clutter width, CLWD, changes from top to bottom. Signal width is  $1 \text{ m}\cdot\text{s}^{-1}$  and signal to clutter power ratio is indicated. Filter 1 is designed to operate well with clutter widths less than  $.16 \text{ m}\cdot\text{s}^{-1}$ , filter 2 with  $\sigma_c \leq .63$  and filter 3 with widths  $\sigma_c \leq .83 \text{ m}\cdot\text{s}^{-1}$ .

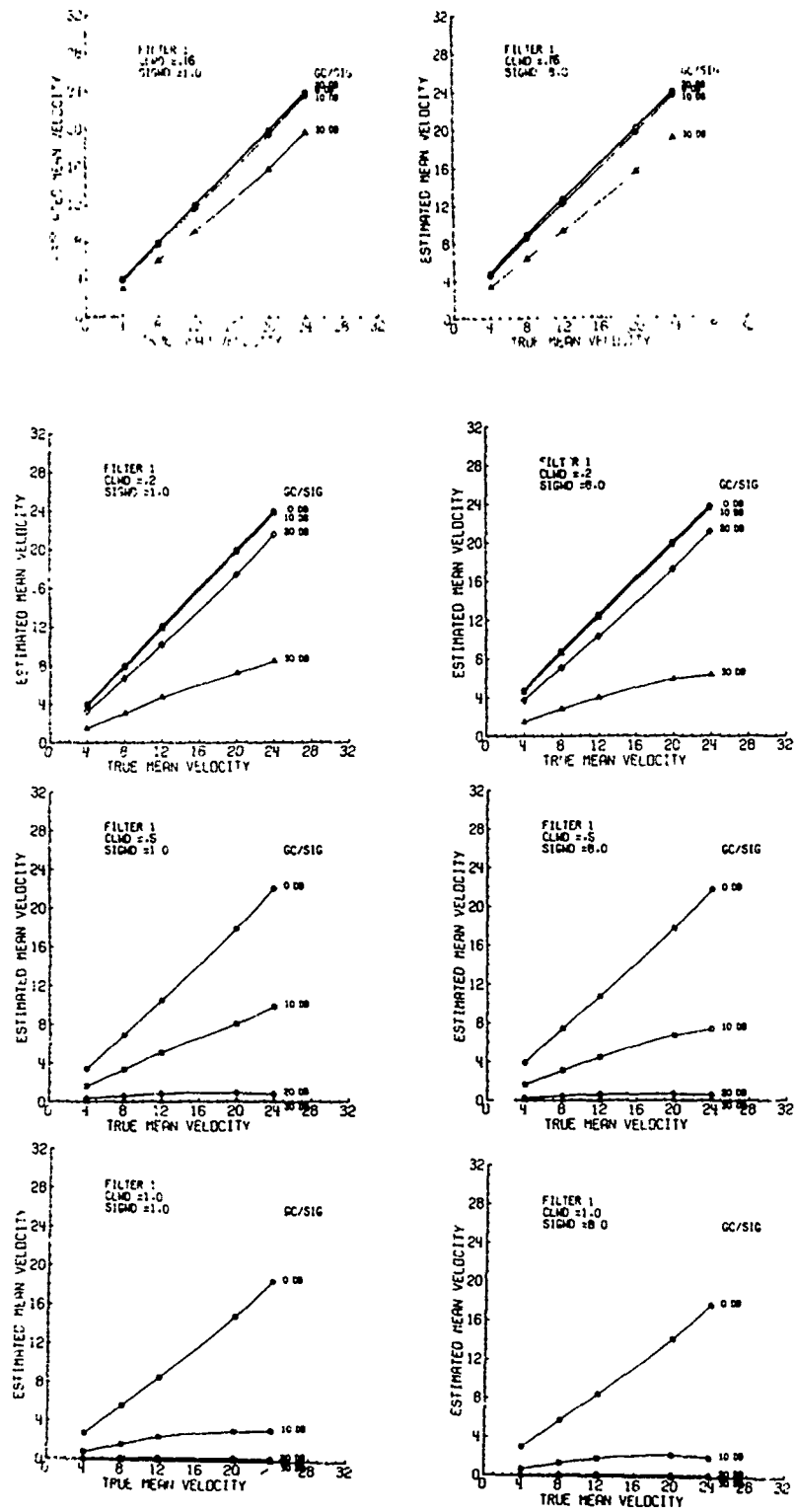


Figure 3.6. Estimated mean velocity versus true mean velocity. Signal widths are  $1 \text{ m} \cdot \text{s}^{-1}$  (on the left) and  $8 \text{ m} \cdot \text{s}^{-1}$  on the right. Clutter width increases from top to bottom, and is indicated together with clutter to signal ratio.

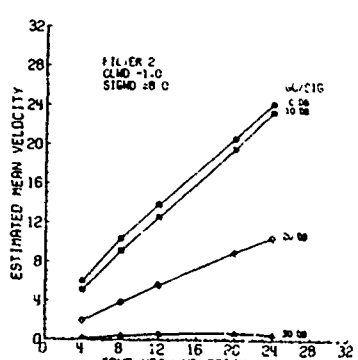
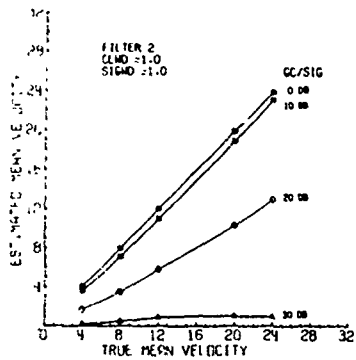
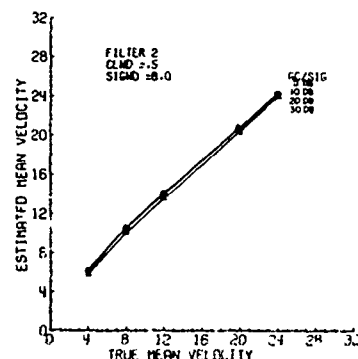
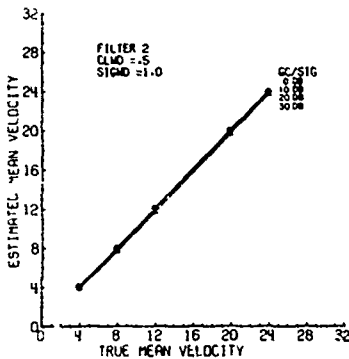
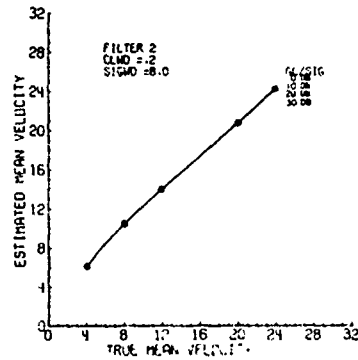
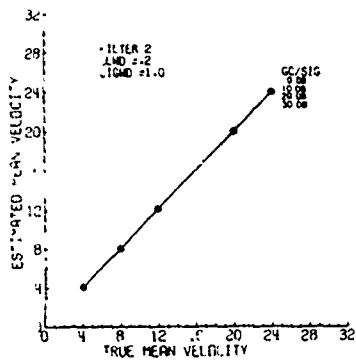


Figure 3.7. Same as 3.6 but filter 2 is used.

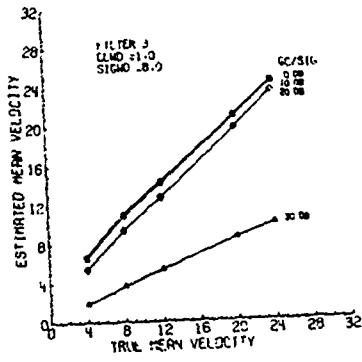
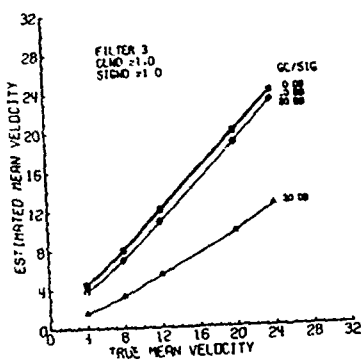
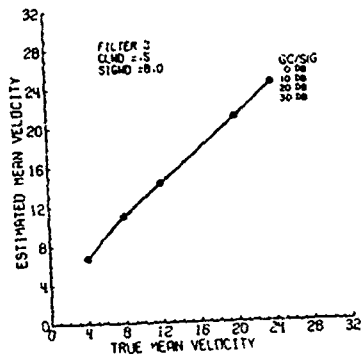
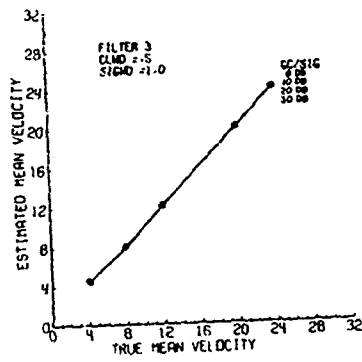
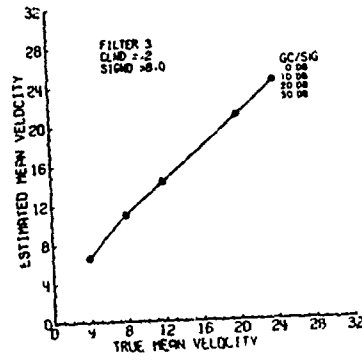
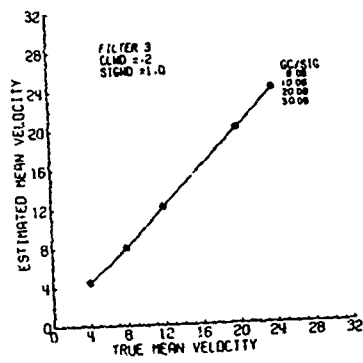


Figure 3.8. Same as 3.6 but filter 3 is used.

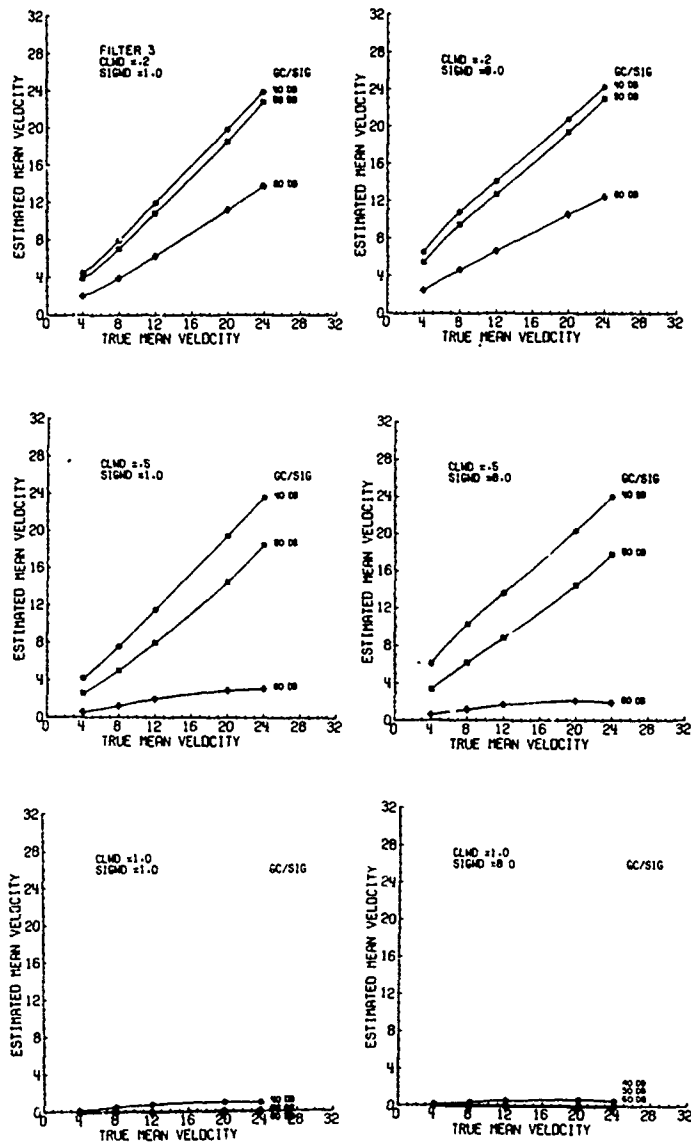


Figure 3.9. Same as 3.8 but the C/S ratios are larger.

The filters perform similarly for the whole range of weather signal widths between 1 and 8  $\text{m}\cdot\text{s}^{-1}$ . To further emphasize the point, larger C/S ratios are shown on Fig. 3.9. The sensitivity to clutter width is apparent. Note that 40 dB of C/S can be tolerated for widths smaller than the matching width ( $0.83 \text{ m}\cdot\text{s}^{-1}$ ). Although the canceler removes 50 dB of clutter in the spectrum domain, the pulse pair processor operates well when spurious peaks are about 10 dB below the signal peak, and therefore 50 dB of C/S ratio (per pulse) results in biased estimate (middle of Fig. 3.9). The bias is quite small for  $\sigma_c = 0.2 \text{ m}\cdot\text{s}^{-1}$ , but that is because at such narrow clutter spectrum width more than 50 dB cancelation is achieved by the steep region of the filter around zero (see Fig. 3.2 for the filter characteristic).

Behavior of the estimates around zero velocity is of interest since that is where the filter characteristic changes most. For the wide notch Filter #3 ( $2v = 8 \text{ m}\cdot\text{s}^{-1}$ ), the mean velocities are plotted on Fig. 3.10. The estimates are reasonably well behaved except for a rather anomalous curve when  $\sigma_c = .2 \text{ m}\cdot\text{s}^{-1}$  and  $\sigma_v = 1 \text{ m}\cdot\text{s}^{-1}$ . It is not clear if this anomaly is real or computational. Apart from it, the estimates are biased, but this should not present a problem for meteorological interpretations since biases are small and predictable. With the narrower filter, the transition through zero is much smoother (Fig. 3.11).

From the above consideration, it is essential to have the passband cutoff  $v_0$  equal to or slightly larger than  $4.8 \sigma_c$ . The filter was operated in steady state and provided 64 samples to the pulse pair estimator. Under these conditions, excellent mean velocity estimates are obtained.

Conclusions concerning spectrum width estimates (Figs. 3.12, 3.13, 3.14, and 3.15) are very similar to the mean velocity estimates. However, the bias can be worse under some circumstances. For instance, Filter 2 is matched to clutter width of  $0.63 \text{ m}\cdot\text{s}^{-1}$ ; thus at smaller widths it should perform well. In Fig. 3.13 we see that at a mean velocity of  $24 \text{ m}\cdot\text{s}^{-1}$  and clutter width of  $.5 \text{ m}\cdot\text{s}^{-1}$  the signal width estimate has a significant bias even though the clutter to signal ratio is only 30 dB. Behavior of width estimates in the transition region is plotted on Figs. 3.16a and b. Biases at mean velocities below  $2 \text{ m}\cdot\text{s}^{-1}$  are evident when data are filtered with the wide notch Filter 3, but such cases can be automatically recognized.

### 3.2 Recursive Filter, Stepped Input and Initialization

The main disadvantage of the recursive elliptic filter is its transient response. Although the steady state frequency response of IIR filters is similar to comparable FIR filters, infinite duration of their impulse response has limited their use in radar application. At low elevation angles ( $< 0.5^\circ$ ) the clutter power is several orders of magnitude stronger than the signal power. Thus, when interlaced samples (batch) for velocity and reflectivity estimation are used, the clutter appears as a step to the filter which produces severe ringing at the output and in effect overwhelms the signal. To reduce this effect, either enough time must be allowed for the transients to settle before pulse pair processing is attempted or some other means of their suppression must be employed. Because settling time is tens of pulses (Fig. 3.17), we consider the alternative which is initialization (Fletcher and Burlage, 1972). The purpose of initialization is to load the memory elements of the recursive filter with their anticipated steady state values. These values can be estimated from the first incoming

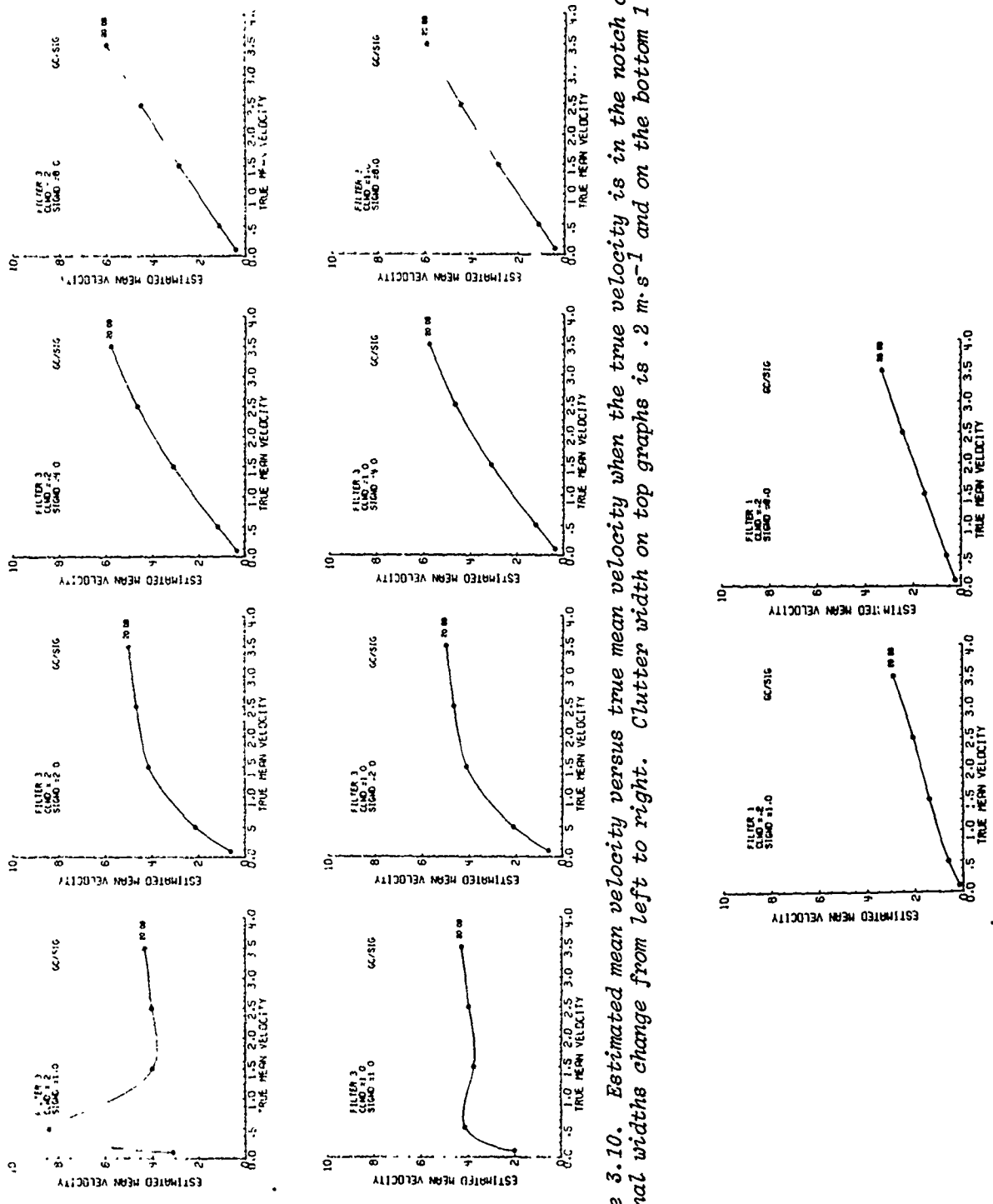


Figure 3.10. Estimated mean velocity versus true mean velocity when the true velocity is in the notch of filter 3. Signal widths change from left to right. Clutter width on top graphs is  $.2 \text{ m}\cdot\text{s}^{-1}$  and on the bottom  $1 \text{ m}\cdot\text{s}^{-1}$ .

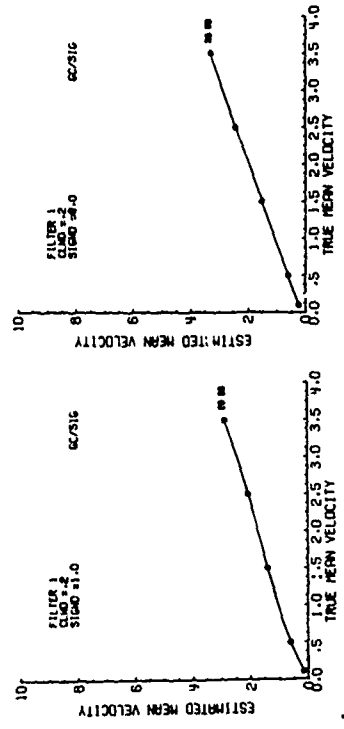


Figure 3.11. Same as 3.10 but filter 1 is used; clutter width is  $.2 \text{ m}\cdot\text{s}^{-1}$ ; and only cases with signal spectrum widths of  $1 \text{ m}\cdot\text{s}^{-1}$  and  $8 \text{ m}\cdot\text{s}^{-1}$  are shown.

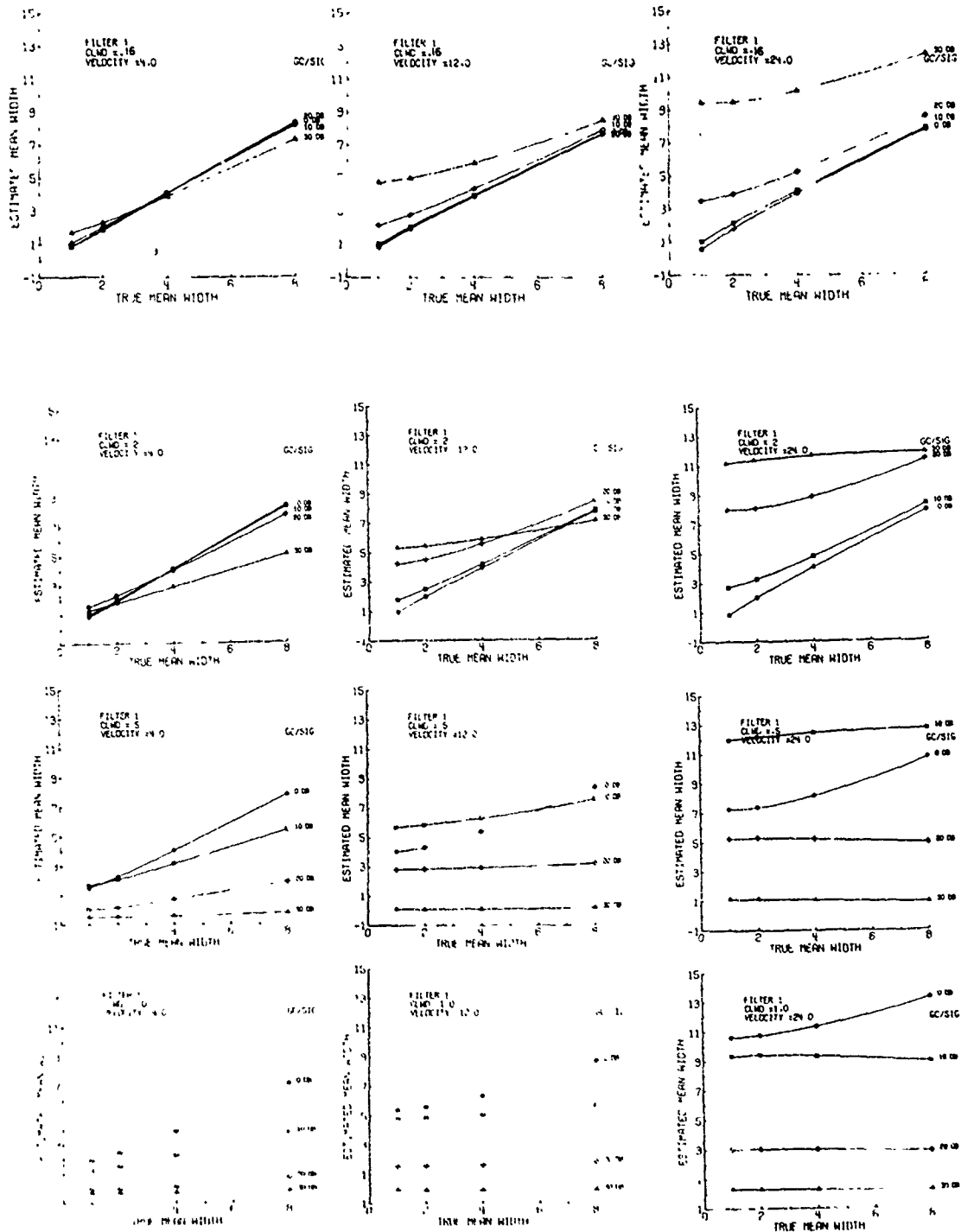


Figure 3.12. Estimated mean signal spectrum width versus true width for simulated time series data processed by the pulse pair processor. Filter 1 is used and clutter width increases from top to bottom. The mean velocity of signal spectrum is  $4 \text{ m}\cdot\text{s}^{-1}$  (left graphs),  $12 \text{ m}\cdot\text{s}^{-1}$  (inside graphs), and  $24 \text{ m}\cdot\text{s}^{-1}$  (right graphs). Ground clutter to signal power ratios are indicated and range from 0 to 30 dB.

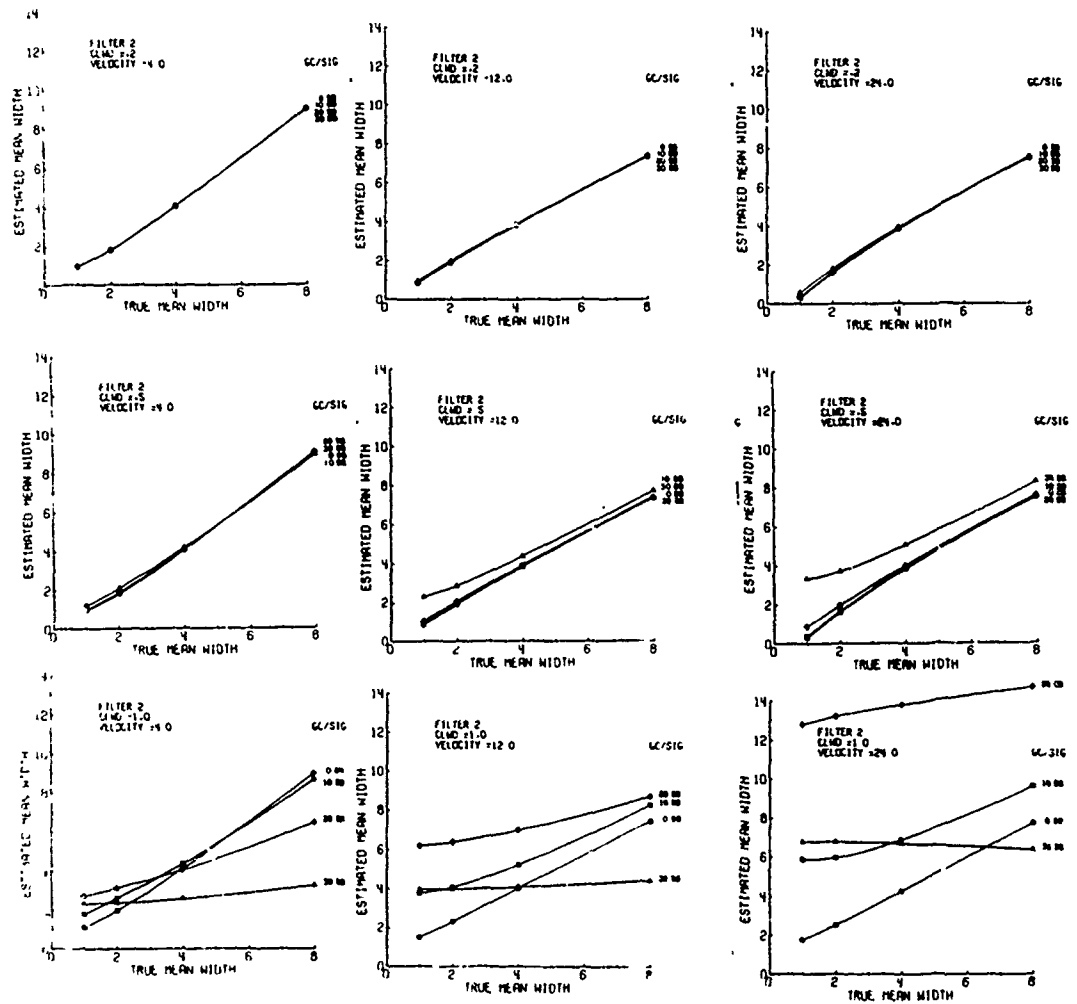


Figure 3.13. Same as 3.12 but filter 2 is used and clutter width of  $.16 \text{ m} \cdot \text{s}^{-1}$  is not considered.

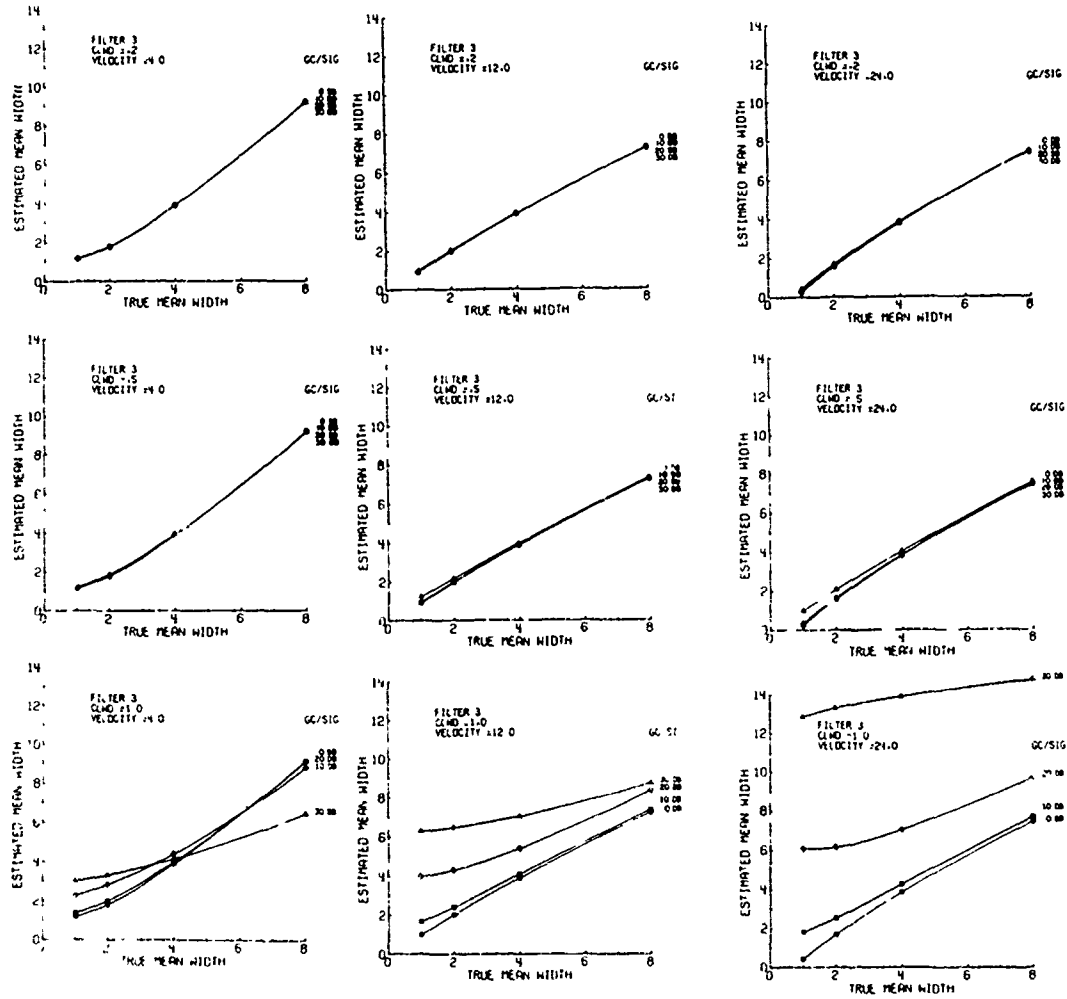


Figure 3.14. Same as 3.13 but filter 3 is used.

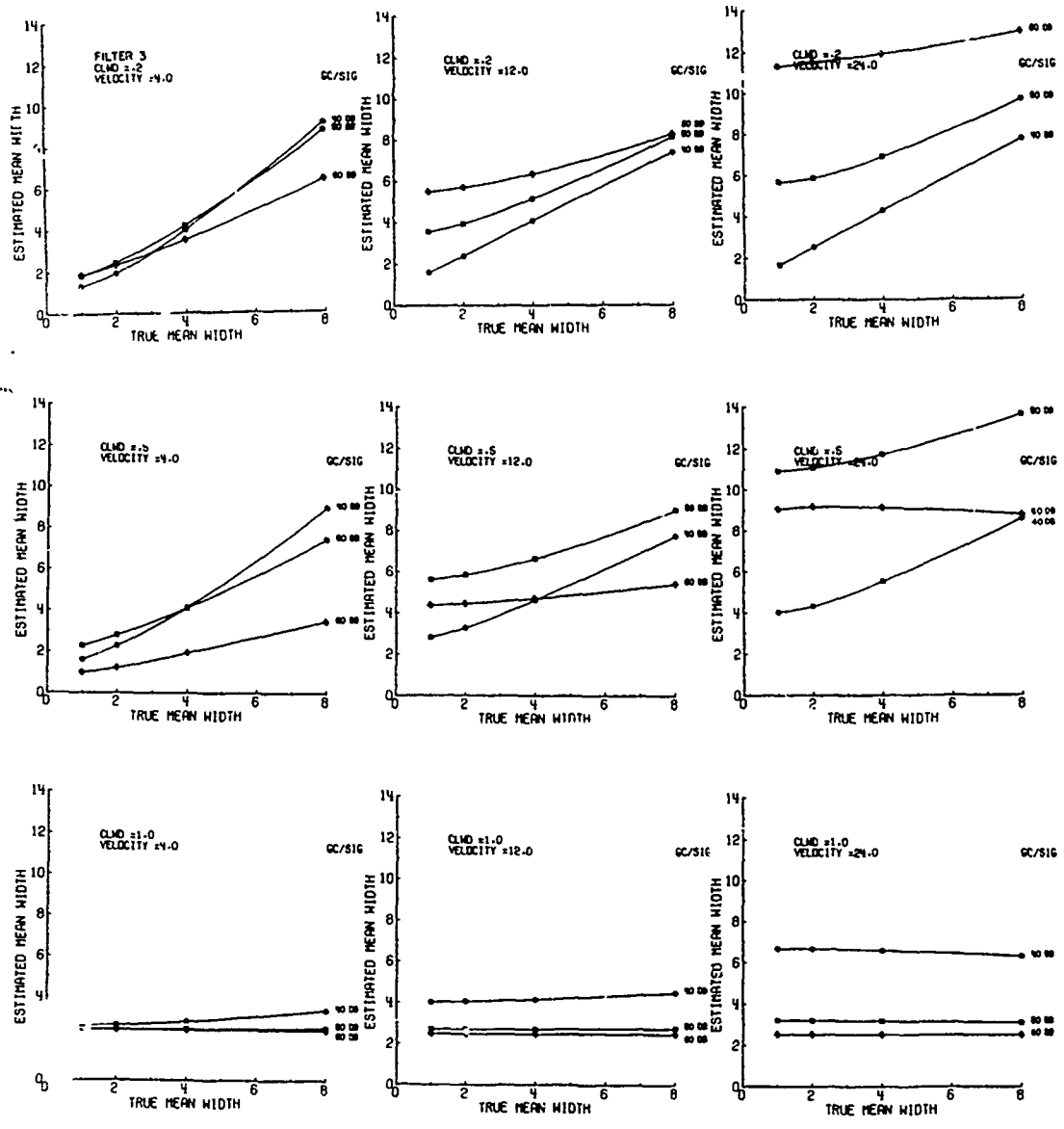


Figure 3.15. Same as 3.14 but the clutter to signal ratios are 40, 50, and 60 dB.

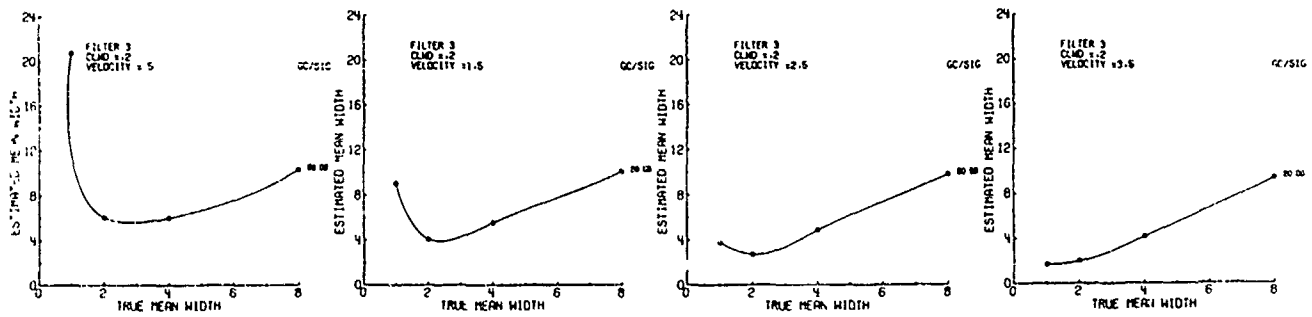


Figure 3.16a. Estimated mean width versus true mean width when the true velocity is in the notch of filter 3. The mean velocity increases in steps of  $1 \text{ m}\cdot\text{s}^{-1}$  from left to right.

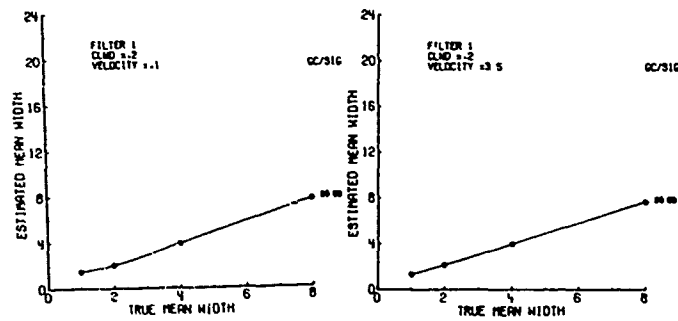


Figure 3.16b. Same as a) but filter 1 was used, and two mean velocities  $.1$  and  $3.5 \text{ m}\cdot\text{s}^{-1}$  are considered. Other velocities between these two produce no noticeable difference in the results.

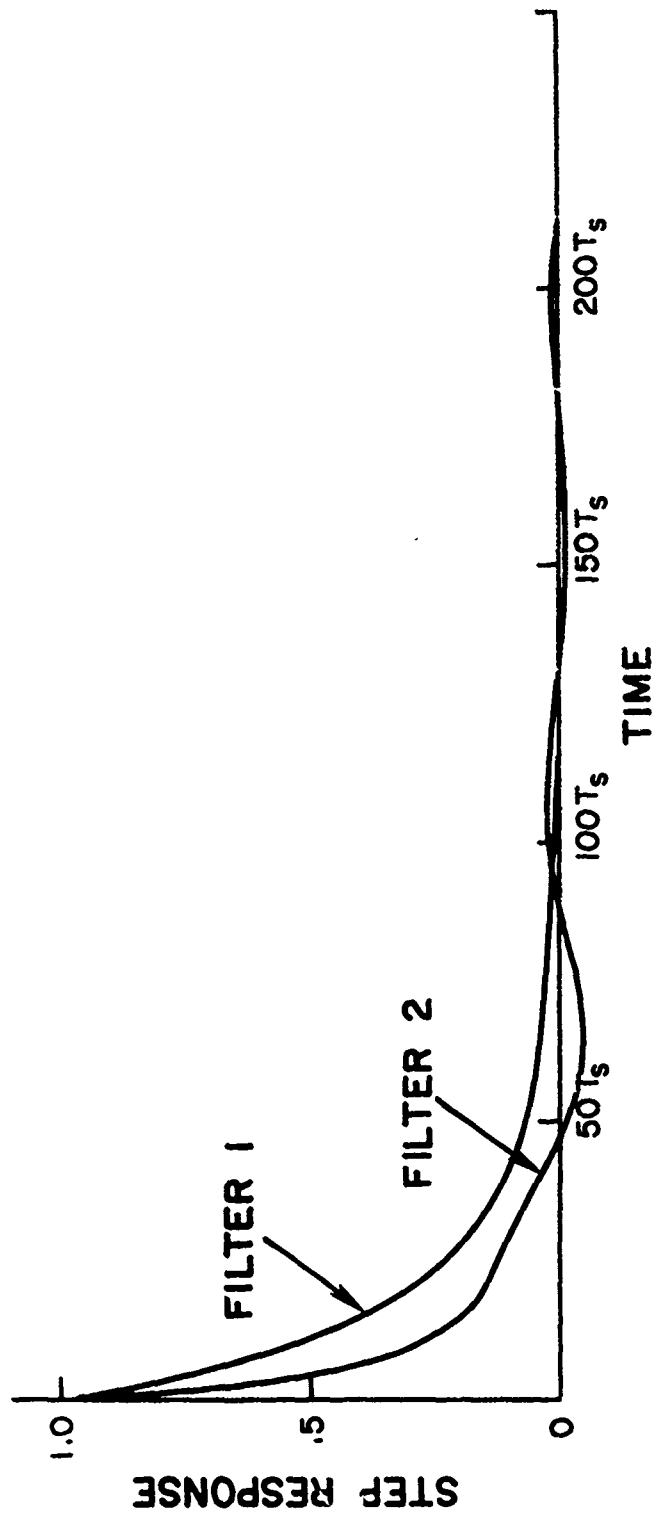


Figure 3.17. Step response of the recursive filter for two different notch widths. Note that the settling time for filters 1 and 2 is over 50 Ts.

pulse. When the ground clutter is a perfect D.C. line and no weather signal is present, the initialization will bring immediately the filter into steady state. Alas, the clutter has finite width and superposed to it is the weather signal which together degrade the initialization.

For the third order filter on Fig. 3.1, the output of the first memory element,  $Z^{-1}$ , would be set to  $A_1/(1-K_4)$  where  $A_1$  is the digital value of the first sample. The outputs of the other two elements must be set to 0. With this the output after the first time sample,  $A_1$ , is 0 and after the second one,  $A_2$ , it is  $A_2 - A_1$ . Thus the filter immediately acts as a delay line canceler so that a large D.C. value does not get through. Simulation of initialization on a digital computer is briefly described in Appendix E, subroutine ELLIPSE 1.

Quantitative measure of the performance of initialization was obtained from simulations. First, we will discuss transient effects on the moment estimates with no initialization. Figure 3.18a shows plots of the estimated mean velocity versus true mean velocity for the case of no clutter and C/S = 10 and 20 dB without any initialization or smoothing. Blocks of 64 time samples were applied repeatedly (70 times) to the recursive filter, and the estimates of the mean velocity and spectrum width were obtained from a 64 sample pulse pair algorithm. The estimates were then averaged to generate the mean values. Throughout this simulation, the clutter spectrum width was set to  $\sigma_v = 0.16 \text{ m}\cdot\text{s}^{-1}$  which is the upper limit for cancellation with Filter No. 1. An unbiased estimate of the mean velocity is obtained in the absence of clutter. Bias is quite evident for both 10 and 20 dB C/S ratios and typical signal spectrum widths  $1.0 \text{ m}\cdot\text{s}^{-1} < \sigma_v < 8.0 \text{ m}\cdot\text{s}^{-1}$ . The width estimate has very little bias when there is no clutter present (Fig. 3.18b). For C/S = 10 dB and velocities  $12.0 \text{ m}\cdot\text{s}^{-1}$ , the width estimate is very poor and is further degraded at C/S = 20 dB.

These biases are mainly there because the filter was in transient during approximately the time half of the samples were applied. Obviously these samples were not properly filtered and their residuals have created biases in the mean velocity and spectrum width.

To suppress the transient response, initialization technique was used, i.e., the first three memory elements were set to anticipated steady state values. Figure 3.19a shows the plot of estimated mean velocity versus true mean velocity for C/S 10 and 20 dB. The estimated values have very little bias for signal spectrum widths  $\sigma_v > 1.0 \text{ m}\cdot\text{s}^{-1}$ . An unbiased estimate of the width (Fig. 3.19b) is obtained for velocities  $8.0 \text{ m}\cdot\text{s}^{-1}$  and C/S = 10 dB. At C/S = 20 dB the bias associated with the estimated signal spectrum width is large except when the mean velocity is  $4 \text{ m}\cdot\text{s}^{-1}$ . In fact, the results are better, i.e., biases are one-half of the ones when C/S=10 dB and no initialization is applied (Figs. 3.18a and b). Thus, in conclusion, filtering over 64 pulses with no initialization is equivalent to about 15 dB S/C improvement, and initialization adds another 15 dB of improvement. In other words, without any filtering a 10 dB S/C ratio for velocity and 15 dB for spectrum width is needed to accurately estimate moments. With recursive filtering of stepped inputs, 64 pulses long at C/S of 0 - 5 dB one may obtain valid  $v$  and  $\sigma_v$  while initialization further raises this ratio to 15-20 dB. In conclusion, recursive filtering on interlaced samples implies a 15-20 dB penalty in ground clutter rejection as opposed to filtering a contiguous pulse train in steady state.

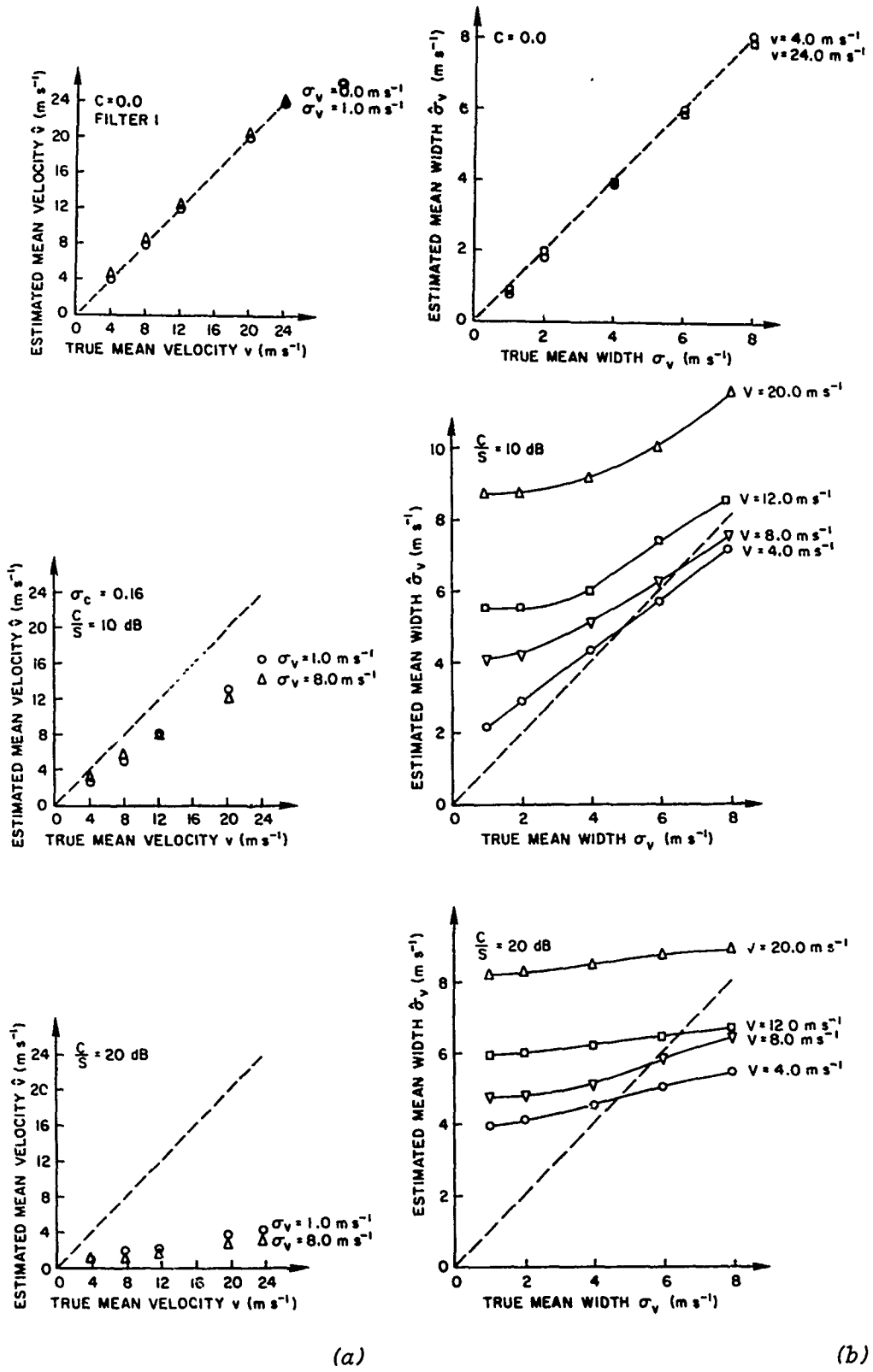


Figure 3.18. a) Mean velocity estimates from the pulse pair algorithm when a 64 sample pulse train is filtered by a recursive filter No. 1 and no provision to suppress transients is applied. b) Mean spectrum width estimates under same conditions as in a).

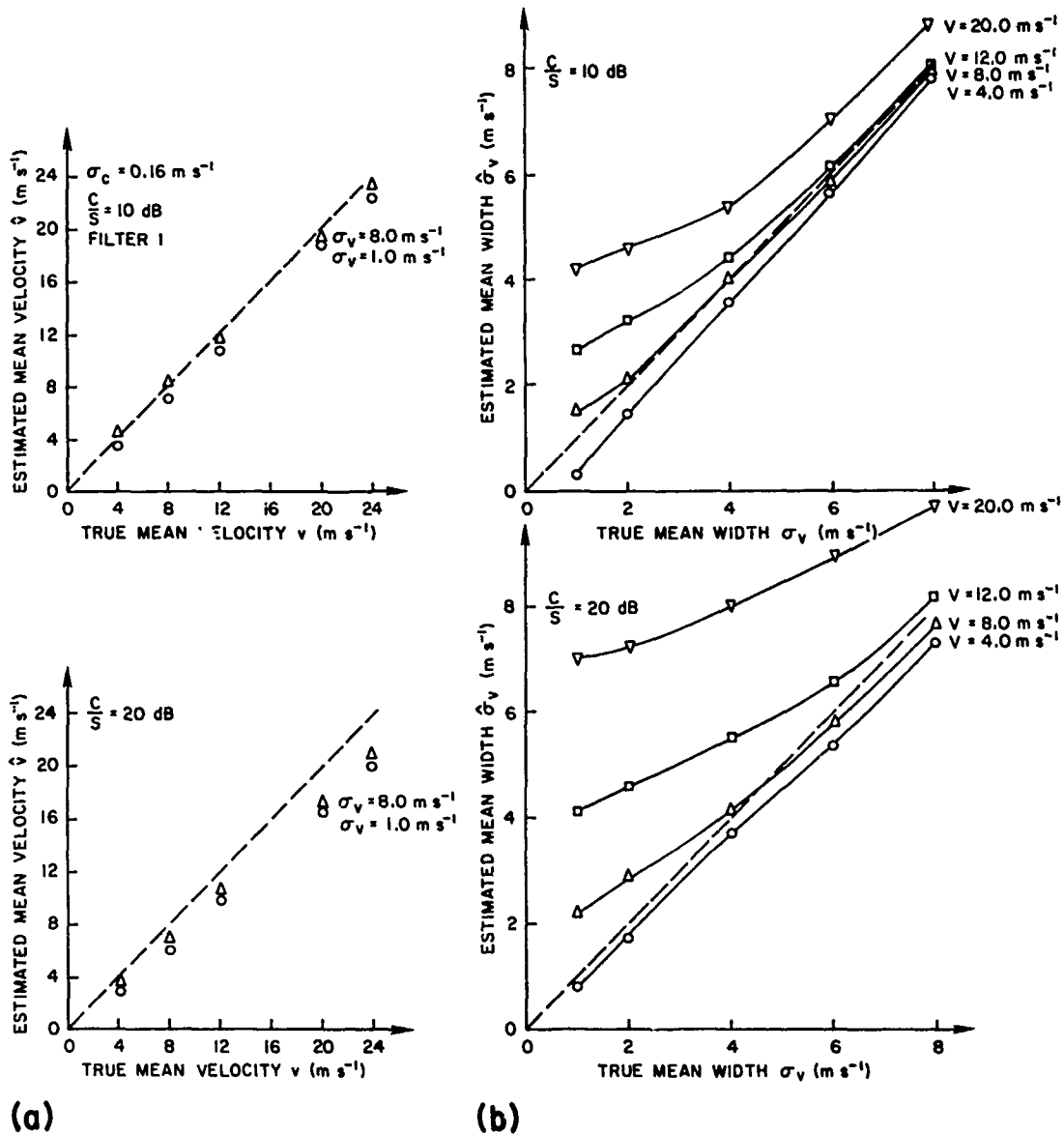


Figure 3.19. a) Same as 3.18a, but the first sample is used to initialize the recursive filter. b) Mean estimates of spectrum width; the filter has been initialized.

It may be possible to reduce this penalty by ignoring the first few samples at the filter's output (after initialization and processing the remaining ones. At present it is not clear what is the minimum number of samples that would allow good clutter canceling and how many of the first samples (if any after initialization) should not be processed.

We have determined that initialization is not detrimental to the weather signal even if ground clutter is weak. For instance, a 64 point spectrum of real signal and clutter is shown in Fig. 3.20a. The signal at  $-8 \text{ m}\cdot\text{s}^{-1}$  is 10 dB above clutter. Next to this graph (Fig. 3.20b) is the spectrum of the filtered signal without initialization, i.e., the 64 time samples were passed through the elliptic filter. On Fig. 3.20c is the spectrum of the same time samples, but the recursive filter has been initialized and on 3.20d the same time samples have been used except that previous 64 samples were also passed through the filter to make it reach steady state. We note that the clutter has been suppressed to about 45 dB below signal when the stepped input is applied to the filter. The residual is 50-55 dB below signal when initialization is applied and is even further down when the filter has reached steady state. The weather spectrum is not affected by the three variations in the filtering.

Very similar conclusions are reached if the clutter power is larger than the signal power. An example on Fig. 3.21a shows a clutter to signal ratio of about 12 dB. Filtering with no initialization removes considerable clutter (Fig. 3.21b), but initialization further decreases the residual by 5 to 10 dB (Fig. 3.21c). Of course, the smallest residual is obtained if the filter reaches steady state, which it approximately does when one also applies the preceding 64 time samples (Fig. 3.21d). In this example, a fairly large image (about 12 dB below the peak of the weather signal) is most likely due to amplitude imbalance of the inphase and quadrature components.

### 3.3 Other Techniques

Two more approaches for filtering ground clutter out of an interlaced pulse sequence were considered. In one, time varying recursive filters with periodic coefficients meant to compensate for the unequal pulse spacing were tried. However, the introduced periodicities created strong spectral peaks (only 5 dB below the DC level) which could not be eliminated. A finite impulse response filter with time varying coefficients would give a better frequency response but due to large storage requirement and the need to change weights at every step makes this filter impractical.

Still another possibility is to use the recursive filter at a reduced rate--let's say every  $kT$ , where  $k$  is a small integer. But this introduces transmission zeroes at frequencies  $(n=1,2,\dots,k)$  which would eliminate considerable amount of weather signal. Furthermore, filtering of pulses between the first and the  $k$ 'th is not trivial.

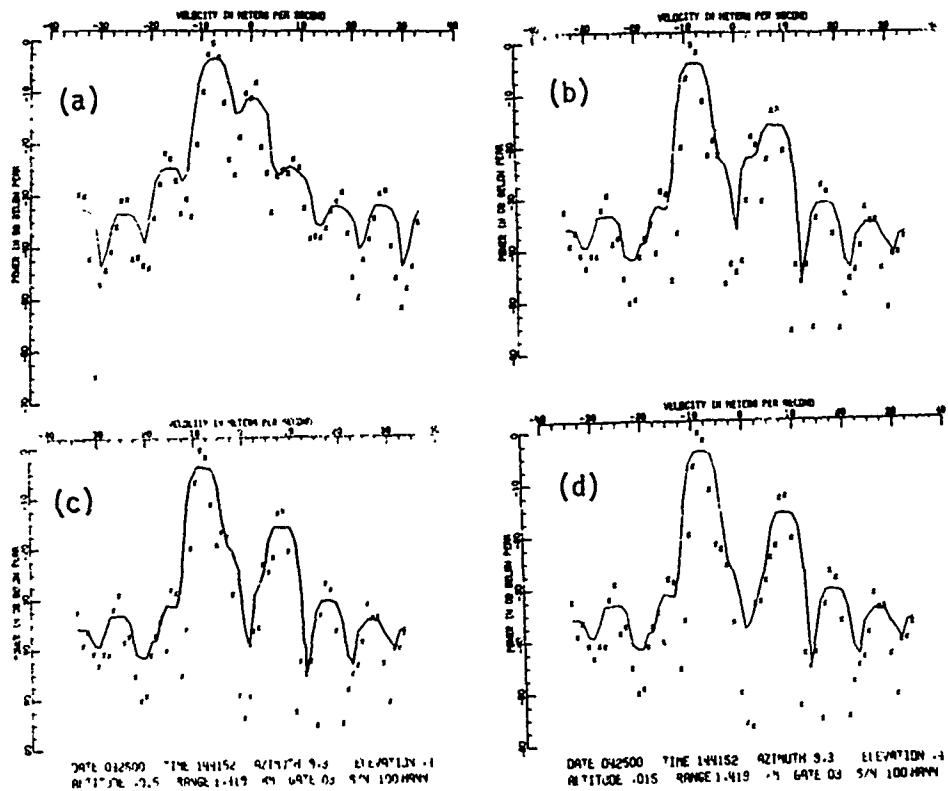


Figure 3.20. a) Doppler spectra of a weather signal (peak at  $-8 \text{ m} \cdot \text{s}^{-1}$ ) and clutter. Spectra are from 64 time samples weighted with a von Hann window.  
 b) Spectra from the same time series but filtered with the recursive filter.  
 c. Same as b) except the recursive filter has been properly initialized.  
 d) Same as b) but the filter has reached steady state since 64 preceding time samples have also been applied.

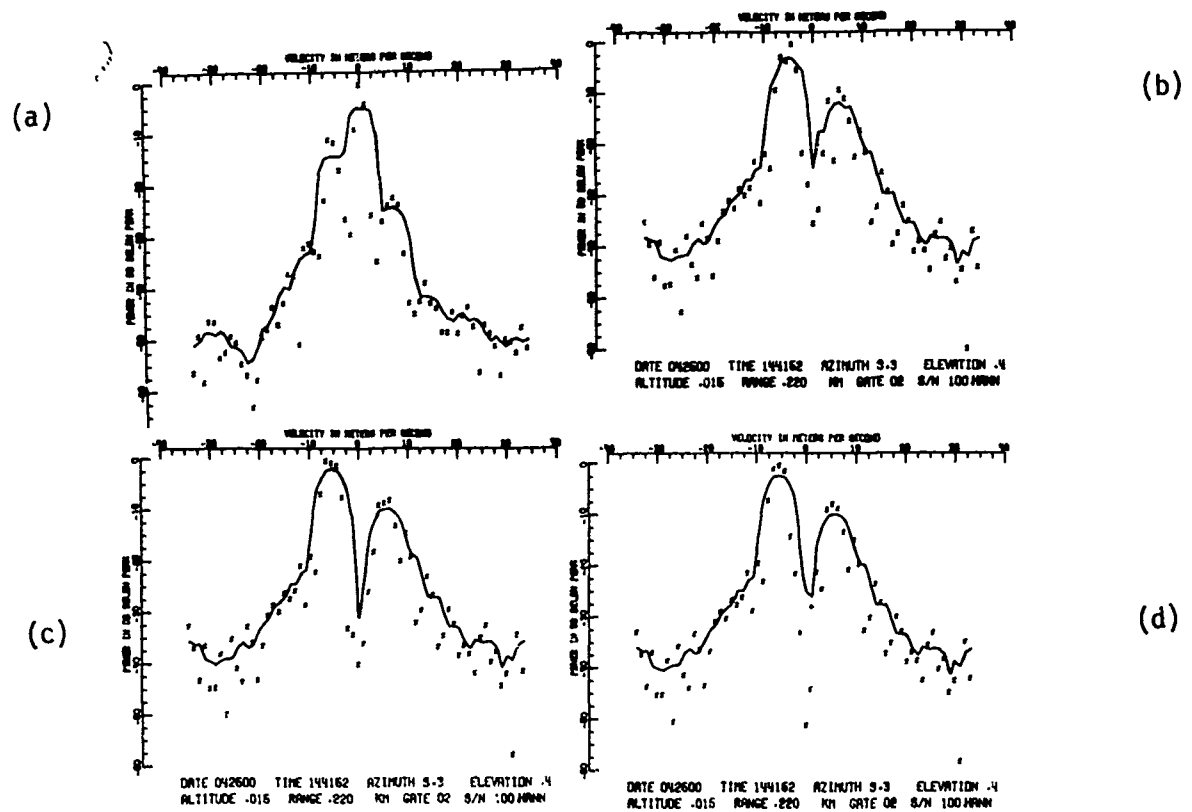


Figure 3.21. a) Spectrum of weather and clutter for  $C/S \approx 12$  dB.  
 b) Time series that generated a) was filtered.  
 c) Time series was filtered and the filter was properly initialized.  
 d) 128 time samples were passed through the filter and the last 64 corresponding to the ones in a), b), and c) are Fourier transformed.

#### 4. CONCLUSIONS

Study of the ground clutter problem at the Norman site indicates that clutter cross sections of 40 to 50 dB below  $1 \text{ m}^2/\text{m}^2$  are typical. These values are small and the clutter extends in range to about 30 km. If a rejection in a stopband of 50 dB can be achieved, then gust fronts with at least -10 dBZ reflectivity would be observed in all but 400  $\text{km}^2$  area at  $0^\circ$  in elevation. Thus, only in 25 percent of the clutter area such weak signals could not be retrieved. On the other hand, reflectivities of 20-30 dBZ would produce viable spectral moments everywhere except at a few spots. Thus, a similar site would be clutter free for storm observations.

Doppler spectrum width,  $\sigma_c$ , of the clutter signal was between 0.1 and  $0.5 \text{ m}\cdot\text{s}^{-1}$  with the mean value of  $.25 \text{ m}\cdot\text{s}^{-1}$  at an antenna rotation rate of  $10^\circ \text{ s}^{-1}$ . The design of clutter filters is very much dependent on this width and for proper cancellation the passband cutoff velocity  $v_p$  must be larger or equal to  $4.8 \sigma_c$ .

Several canceling schemes were investigated, and the most efficient one is with a third order recursive filter. This filter achieves a 50 dB rejection in the stop band with total annihilation of DC. One dB ripple is in the passband, and the ratio of passband cutoff  $v_p$  to stop band cutoff  $v_s$  is about 3.5. The filter operates best in steady state, but it can also be made to operate in transient by properly initializing its memory elements. Performance on 64 simulated and real time samples show that no more than 10 dB loss in effective canceling over steady state occurs if the filter is initialized. Thus, there is no doubt that canceling will be effective on a contiguous 64 pulse sequence. The remaining question is, how well would the scheme work with a smaller number of pulses (16 or 32) and if the first few pulses from the filter's output should not be processed. In our initialization scheme only the first incoming pulse was used to set the filter memory elements, after which the system was left to itself. One may perhaps benefit if some of the storage elements are reinitialized after the second and also after the third pulse.

The autocovariance processor of mean velocity requires 10 dB of signal to clutter power ratio while for second moment estimation 15 dB insures adequate accuracy. Therefore, the two estimates will not behave in a same manner for a fixed amount of clutter canceling. For instance, a properly initialized filter would allow processing of samples with 20 to 40 dB of C/S for mean velocity and 15 to 35 dB for Doppler spectrum width.

It is shown that a scan sequence can be accomplished in about 4 minutes if the rotation at the two lowest elevations is slow (2 rpm) and at the next 18 levels it is increased to 6 rpm. The purpose here was not to investigate scanning strategies, but rather to point out that 4 to 5 minutes update times are feasible with good clutter canceling at low levels where it counts. Other possible schemes such as interlaced elevation angles, etc., would also need to have antenna speeds reduced to 2 rpm at the lowest elevations. Beside the variable antenna speed it may be wise to consider an adaptive canceling scheme. For instance, canceling should be done only where needed, i.e. up to a maximum range that depends on elevation. Also the filter notch may change with elevation.

We stress that clutter canceling throughout the volume would be easiest if a dual frequency transmitter is employed, because then the recursive filter would not be subjected to transients (if block AGC is utilized, transients due to gain change are easier to control). Furthermore, rotation rate at the lowest elevations could be somewhat increased, and there would be more samples for velocity estimation at

higher elevations. Also, more samples for reflectivity calculations would be made available. This last parameter may prove difficult to estimate in an interlaced mode with a long string of velocity pulses. It may even be necessary to transmit a broadband pulse for reflectivity estimation.

The part of weather signal that is within the stop band cutoff of the filter is totally lost but that is a small penalty since zero radial velocities occupy a small portion of a storm and can usually be identified. But large spectrum widths indicative of turbulence and other hazards would still be measurable. Reflectivities would be underestimated if the signal is directly in the notch, and would be in error by about 1 dB in the immediate vicinity of the notch. Therefore, canceling should be done selectively at those ranges and elevation angles where ground clutter is significant.

Filtering via a weighted discrete Fourier transform was briefly investigated (Appendix B) and although the number of pulses needed to achieve comparable characteristics is about 70, the filter itself is not subject to transients. Therefore, its effects can be exactly predicted and with some fitting of weather and clutter spectrum models it may be even possible to retrieve considerable information about the weather signal of zero velocity. Another possible advantage of the Fourier method is that it can be implemented in conjunction with a phase diversity radar. By this we mean that the Fourier transform may be performed on samples that are phase adjusted for the first trip. Then after rejecting clutter spectrum coefficients, an inverse transform is made and the resulting time samples can be phase readjusted for the second trip. Another transform or autocovariance processing of these samples will reveal the echoes from the second trip while the clutter residual would be spread uniformly through the Nyquist interval. All this is computationally very intense; it is not clear if and how an analogous algorithm with the recursive filter could unscramble the second trip echoes in a phase diversity radar.

The first trip clutter overlaid on storms of interest in the second trip is very bothersome because the obscuration area increases 10 or more times and the second trip signal strength has a 10 to 15 dB disadvantage due to range. Effective ground clutter canceling is therefore very important in operational Doppler weather radar.

## APPENDIX A

### Errors in Pulse Pair Derived Velocity and Spectrum Width Due to Anomalous Signal

The signal of interest, with power 'S' and the anomalous signal (for instance ground clutter) with power 'C' are both assumed to have Gaussian shaped power spectra with mean frequencies  $f_s$  and  $f_c$  and widths  $\sigma_s$  and  $\sigma_c$ . The error we are interested in is the difference between  $v_{s+c}$  and  $v_s$ . Where  $v_{s+c}$  is the pulse pair velocity for the total signal (signal + clutter) and  $v_s$  is the pulse pair velocity of the signal of interest.

$$v_s = \frac{v_a}{\pi} \arg [R_s(T_s)] \quad (A.1)$$

$R_s(T_s)$  is the signal autocovariance function;  $v_a$  is the Nyquist velocity.

$$v_c = \frac{v_a}{\pi} \arg [R_c(T_s)] \quad (A.2)$$

If the signals that give  $v_c$  and  $v_s$  are uncorrelated, then

$$v_{s+c} = \frac{v_a}{\pi} \arg [R_{s+c}(T_s)] \quad (A.3)$$

where

$$R_{s+c}(T_s) = R_c(T_s) + R_s(T_s)$$

for Gaussian shaped spectra  $R_s(T) = S e^{-2\pi^2 \omega_s^2 T_s^2 + j\omega_s T_s}$

$$\omega_s T_s = \frac{\sigma_s}{2v_a} \quad (A.4)$$

$$\omega_s = 2\pi f_s$$

$T_s$  is PRT, and a similar expression holds for  $R_c(T_s)$ .

$$\text{Normalized error} = e_n = \frac{|v_{s+c} - v_s|}{v_a} = \frac{1}{\pi} \text{Arg} \left[ S e^{-2\pi^2 \left[ \frac{\sigma_s}{2v_a} \right]^2 + j\omega_s T_s} + C e^{-2\pi^2 \left[ \frac{\sigma_c}{2v_a} \right]^2 + j\omega_c T_s} \right] - \frac{v_s}{v_a} \quad (A.5)$$

$$\text{Let } \beta = \frac{S\rho_S}{C\rho_C} \text{ and } \rho_S = e^{-2\pi^2 \left[ \frac{\sigma_S}{2v_a} \right]^2} \quad \rho_C = e^{-2\pi^2 \left[ \frac{\sigma_C}{2v_a} \right]^2}$$

$$\text{then } e_n = \frac{1}{\pi} \text{Tan}^{-1} \left[ \frac{\beta \sin \omega_S T_S + \sin \omega_C T_S}{\beta \cos \omega_S T_S + \cos \omega_C T_S} \right] - \frac{v_S}{v_a} \quad (\text{A.6})$$

It can be shown that  $e_n$  is a function of  $|v_S - v_C|$ , i.e., the absolute value of  $v_S$  is of no consequence if  $|v_S - v_C|$  is a constant.

Now with  $v_S = \frac{\omega_S \lambda}{4\pi}$  and  $v_a = \frac{\lambda}{4T_S}$ ;  $\omega_S T_S = \frac{\pi v_S}{v_a}$  and  $v_d$  (velocity difference) =  $v_C - v_S$ .

$$e_n = \left| \frac{1}{\pi} \text{Tan}^{-1} \left[ \frac{\beta \sin \left( \frac{\pi v_d}{v_a} \right)}{\beta \cos \left( \frac{\pi v_d}{v_a} \right) + 1} \right] \right| \quad (\text{A.7})$$

Figure A.1 shows  $e_n$  for various power ratios. For typical clutter width of  $0.1 \text{ m}\cdot\text{s}^{-1}$  to  $0.5 \text{ m}\cdot\text{s}^{-1}$  and signal width of  $1$  to  $8 \text{ m}\cdot\text{s}^{-1}$ , the ratio  $\rho_S/\rho_C$  is less than  $1.3 \text{ dB}$  (Fig. A.2) which means that the performance of the pulse pair mean velocity (through  $\beta$ ) depends primarily on the S/C ratio. From Fig. A.1 we note that a signal  $10 \text{ dB}$  larger from clutter will suffer less than  $1 \text{ m}\cdot\text{s}^{-1}$  error in its velocity estimate. Thus, with no other suppression, a  $10 \text{ dB}$  margin of signal over clutter can be considered more than adequate for precise Doppler estimation via a pulse pair algorithm.

#### Spectrum width error

Formulas for the spectrum width when two narrow band Gaussian signal are superimposed can be found in Zrnic' (1979). The formula reads:

$$\sigma_b^2 = \frac{2v_a^2}{\pi^2} \cdot \ln \left\{ \frac{1 + R_C/S}{\left[ \rho_S^2 + 2\rho_S R_C \cos(\pi v/v_a)/S + R_C^2/S^2 \right]} \right\} \quad (\text{A.8})$$

where  $\sigma_b$  is the biased width,  $\bar{v}$  the mean velocity of weather signal and the other symbols are defined in the preceding section. The plot of this equation (Fig. A.3 and A.4) shows large biases for narrow widths, which are also strongly dependent on the signal's mean velocity. Doppler spectrum width of  $4 \text{ m}\cdot\text{s}^{-1}$  indicates moderate turbulence, thus if we want to be near or below that value for typical widths of  $1\text{-}3 \text{ m}\cdot\text{s}^{-1}$ , we need a margin of at least 15 dB between signal and clutter. Results of simulations on the same figures and also in Appendix C confirm the validity of these curves.

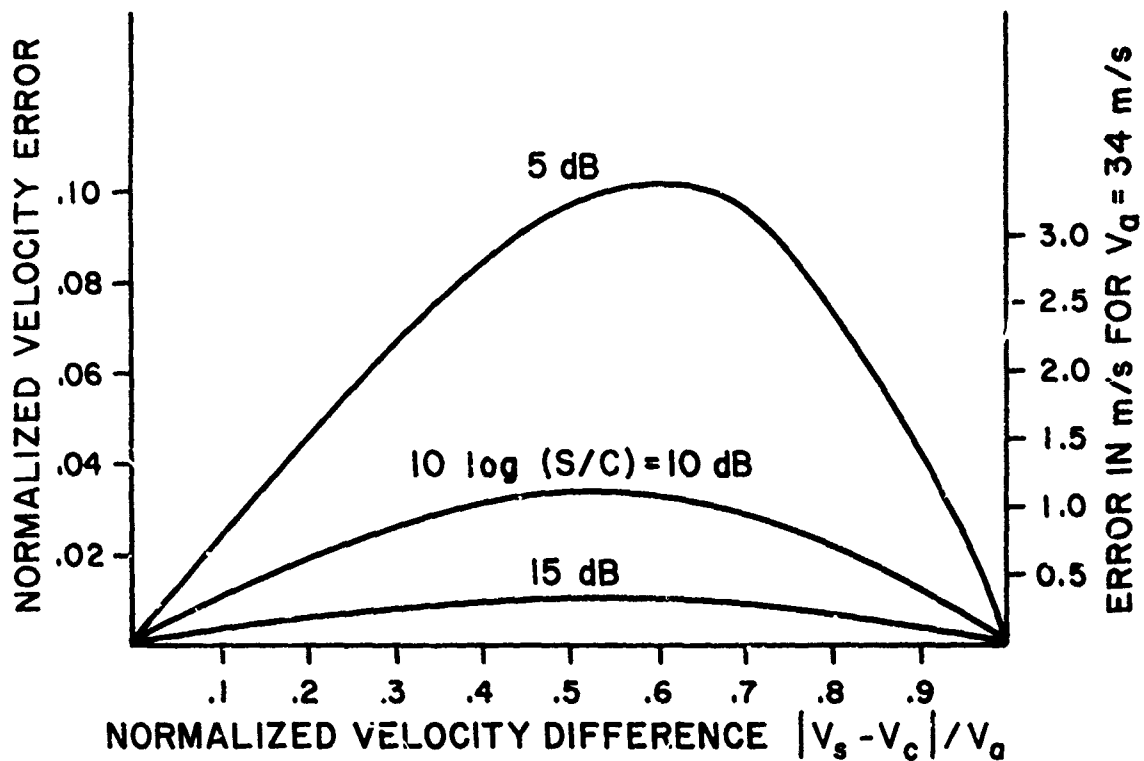


Figure A.1. Magnitude of the normalized velocity error versus the magnitude of the difference between the signal mean velocity and ground clutter mean velocity. For ground based radars  $v_c = 0$ . Signal to clutter power ratio is indicated, and the curves are strictly correct for  $\sigma_c < \sigma_v \ll v_a$ .

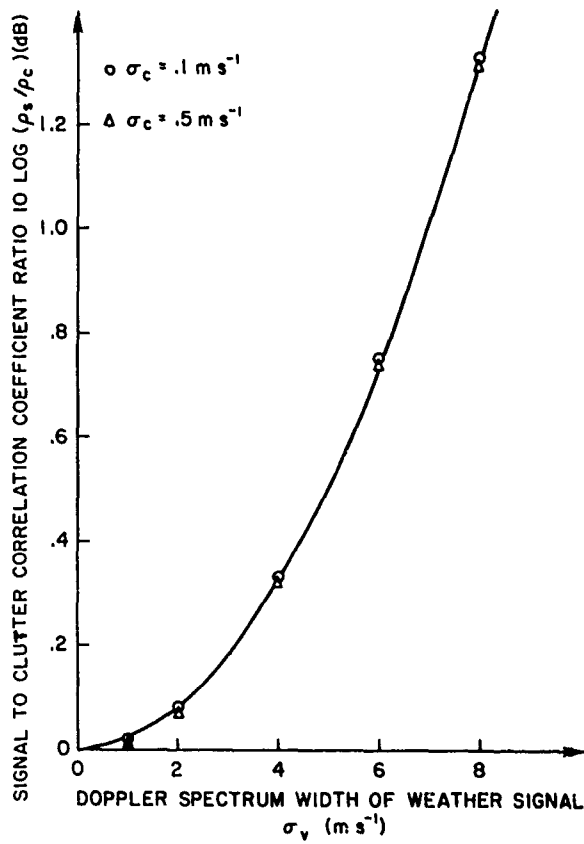


Figure A.2. The ratio of signal and clutter correlation coefficients for Gaussian shaped spectra. Clutter widths are indicated. Unambiguous velocity  $v_a \approx 32 \text{ m}\cdot\text{s}^{-1}$ .

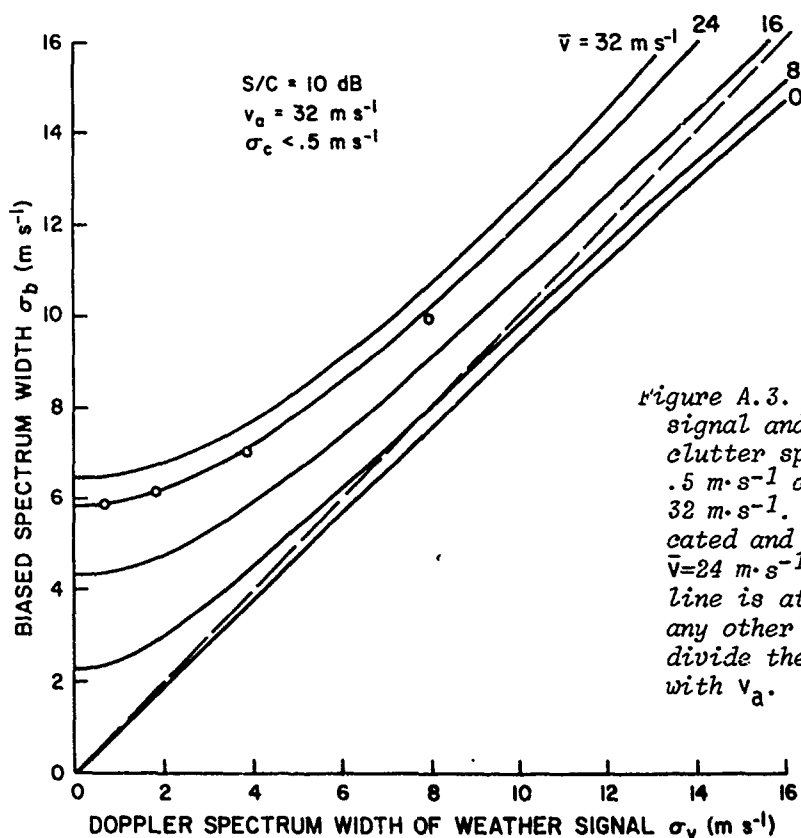


Figure A.3. Biased spectrum width when signal and clutter are present. The clutter spectrum width is less than  $.5 \text{ m}\cdot\text{s}^{-1}$  and unambiguous velocity is  $32 \text{ m}\cdot\text{s}^{-1}$ . Mean velocities are indicated and results of simulations for  $\bar{v}=24 \text{ m}\cdot\text{s}^{-1}$  are superimposed. Dashed line is at  $45^\circ$ . To obtain values for any other unambiguous velocity  $v_a$ , divide the scale by 32 and multiply with  $v_a$ .

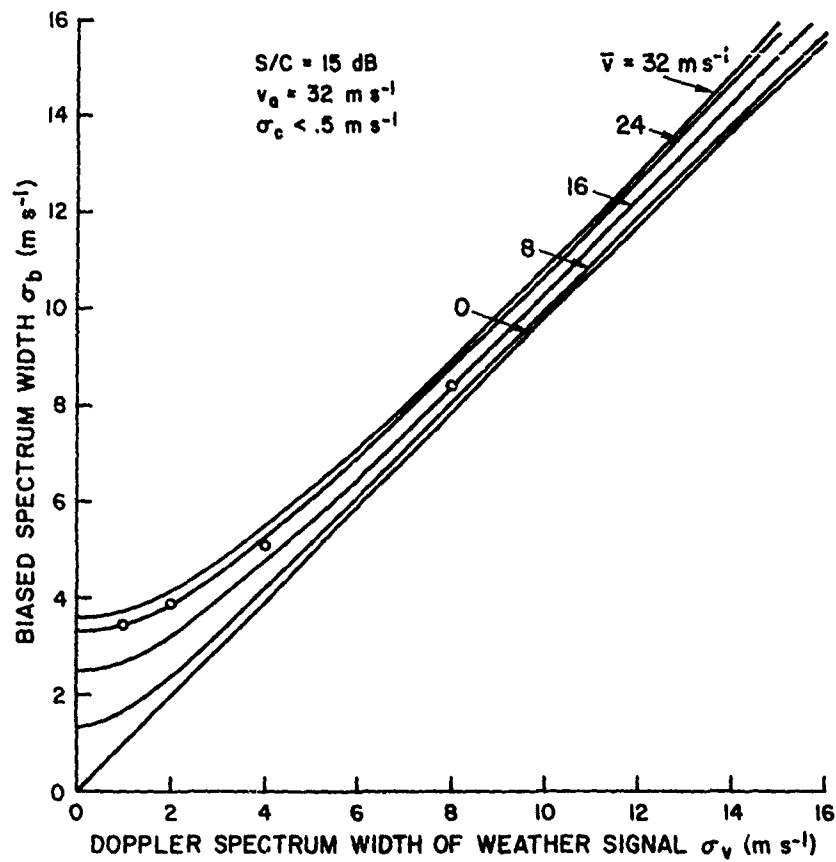


Figure A.4. Same as A.3 but  $S/C = 15 \text{ dB}$ .

## APPENDIX B

### Finite Impulse Response - FIR Filter

The objective is to estimate the number of sample points for a ground clutter filter with a 1 dB ripple in the passband and a stopband rejection of -50 dB (with respect to passband) for a desired set of passband and stopband cutoff frequencies. Figure B.1a shows the amplitude response of a typical FIR high pass filter with stopband cutoff radian frequency  $\omega_s$ ; passband cutoff frequency  $\omega_p$ ; passband deviation  $\delta_1$ ; and stopband deviation  $\delta_2$ . Figure B.1b shows the magnitude response described in terms of passband parameter  $\epsilon$  and stopband parameter A. Comparing Figs. B.1a and B.1b,  $\epsilon$  and A are related to  $\delta_1$  and  $\delta_2$  as

$$\frac{1}{\sqrt{1 + \epsilon^2}} = \frac{1 - \delta_1}{1 + \delta_1} \quad (\text{B.1})$$

$$\frac{1}{A} = \frac{\delta_2}{1 + \delta_1} \quad (\text{B.2})$$

where

$$10 \log \frac{1}{A^2} = -50 \text{ dB} \quad (\text{B.3})$$

$$10 \log \frac{1}{1 + \epsilon^2} = 1 \text{ dB} \quad (\text{B.4})$$

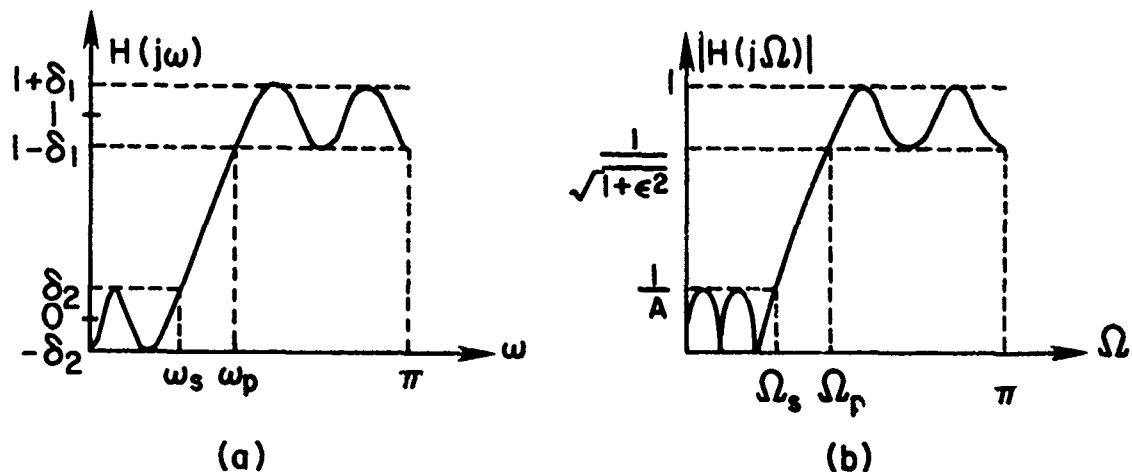


Figure B.1. Terminology used to describe high pass FIR characteristics.  
 a) Amplitude response, and b) Magnitude response.

$$\omega_s = \Omega_s \text{ and } \omega_p = \Omega_p \quad (\text{B.5})$$

To obtain the estimate of the value of M required to meet specifications on  $\delta_1$ ,  $\delta_2$ ,  $f_p$ , and  $f_s$ , the following equation can be used (Rabiner et al. 1974).

$$M = \frac{D_\infty(\delta_1, \delta_2)}{\Delta f} - f(\delta_1, \delta_2)(\Delta f)^2 + 1 \quad (\text{B.6})$$

where

$$D_\infty(\delta_1, \delta_2) = [5.309 \cdot 10^{-3} (\log_{10} \delta_1)^2 + 7.114 \cdot 10^{-2} \log_{10} \delta_1 - 4.761 \cdot 10^{-1}] \cdot \log_{10} \delta_2 - [2.66 \cdot 10^{-3} (\log_{10} \delta_1)^2 + 5.241 \cdot 10^{-1} \log_{10} \delta_1 + 4.278 \cdot 10^{-1}] \quad (\text{B.7a})$$

$$f(\delta_1, \delta_2) = 11.01217 + 0.51244 \log_{10} \delta_1 - 0.51244 \log_{10} \delta_2 \quad (\text{B.7b})$$

and the normalized transition width  $\Delta f$  is defined as

$$\Delta f = (f_p - f_s) T_s \quad (\text{B.7c})$$

Table B.1. The number of sample points needed for various passband and stopband cutoff frequencies,  $T_s^{-1} = 1302 \text{ Hz}$  ( $v_a = 32.5 \text{ m} \cdot \text{s}^{-1}$ ).

Stopband cutoff frequency		Passband cutoff frequency		Number of points M	
$v_s$	$f_s$	$v_p$	$f_p$	Rejection 50 dB	Rejection 30 dB
$\text{m} \cdot \text{s}^{-1}$	Hz	$\text{m} \cdot \text{s}^{-1}$	Hz		
.225	4.5	.8	16	197	126
.56	11.2	2	40	76	51
.85	17.0	3	60	51	35
1.13	22.6	4	80	39	26

Figure B.2 shows the number of sample points versus the notch width associated with the FIR filter where the width is defined as twice the passband cutoff velocity. From the figure it is clear that in order to achieve narrow widths, one needs to collect a lot of sample points ( $M > 125$ ), whereas for wider widths fewer samples are required ( $M < 75$ ). Therefore, for the actual design of the filter, specifications as well as the limitations on the data collection must be considered. Because the pulse repetition time for these calculations is  $768 \mu\text{s}$ , the dwell time to achieve a desired cutoff width can be calculated by multiplying  $M$  on Fig. B.2 with  $768 \mu\text{s}$ . This is shown on the auxiliary axis. It can be seen by evaluating (B.6) for this type of filter that:

$$M \approx D_{\infty} (\delta_1, \delta_2) / \Delta f \quad (\text{B.8})$$

or from (B.7c)  $MT_s \approx D_{\infty} (\delta_1, \delta_2) / (f_p - f_s)$

Thus it takes a minimum dwell time  $MT_s$  to achieve desired specifications.

Two hardware implementations of this filter are possible. In one filter weights are determined and a weighting average with these weights is computed, i.e.,:

$$y(k) = \sum_{n=k-M}^k w(n)x(k-n) \quad (\text{B.9})$$

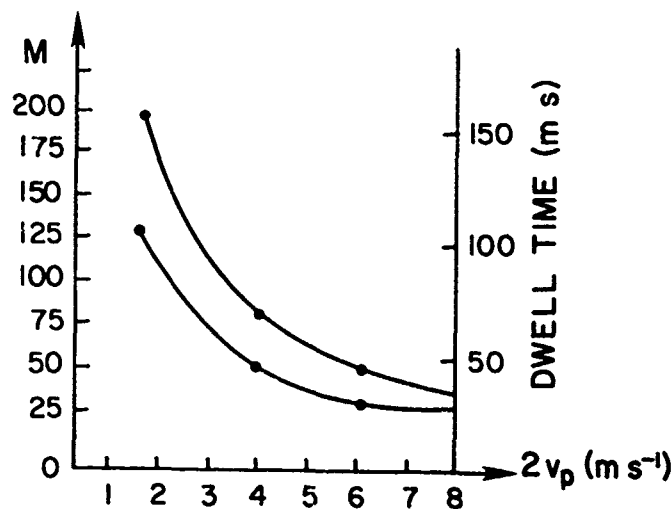


Figure B.2. Number of sample points  $M$  for various passband cutoff widths  $2 v_p$ . The upper curve is for 50 dB rejection while the lower one is for 30 dB.

where  $y(k)$  are filtered samples of the inphase or quadrature components  $x(k)$ , and  $w(n)$  are the weights. This realization requires  $2M$  contiguous input samples to produce  $M$  output samples without transients. Because of this long dwell time and due to large storage requirement, the scheme makes a poor candidate for interlaced processing.

If one accepts a Fourier Transform as a viable alternative to pulse pair processing, then the weights  $w(k)$  obtained for the FIR filter can be utilized as data window coefficient in which case the Fourier filter will have exactly the desired characteristic.

To illustrate the point, Hamming, von Hann, and rectangularly windowed time series data containing ground clutter were Fourier analyzed for antenna rotation rates of  $1^\circ\text{s}^{-1}$  and  $10^\circ\text{s}^{-1}$ . With a 32-point Fourier transform, the von Hann window offers 40 dB or more rejection if three spectral points (one either side of zero and zeroth) are eliminated (Fig. B.3). However, this type of filtering implies a notch of about  $4\text{ m}\cdot\text{s}^{-1}$ , which may still be acceptable. The notch decreases to about  $2\text{ m}\cdot\text{s}^{-1}$  when 64 pulses are utilized (Fig. B.4).

An important point that must be considered in using the weighted Fourier Transform for clutter rejection is the desirability to achieve perfect DC cancellation for all but a few spectral lines. This can be obtained only with some weighting functions (rectangular, von Hann, Hamming, see Figs. B.5 and B.6). In general, Fourier Transform of optimum weights will have nonzero lobes at the location of Fourier coefficients if these are equally spaced such as in the FFT. This implies that a pure DC line would spill into other coefficients when FFT is used to calculate the transform. A Discrete Fourier Transform (DFT) can be chosen such that the coefficients are in the zeroes of the lobes, but the computations are lengthy.

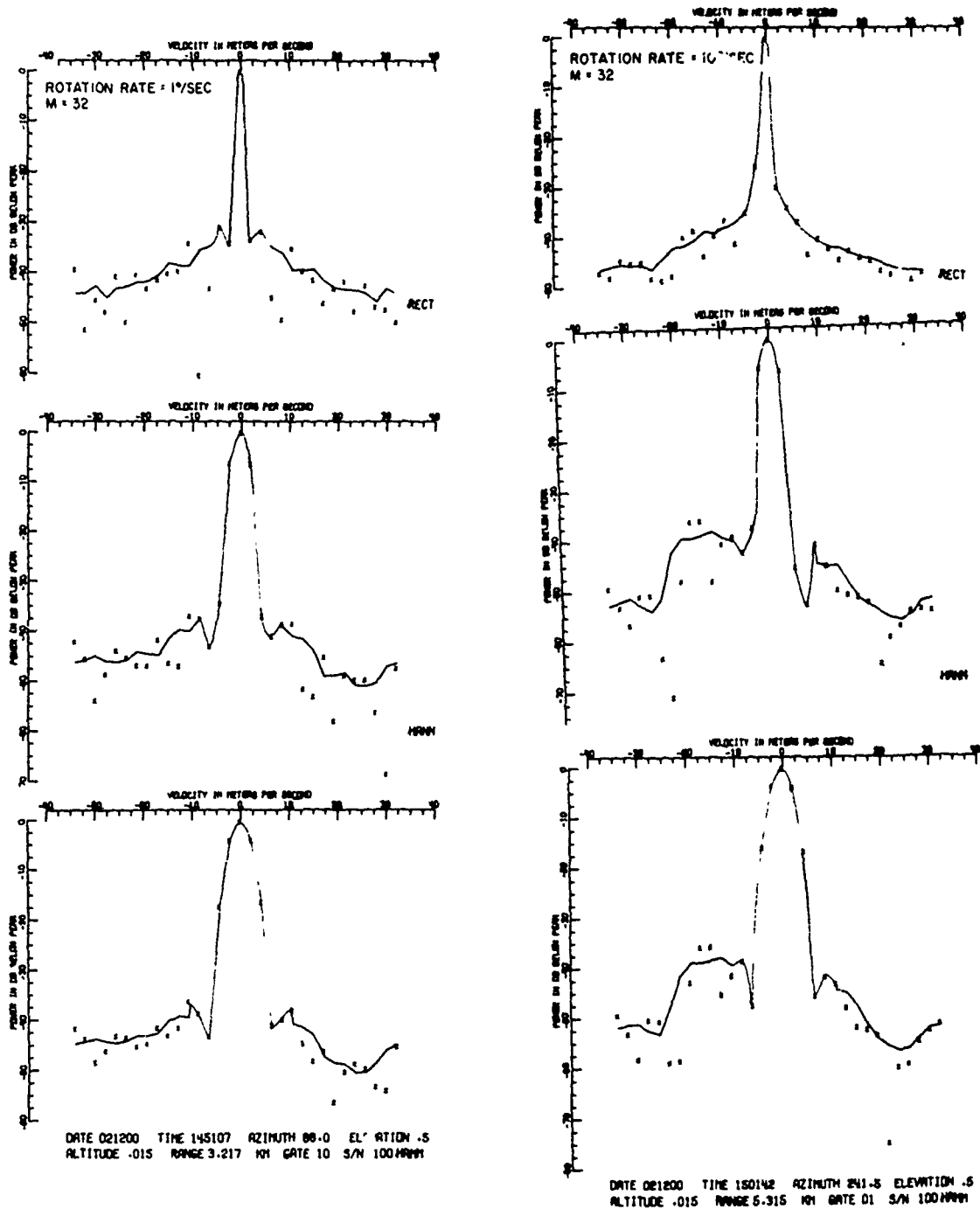
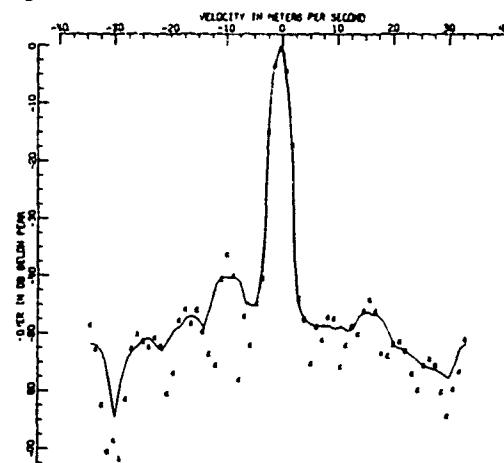
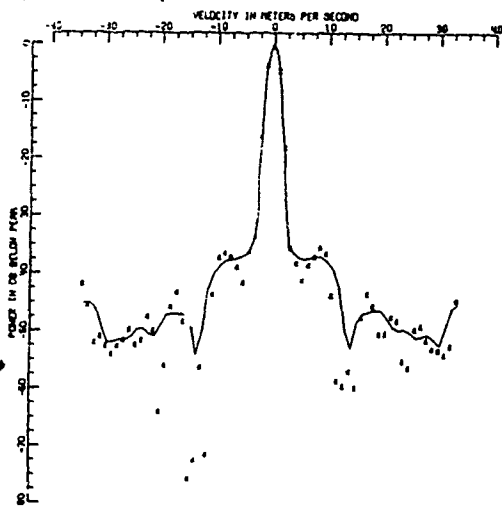
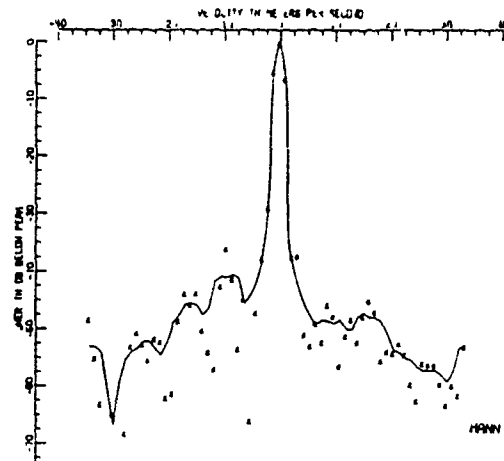
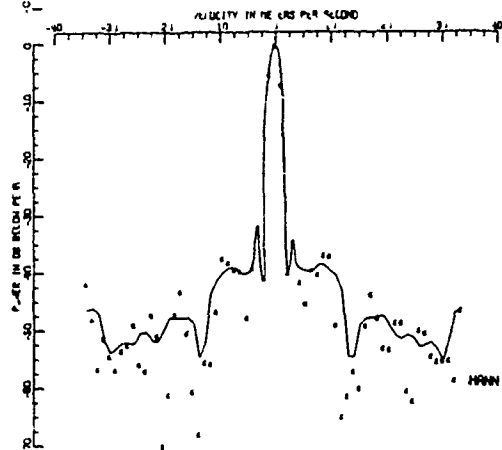
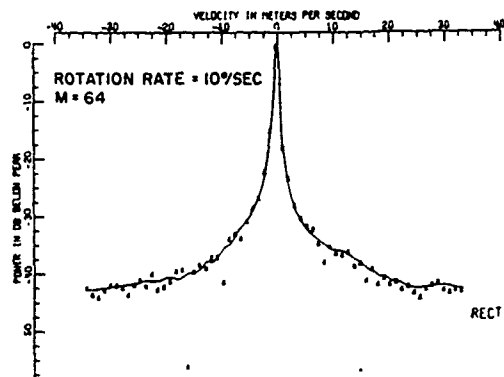
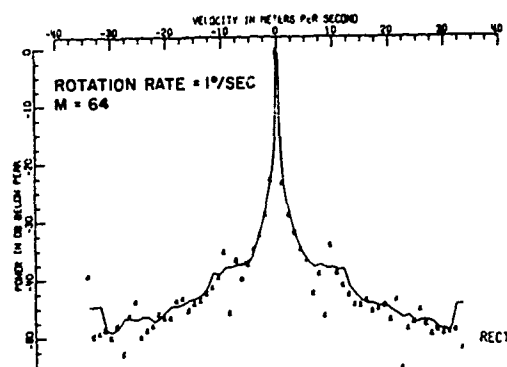


Figure B.3. Power spectra of ground clutter at antenna rotation rates of  $1^{\circ}\text{s}^{-1}$  (left graphs) and  $10^{\circ}\text{s}^{-1}$  (right graphs). Data windows applied to time series are indicated. Number of samples is 32. Solid curve connects the data points of the main peak (lobe) while in the noise it is a five point running average.



DATE 021210 TIME 145107 AZIMUTH 88.0 ELEVATION .5  
ALTITUDE .015 RANGE 3.217 CH GATE 10 S/N 100 HANN

DATE 021201 TIME 150142 AZIMUTH 241.5 ELEVATION .5  
ALTITUDE .015 RANGE 5.315 CH GATE 11 S/N 111 HANN

Figure B.4. Same as B.3 but the number of samples is 64.

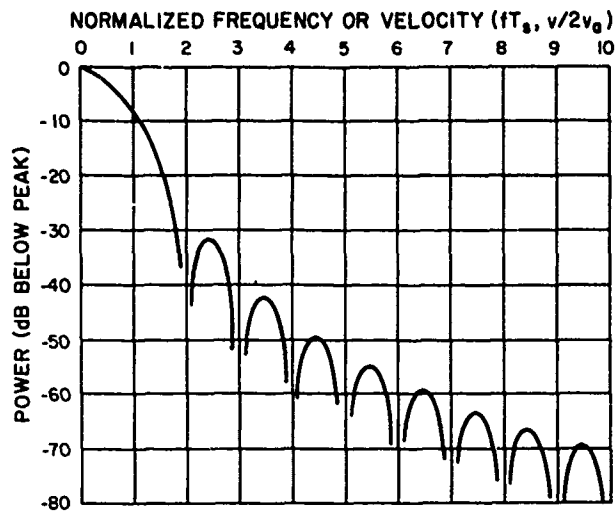


Figure B.5. Spectral window corresponding to the von Hann data window.

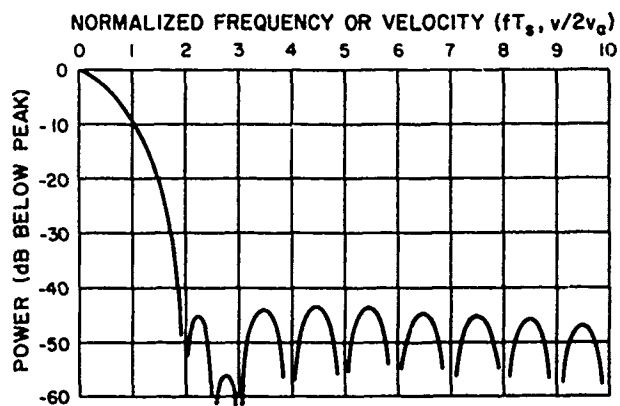


Figure B.6. Spectral window corresponding to Hamming data window.

## APPENDIX C

### Clutter Rejection in the Autocovariance Domain

The ground clutter echoes have generally narrow Gaussian shaped power spectrum and are nearly always centered on zero Doppler frequency. Therefore, it may be feasible to remove the clutter autocorrelation function from the real part of the composite autocorrelation prior to calculation of power, velocity, and spectrum width by pulse pair algorithm. We refer to this technique as the autocovariance technique for obtaining spectral moment estimates in the presence of ground clutter.

#### 1. Power Spectrum Estimation

The total echo power  $\hat{P}$  in the presence of clutter can be defined as

$$\hat{P} = \hat{S} + \hat{C} + \hat{N} = \frac{1}{M} \sum_{i=1}^M (I_i^2 + Q_i^2) \quad (C.1)$$

where  $I_i$  and  $Q_i$  are the quadrature video components.

It can be shown that for an assumed Gaussian spectrum, the clutter power estimate may be obtained from the equation

$$\hat{C} = \left[ \left( \frac{1}{M} \sum_{i=1}^M I_i \right)^2 + \left( \frac{1}{M} \sum_{i=1}^M Q_i \right)^2 \right] \sqrt{2\pi} \hat{w}_c MT_s \quad (C.2)$$

where  $\hat{w}_c$  is the clutter spectrum width estimate in (Hz) as opposed to ( $m \cdot s^{-1}$ ),  $M$  is the number of sample points;  $T_s$  is the time lag, and terms in parenthesis are the DC values squared. To estimate  $w_c$ , we may use the known antenna rotation rate and equation (1.6). Equation (C.1) was programmed using simulated data and estimates of logarithmic signal power ( $\log \hat{S}$ ) for different clutter to signal ratios (C/S) are plotted on Fig. C.1. In these, simulations in lieu of an estimated  $w_c$ , a true input clutter spectrum width, was used. At C/S = 0 dB and no filtering, a bias error of 3 dB in the power estimate is obtained because the power is a sum of clutter and signal power. However, with the partial compensation via the autocovariance technique (C.1) this bias is reduced to 2 dB. This is not a significant reduction and thus the technique cannot be recommended for power estimation in presence of ground clutter.

#### 2. Mean Velocity Estimation

The total autocovariance estimate  $\hat{R}_t(T_s)$  for a signal and clutter that are not correlated is the sum of the individual autocovariances:

$$\hat{R}_t(T_s) = \hat{R}_s(T_s) + \hat{R}_c(T_s) \quad (C.3)$$

where  $\hat{R}_s(T_s)$  and  $\hat{R}_c(T_s)$  are the estimated signal and clutter autocovariances.

The pulse pair velocity estimate in the presence of the clutter is defined as

$$\hat{v} = \frac{\lambda}{4\pi T_s} \arg \left\{ \frac{\text{Im}[\hat{R}_s(T_s)]}{\text{Re}[\hat{R}_s(T_s)]} \right\} \quad (\text{C.4})$$

where

$$\text{Im}[\hat{R}_s(T_s)] = \text{Im}[\hat{R}_t(T_s)] - \text{Im}[\hat{R}_c(T_s)] \quad (\text{C.5})$$

Since the mean of  $\hat{R}_c(T_s)$  is real, the following relationships hold between the mean or true values:

$$\text{Im}[R_s(T_s)] = \text{Im}[R_t(T_s)] \quad (\text{C.6})$$

and

$$\text{Re}[R_s(T_s)] = \text{Re}[R_t(T_s)] - \text{Re}[R_c(T_s)] \quad (\text{C.7})$$

These equalities are assumed to hold also for the respective estimates.

The real and imaginary part of the total estimated autocovariance,  $\hat{R}_t(T_s)$ , can be represented in terms of the inphase and quadrature components as

$$\text{Re}[\hat{R}_t(T_s)] = \frac{1}{M} \sum_{i=1}^M (I_{i+1} I_i + Q_{i+1} Q_i) \quad (\text{C.8})$$

$$\text{Im}[\hat{R}_t(T_s)] = \frac{1}{M} \sum_{i=1}^M (Q_{i+1} I_i - I_{i+1} Q_i)$$

The autocovariance estimate for Gaussian shaped ground clutter,  $\hat{R}_c(T_s)$ , is

$$\hat{R}_c(T_s) = \hat{c} e^{-\pi^2 \hat{\sigma}_c^2 / 2v_a^2} \quad (\text{C.9})$$

where,  $\hat{\sigma}_c$  is the clutter spectrum width estimate, ( $\text{m}\cdot\text{s}^{-1}$ ). Thus, equation (C.4) in terms of the estimated velocity becomes:

$$\hat{v} = \frac{\lambda}{4\pi T_s} \arg \left\{ \frac{\text{Im}[\hat{R}_t(T_s)]}{\text{Re}[\hat{R}_t(T_s)] - \hat{c} e^{-\pi^2 \sigma_c^2 / 2v_a^2}} \right\} \quad (\text{C.10})$$

The above equation was tested on simulated data and estimates of velocity for different ground clutter to signal ratios C/S are plotted on Fig. C.2.

When C/S = 0 dB,  $\sigma_c = 0.2 \text{ m}\cdot\text{s}^{-1}$ , and  $1.0 \text{ m}\cdot\text{s}^{-1} < \sigma_v < 8.0 \text{ m}\cdot\text{s}^{-1}$ , the bias of the mean velocity estimate decreases by 33 percent which translates to an effective S/C improvement of about 3-5 dB. For C/S = 10, 20, and 30 dB, a heavily biased estimate of the mean velocity is obtained which indicates that the autocovariance technique does not really perform well when C/S > 0 dB. Estimated mean velocities for  $\sigma_c = .1 \text{ m}\cdot\text{s}^{-1}$  and  $\sigma_c = .3 \text{ m}\cdot\text{s}^{-1}$  were also obtained. The results are similar to the ones when  $\sigma_c = 0.2 \text{ m}\cdot\text{s}^{-1}$  and thus are not presented here. The algorithm did poorly for the clutter width values  $\sigma_c = 0.3 \text{ m}\cdot\text{s}^{-1}$ . Note that the pulse pair processor generates unbiased mean velocity estimates (if no filtering is done) only for C/S < -10 dB in agreement with theoretical predictions of Appendix A.

### 3. Spectrum Width Estimation

For Gaussian spectra, the spectrum width estimate in the presence of ground clutter is defined as

$$\hat{\sigma}_v = \frac{1}{\sqrt{2} \pi T_s} \left[ \ln \left| \frac{\hat{S}}{|\hat{R}_s(T_s)|} \right| \right]^{1/2} \left[ \text{sgn} \left[ \ln \frac{\hat{S}}{|\hat{R}_s(T_s)|} \right] \right] \quad (\text{C.11})$$

where  $\hat{S}$  is the signal power as defined in equation (C.1) and  $|\hat{R}_s(T_s)|$  is defined with (C.6) and (C.7). Using equations (C.8) and (C.9)  $|\hat{R}_s(T_s)|$  can be represented in discrete form as

$$|\hat{R}_s(T_s)| = \left\{ \left[ \frac{1}{M} \sum_{i=1}^M (I_{i+1} I_i + Q_{i+1} Q_i) - \hat{c} e^{-\pi^2 \sigma_c^2 / 2v_a^2} \right]^2 + \left[ \frac{1}{M} \sum_{i=1}^M (Q_{i+1} I_i - I_{i+1} Q_i) \right]^2 \right\}^{1/2} \quad (\text{C.12})$$

Simulated data were run through the estimator for different ground clutter to signal ratios (C/S). Figure (C.3) shows the plot of estimated mean width versus true mean width without filtering and for the autocovariance filtering.

Comparison of the two cases for a C/S = 0 dB reveals that the bias of the spectrum width estimate decreases by about 50 percent when the autocovariance

technique is used. But even then the bias is significant and what's more it does depend on both the mean velocity and clutter to signal ratio. This means the technique is unacceptable for spectrum width estimation. Moreover, we see that accurate estimation of spectrum widths with the pulse pair technique requires larger S/C ratio (15 dB) than the mean velocity estimation (10 dB) in agreement with results of Appendix A. Clutter width values larger than  $0.3 \text{ m}\cdot\text{s}^{-1}$  were also tried but the algorithm failed likewise.

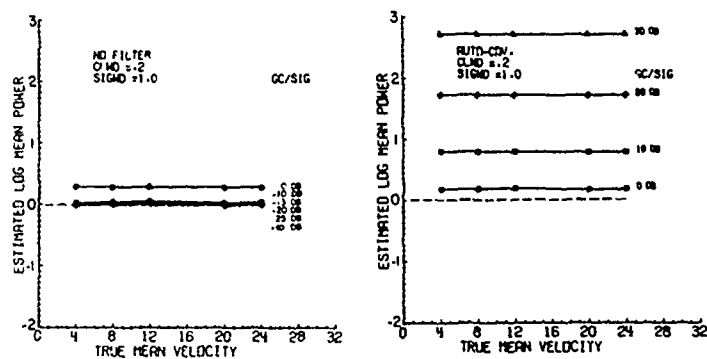


Figure C.1. Logarithm of estimated mean power versus true mean velocity for no filtering (left figure) and autocovariance technique (right figure). Clutter spectrum width  $CLWD$  of  $.2 \text{ m}\cdot\text{s}^{-1}$  is indicated, and so is signal width  $SIGWD = 1.0 \text{ m}\cdot\text{s}^{-1}$ . Clutter to signal ratios range from 0 to  $-\infty$  dB in the no filter graph and 0 to 30 dB in the autocovariance graph.

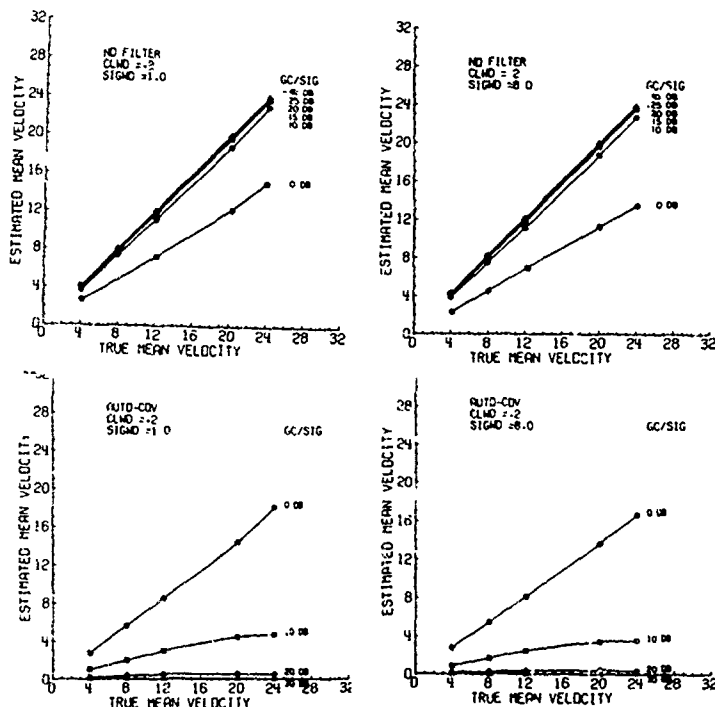


Figure C.2 Plot of estimated mean velocity versus true mean velocity for no filtering (upper graphs) and autocovariance technique (lower graphs).

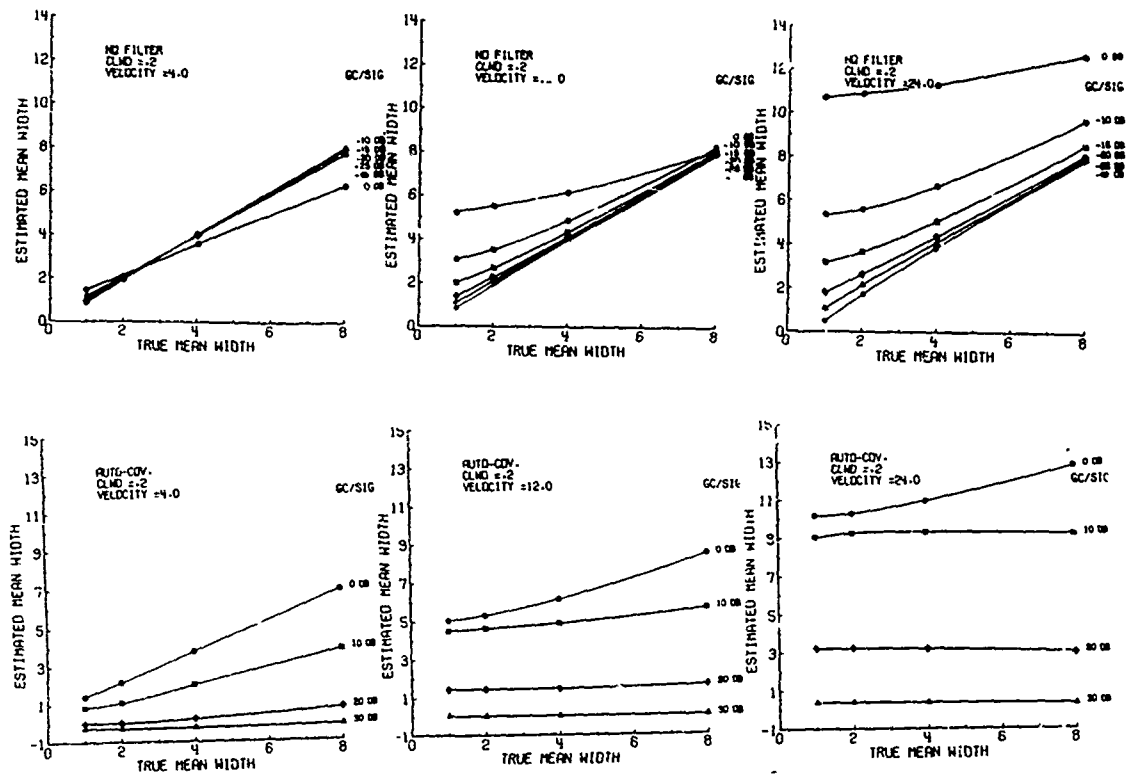


Figure C.3 Plot of estimated mean width versus true mean width with no filtering (top graphs) and with autocovariance filtering (bottom graphs). Mean velocities of the signal spectrum (4, 12, and 24  $\text{m}\cdot\text{s}^{-1}$ ) as well as the clutter to signal ratios are indicated. Note that C/S ratios are less than 0 dB for no filtering and are larger than 0 dB for autocovariance filtering.

In summary, simply removing the ground clutter from the composite autocovariance improves very little the estimates of reflectivity, mean velocity and Doppler spectrum width. The improvement is equivalent to about 3-5 dB increase in signal to clutter power ratios. Therefore, this technique is not suitable for Doppler weather radars.

## APPENDIX D

### Antenna Speed, Apparent Pattern, and Dwell Time

We have examined the various rotational rates that could apply to a radar such as the NSSL Doppler. The philosophy of design and curves depicting the errors are listed.

Let's start with the beamwidth,  $\theta_1 = .8^\circ$  which is the beamwidth of NSSL Doppler radars. Now if we agree that the resolution should not be less than  $1.2^\circ$  (i.e., 50 percent worse than beamwidth), we can find the relationship between the antenna rotation  $\alpha$ , dwell time  $MT_s$ , and apparent beamwidth  $\phi_a$ . From Fig. D.1 (Zrnic' and Doviak, 1976) we see that

$$\phi_a/\theta_1 = 1.5 \quad (D.1a)$$

$$\alpha MT_s/\theta_1 = 1. \quad (D.1b)$$

Thus, Eq. D.1b is basic as it ties the rotation rate and dwell time to the beamwidth. As illustration, consider the following three rotation rates:  $18^\circ/s$  (3 rpm),  $36^\circ/s$ , and  $54^\circ/s$ .

#### 1. Velocity Estimation

On Fig. D.2a and b are plotted the standard deviation of velocity estimates for a radar transmitting contiguous pulses with parameters as at NSSL. Auto-covariance processing is assumed.

We note from Fig. D.2b that at 9 rpm  $\sigma_v$ 's up to  $5.25 \text{ m}\cdot\text{s}^{-1}$  produce errors less than  $2 \text{ m}\cdot\text{s}^{-1}$ . This indicates that there is no need for exotic improvements in the signal design and processing algorithms for mean velocity estimation.

#### 2. Reflectivity Estimation

This subject has been treated intensely in the literature and suffices to state here that the number of independent samples for large M is (Zrnic' 1979):

$$M_I = M 2\pi^{5/2} \sigma_v T_s / (\lambda \cdot 3 \cdot 1.34) \quad (D.2)$$

Let  $T_s = 768 \mu\text{s}$ ,  $\lambda = .1\text{m}$  and examine the case of  $M=57$  (i.e., rotation rate equals  $18^\circ/s$ ). Substitution of those values into (D.2) gives:

$$M_I = M \sigma_v \cdot 6.7 \cdot 10^{-2} = \sigma_v \cdot 3.8 \quad (D.3)$$

Then the SD of reflectivity Z is:

$$\text{SD}(Z) = 5.57/\sqrt{(\sigma_v \cdot 3.8)} \text{ dB} \quad (D.4)$$

Take  $\sigma_v = 1 \text{ m}\cdot\text{s}^{-1}$  as the smallest width and we get  $\text{SD}(Z) \approx 2.86 \text{ dB}$ . This value can be further reduced by averaging in range. For instance, if 6 samples are averaged, we obtain

$$\text{SD}_6(Z) = 2.86/\sqrt{6} = 1.16 \text{ dB} \quad (\text{D.5})$$

In order to have the SD below 1 dB, one must average about 8 samples in range. This illustrates that the reflectivity estimation imposes a more stringent requirement to the number of samples and rotation rate than the velocity estimation!

### 3. Spectrum Width Estimation

Conclusions concerning spectrum width are compatible with the ones concerning the mean velocity. Figures D.2c and d illustrate the standard deviations for two different SNR's. Therefore, a 3 rpm or even higher rotation rate can be achieved with little degradation in the estimates and with simple contiguous processing of samples.

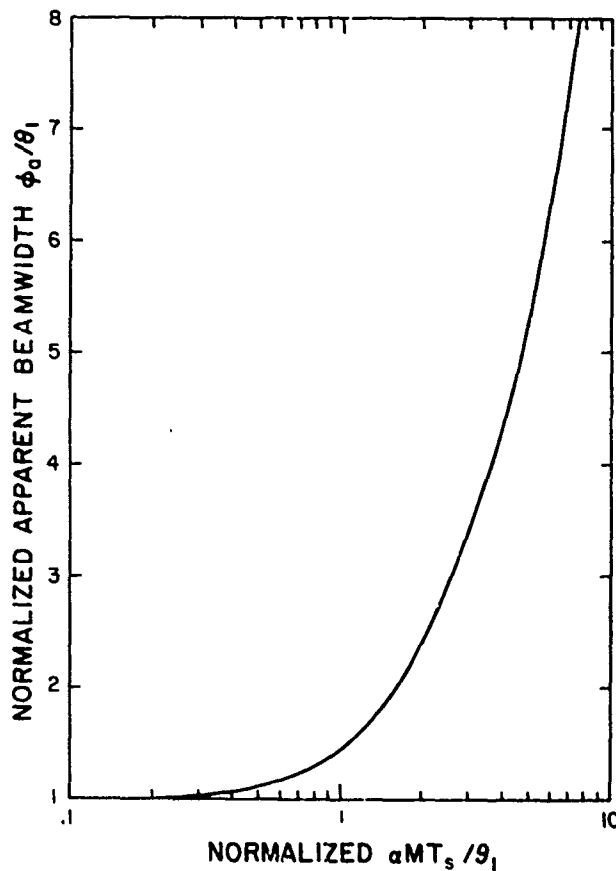


Figure D.1 Apparent beamwidth normalized to the 3 dB beamwidth versus the normalized rotation rate ( $\alpha M T_s / \theta_1$ ). A 50 percent increase of the apparent beamwidth with respect to the 3 dB beamwidth occurs at  $\alpha M T_s / \theta_1 = 1$ .

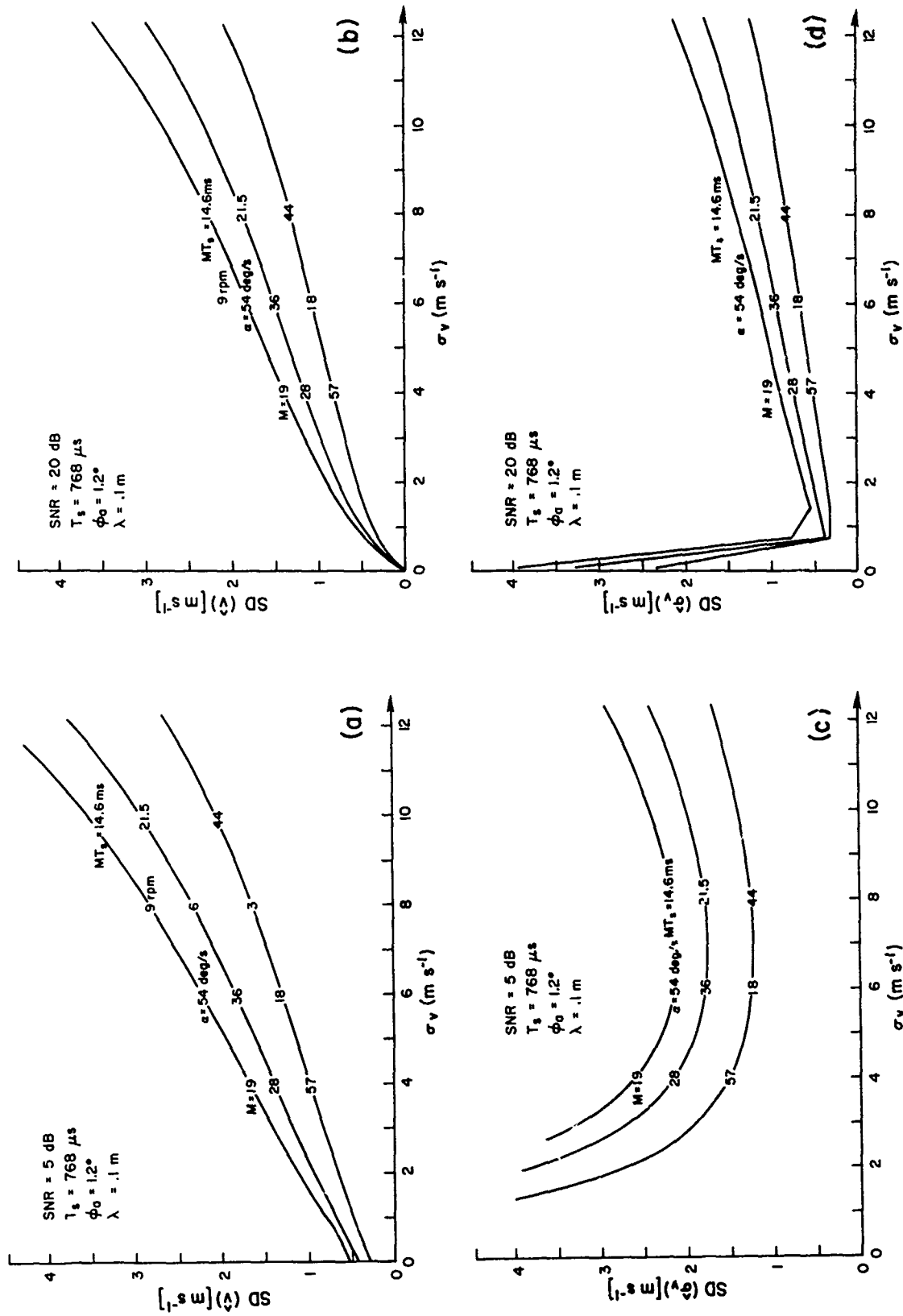


Figure D.2 a) Standard deviation of pulse pair derived mean velocity estimates. Antenna 3 dB beamwidth  $\theta_1$  is .80 and rotation rates and number of samples needed to achieve constant apparent beamwidth of  $\phi_a = 1.2^\circ$  are indicated. Signal to noise ratio is 5 dB. b) Same as a) except SNR is 20 dB. c) Standard deviation of pulse pair derived Doppler spectrum width. Other parameters are as in a). d) Same as c) but the SNR is 20 dB.

## APPENDIX E

### Program Flow Charts

This Appendix contains flow charts of various programs that were used throughout this study. The most important subroutines are described in the few paragraphs that follow:

ESTPP	This subroutine calculates the signal power, velocity, and spectrum width using pulse-pair algorithm.
ESTCOV	Signal power, velocity, and spectrum width are calculated using autocovariance techniques (outlined in Appendix C).
IQREAD	This subroutine combines the 51 blocks (each containing 5120 bytes, 4096 samples for the 16 gates) into one 262,190 bytes block.
IQDECODE	I and Q time series data for each gate are obtained from the 262,190 bytes, i.e., 4096 sample points.
ELLIPSE	Third order elliptic filter.
AGC	Every 64 sample points are successively multiplied and divided by two.
TIMDOP	It generates simulated I and Q time series data with a specified mean velocity, CNR, SNR, $\sigma_c$ and $\sigma_v$ .
DPVLWD	From the input I and Q time series data it computes the power, velocity, and spectrum width using pulse-pair algorithm and FFT.
DPDSPY	Prints the weather signal power spectrum on the printer from the I and Q time series data.
SHIFTIQ	It eliminates specified number of time series data points from the beginning of the series after filtering in order to reduce the transient effects.
WINDOW	The I and Q time series data are weighted with the von Hann (raised cosine) or Hamming window.
SMOOTH	The first forty points of the simulated I and Q time series data are smoothed with the raised cosine before the entire 8192 sample points are run through the filter.
IQPLOT	Plots I and Q time series data on the printer.

START

```
REAL AVS(5),ASIGWID(4),AGCNR(4),AGCN(3),ZIQ(2,8192)
NAVG = 70          MSAM = 128          SNR = 20
```

```
DO IGCW = 1,3
  DO IVS = 1,5
    DO ISIGWID = 1,4
      DO IGCNR = 1,4
```

```
N1 = 8192
CALL TIMDOP(ZIQ,N1,VS,SIGWID,SNR,NORMAL,GCNR,GCWID)
I = 1
CALL SMOOTH(ZIQ(1,I),8192,40)
CALL ELLIPSE(IFILTER,ZIQ(1,I),8192)
CALL SHIFTIQ(ZIQ(1,I),ZIQ(1,I),8064,128)
```

```
DO IIV = 1,NAVG
CALL ESTPP(ZIQ(1,I),64,PARAM(1),PARAM(2),PARAM(3),GCWID,SNR)
I = I + MSAM
```

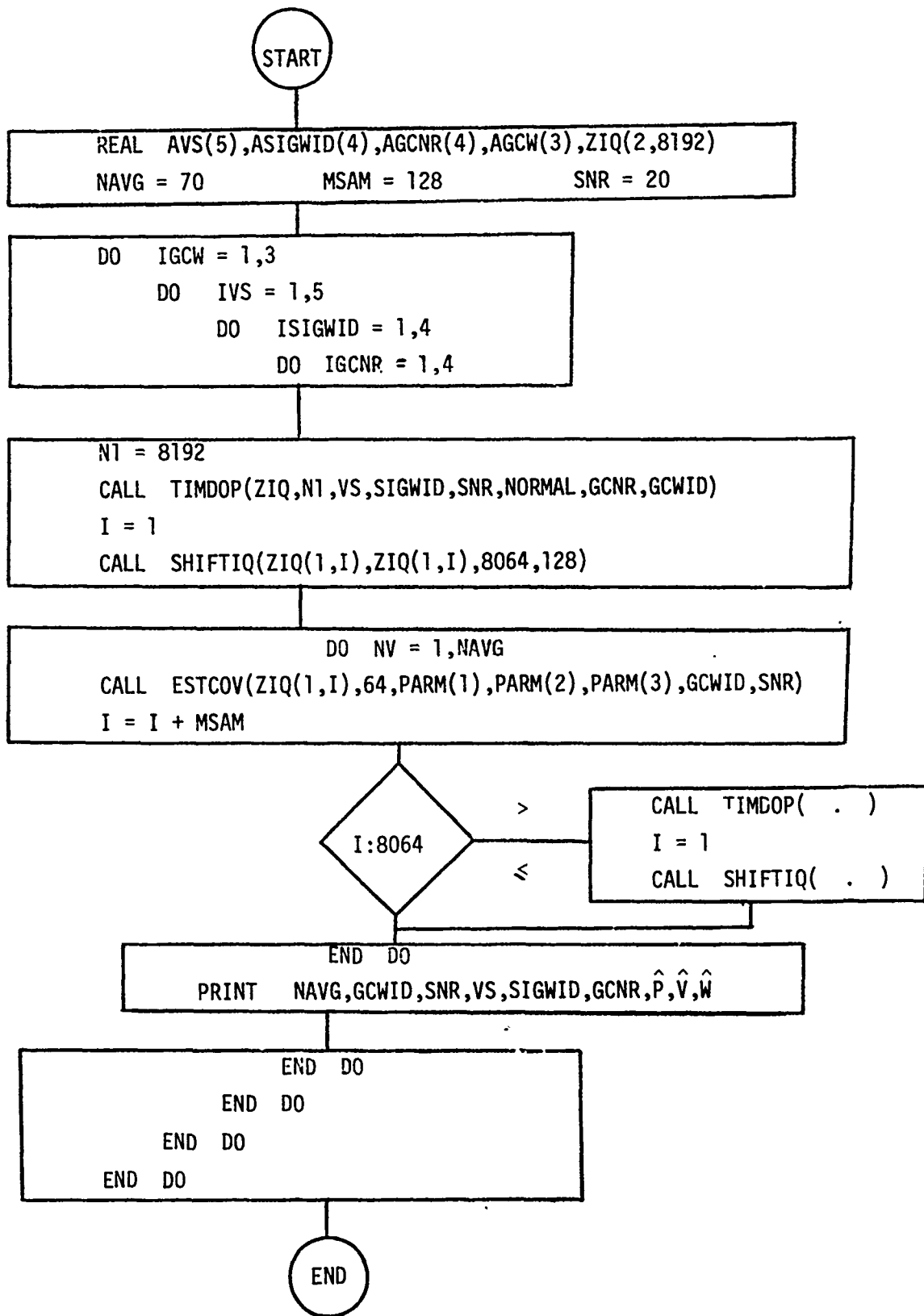
I:8064

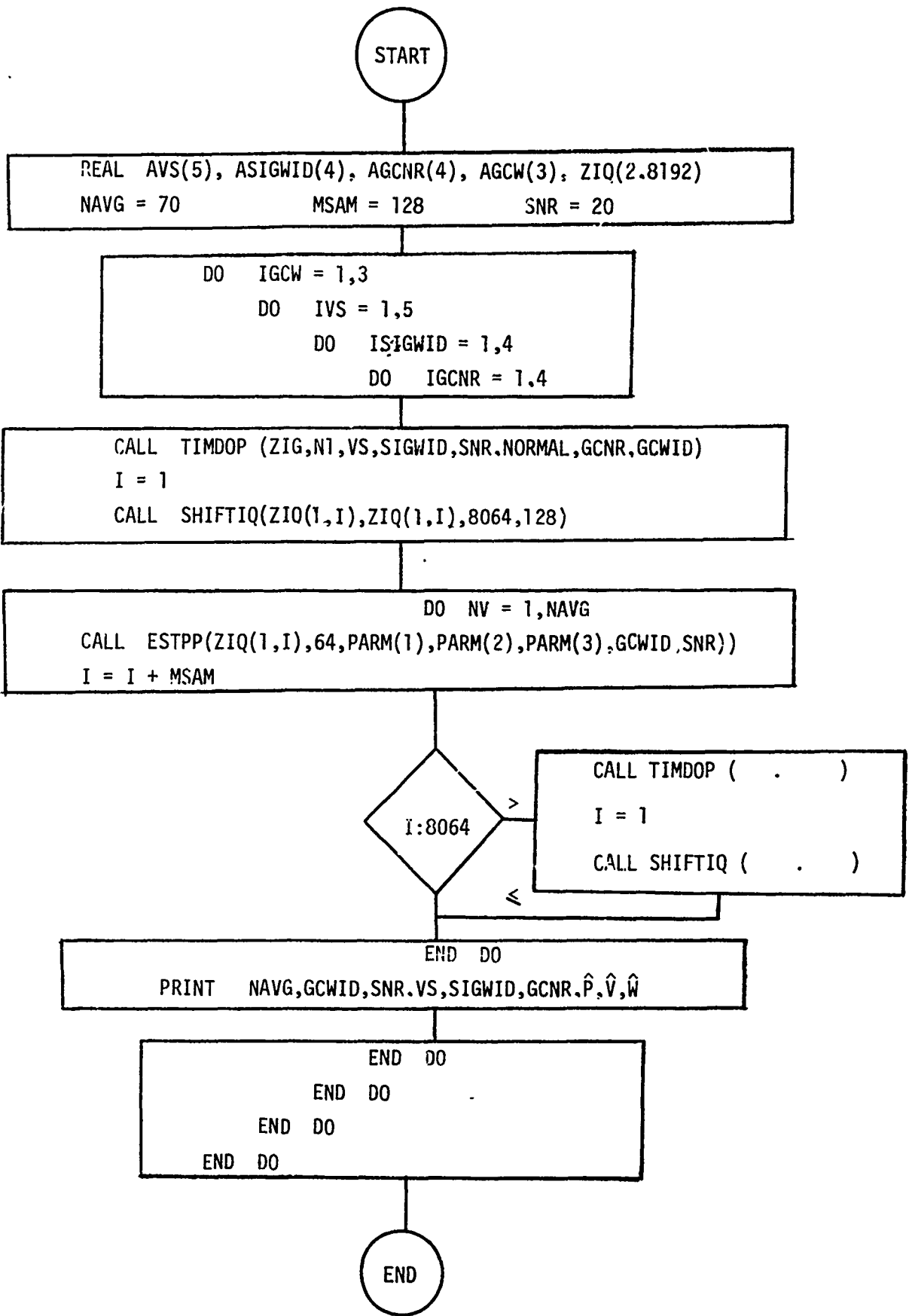
```
> CALL TIMDOP( . )
I = 1
CALL SMOOTH( . )
CALL ELLIPSE( . )
CALL SHIFTIQ( . )
```

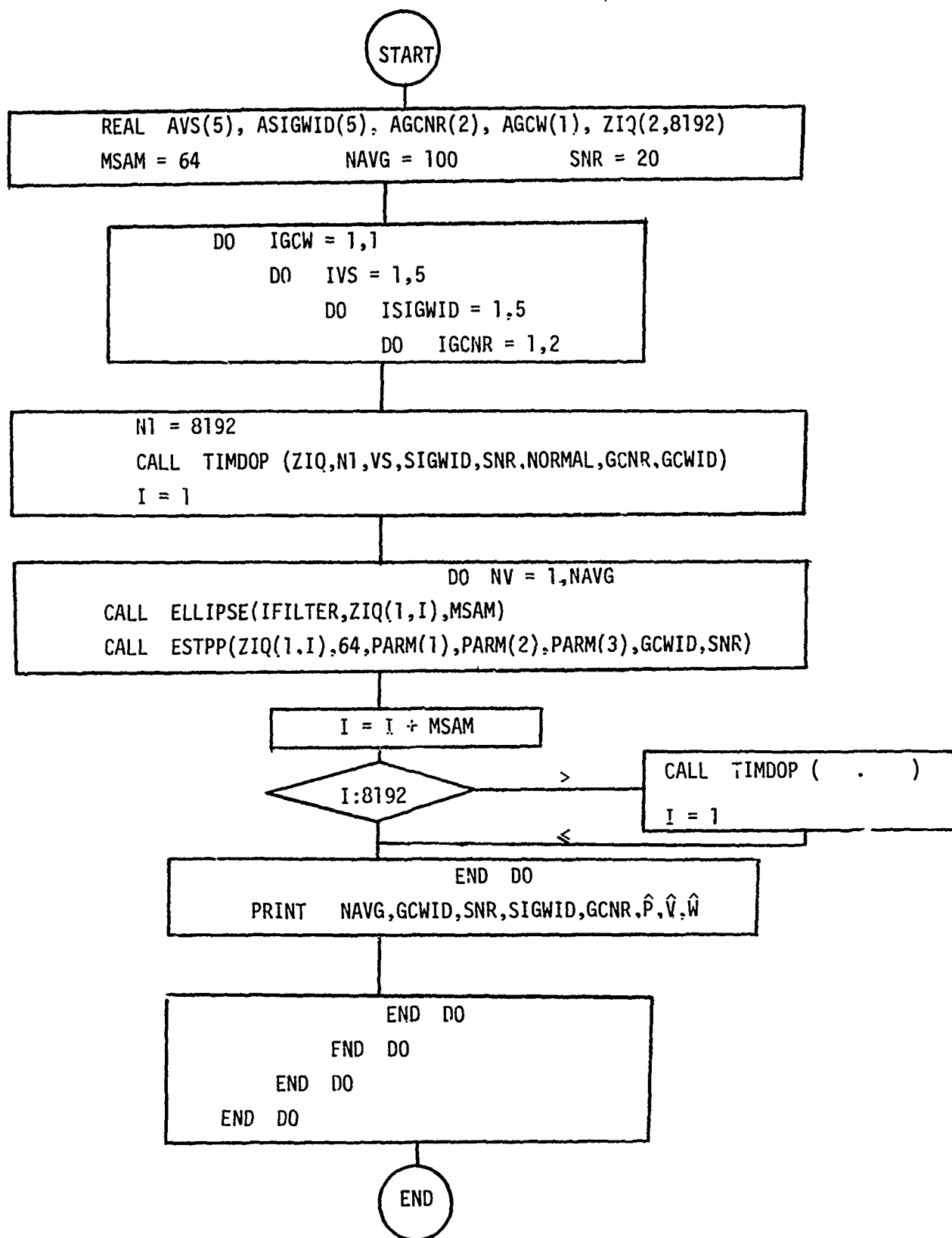
```
END DO
PRINT NAVG,GCWID,SNR,VS,SIGWID,GCNR, $\hat{P}$ , $\hat{V}$ , $\hat{W}$ ,
```

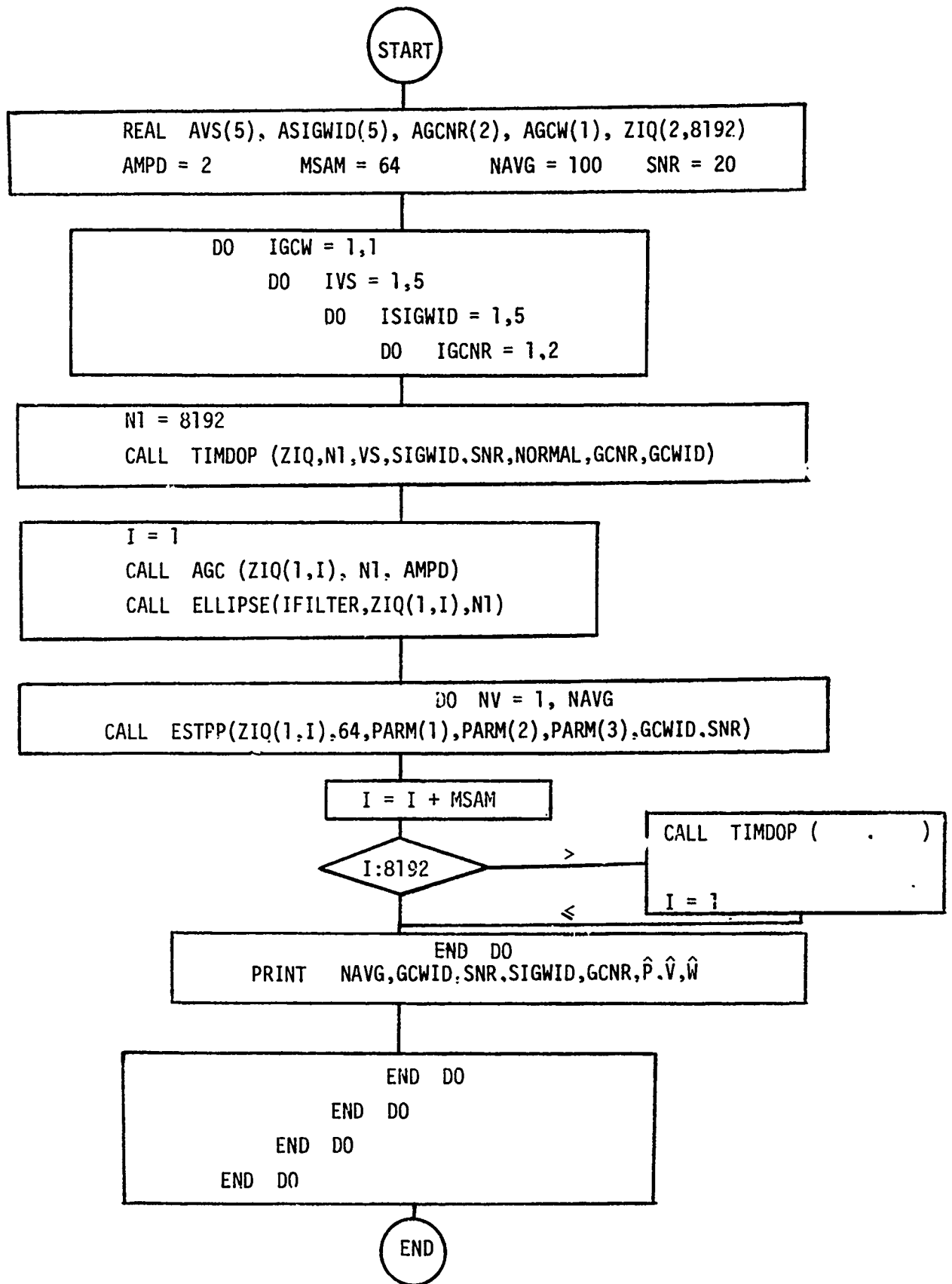
```
END DO
END DO
END DO
END DO
```

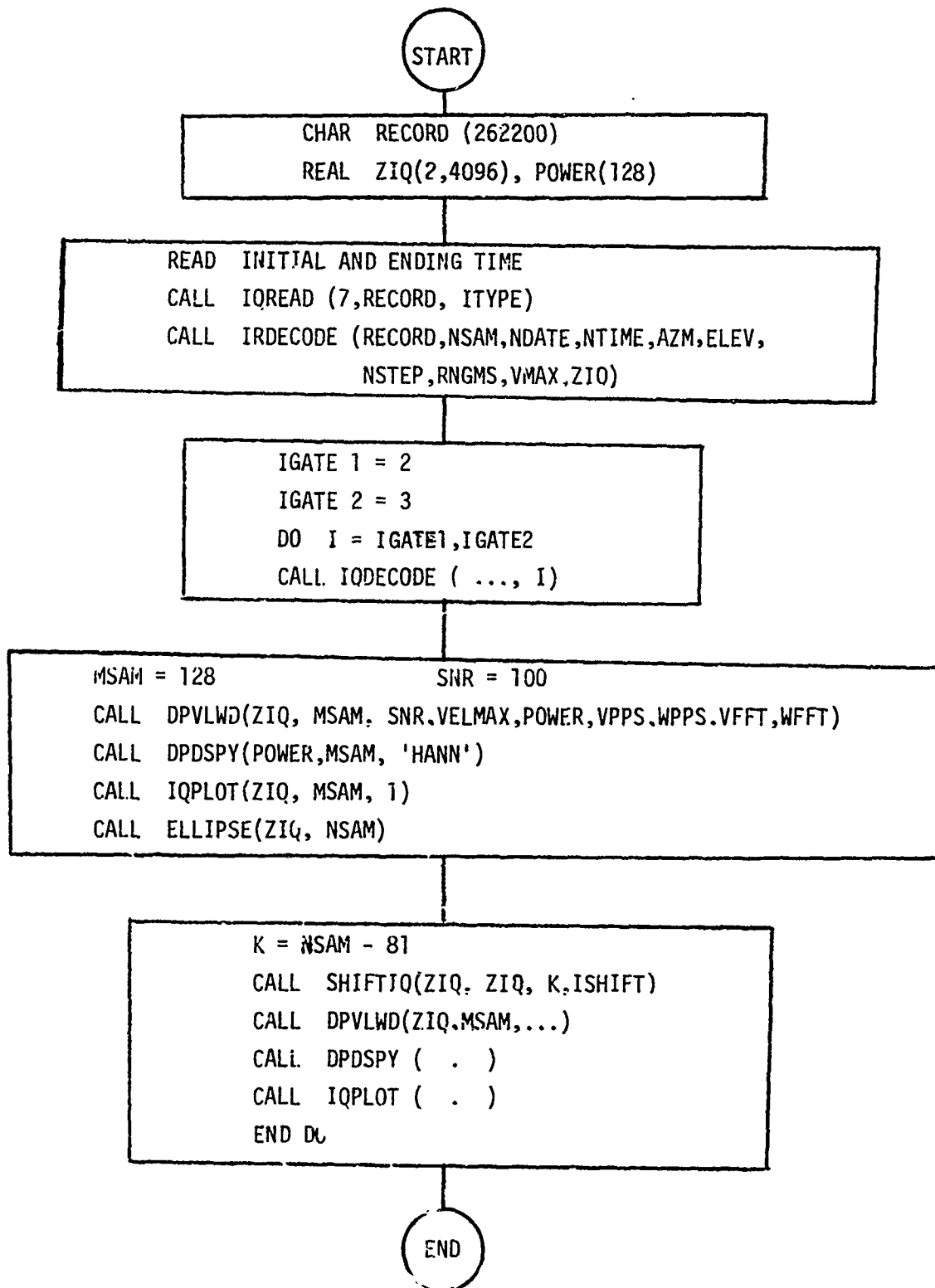
END











START

```
REAL ZIQ(2,256), XIQ(2,128)
200 READ IBTM, IETM, DELAY1, DELAY2
```

```
IGATE 1 = 2
IGATE 2 = 3
DO 300 I = IGATE1, IGATE2
MSAM = 128          SNR = 100
```

```
CALL MOVEARRY(ZIQ, XIQ, MSAM)
A = B = 0.5
CALL WINDOW(ZIQ, MSAM, A, B)
CALL DPVLWD(ZIQ, MSAM, SNR, VELMAX, POWER, VPPS, WPPS, VFFT, WFFT)
CALL DPDSY(PPOWER, MSAM, 'HANN')
CALL IQPLOT(ZIQ, MSAM, 1)
```

```
CALL MOVEARRY(XIQ, ZIQ, MSAM)
CALL SMOOTH(ZIQ, MSAM, 40)
CALL ELLIPSE(ZIQ, MSAM)
CALL SHIFTIQ(ZIQ, ZIQ, 64, 64)
```

```
MSAM = 64
A = B = 0.5
CALL WINDOW(ZIQ, MSAM, A, B)
CALL DPVLWD(ZIQ, MSAM, ....)
CALL DPDSY(PPOWER, MSAM, 'HANN')
CALL IQPLOT(ZIQ, MSAM, 1)
```

```
GO TO 200
END DO
```

END

START

200 READ MSAM, VS, GCNR, SNR, GCWID, SIGWID  
MSAM = 128

CALL TIMDOP(ZIQ, N1, VS, SIGWID, SNR, NORMAL, GCNR, GCWID)  
CALL DPVLWD(ZIQ, MSAM, SNR, VELMAX, POWER, VPPS, WPPS, VFFT, WFFT)  
CALL DPDSY(Power, MSAM, 'RECT')  
CALL IQPLOT(ZIQ, MSAM, 1)

CALL SMOOTH(ZIQ, 256, 20)  
A = B = 0.5  
CALL ELLIPSE(ZIQ, 256)  
CALL WINDOW(ZIQ, MSAM, A, B)

CALL DPVLWD(ZIQ, MSAM, ....)  
CALL DPDSY(Power, MSAM, 'HANN')  
CALL IQPLOT(ZIQ, MSAM, 1)  
GO TO 200

END

SUBROUTINE ESTCOV(ZIQ,MSAM, $\hat{P}$ , $\hat{V}$ , $\hat{W}$ ,GCWID,SNR)

$$\hat{P}_T = \frac{\sum_{i=1}^{MSAM} (I_i^2 + Q_i^2)}{MSAM} \quad \begin{matrix} SNR/10 \\ \beta=10 \end{matrix}$$

$$\hat{S}_C = \left[ \left( \frac{\sum_{J=1}^{MSAM} I_J}{MSAM} \right)^2 + \left( \frac{\sum_{J=1}^{MSAM} Q_J}{MSAM} \right)^2 \right] \sqrt{\frac{2\pi}{64}} * MSAM$$

$$\hat{P} = (\hat{P}_T - \hat{S}_C) \left( \frac{\beta}{1+\beta} \right)$$

$$T = .00078125$$

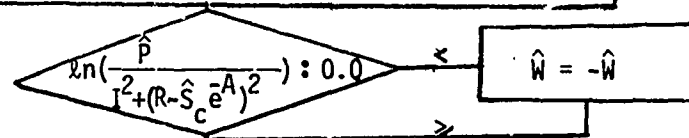
$$R = \frac{\sum_{l=2}^{MSAM} I_{l-1} * I_l + Q_{l-1} * Q_l}{MSAM-1}$$

$$I = \frac{\sum_{l=2}^{MSAM} Q_{l-1} * I_l - I_{l-1} * Q_l}{MSAM-1}$$

$$A = 2\pi^2 \left( \frac{GCWID}{64} \right)^2$$

$$\hat{V} = \frac{1}{(2\pi)(20T)} \tan^{-1} \left( \frac{I}{R - \hat{S}_C e^{-A}} \right)$$

$$\hat{W} = \frac{1}{(20T)(\sqrt{2\pi})} \sqrt{\left| \ln \left( \frac{\hat{P}}{I^2 + (R - \hat{S}_C e^{-A})^2} \right) \right|}$$



PRINT  $\hat{P}, \hat{V}, \hat{W}$

RETURN

END

SUBROUTINE ESTPP(ZIQ,MSAM, $\hat{P}$ , $\hat{V}$ , $\hat{W}$ ,GCWID,SNR)

$$\text{MSAM } \alpha = 10^{\text{SNR}/10}$$

$$\hat{P}_T = \frac{\sum_{i=1} (I_i^2 + Q_i^2)}{\text{MSAM}}$$

$$\hat{P} = \hat{P}_T * \left(\frac{\alpha}{1+\alpha}\right)$$

$$T = .00078125$$

$$R = \frac{\sum_{\ell=2}^{\text{MSAM}} I_{\ell-1} * I_{\ell} + Q_{\ell-1} * Q_{\ell}}{\text{MSAM}-1}$$

$$I = \frac{\sum_{\ell=2}^{\text{MSAM}} Q_{\ell-1} * I_{\ell} - I_{\ell-1} * Q_{\ell}}{\text{MSAM}-1}$$

$$\hat{V} = \frac{1}{(20T)(2\pi)} \text{TAN}^{-1} \left(\frac{I}{R}\right)$$

$$\hat{W} = \frac{1}{(20T)(\sqrt{2\pi})} \sqrt{\left| \ln \left( \frac{\hat{P}}{(R^2 + I^2)^{1/2}} \right) \right|}$$

$$\ln \left( \frac{\hat{P}}{(R^2 + I^2)^{1/2}} \right) : 0.0$$

$$\hat{W} = -\hat{W}$$

PRINT  $\hat{P}$ ,  $\hat{V}$ ,  $\hat{W}$   
 RETURN  
 END

Two versions of the elliptic filter subroutine are listed. The first one uses initialization to anticipate steady state. The second one initializes memory elements to zero. The first subscript (i.e., 1) refers to I while 2 refers to the J component. Z's are input time samples; y's are filtered time samples. XK's are filter coefficients corresponding to Fig. 3.1 and Table 3.1.

Subroutine ELLIPSE 1 (IFILTER,Z,N)

REAL Z(2,N),Y(2,8192),XK(4)

$A_0 = 1$	$B_0 = 1$
$A_1 = -(1 + XK(1))$	$B_1 = XK(2) + XK(4)$
$A_2 = (1 + XK(1))$	$B_2 = XK(3) + XK(2) * XK(4)$
$A_3 = -1$	$B_3 = -XK(3) * XK(4)$

$y_{11} = 0$   
 $y_{21} = 0$   
 $y_{12} = A_0 Z_{12} + (A_1 + A_2 + A_3) Z_{11} - B_1 y_{11}$   
 $y_{22} = A_0 Z_{22} + (A_1 + A_2 + A_3) Z_{21} - B_1 y_{21}$   
 $y_{13} = A_0 Z_{13} + A_1 Z_{12} + (A_2 + A_3) Z_{11} - B_1 y_{12} - B_2 y_{11}$   
 $y_{23} = A_0 Z_{23} + A_1 Z_{22} + A_2 Z_{21} + (A_2 + A_3) Z_{21} - B_1 y_{22} - B_2 y_{21}$

DO I = 4,N

$y_{1I} = A_0 Z_{1I} + A_1 Z_{1I-1} + A_2 Z_{1I-2} + A_3 Z_{1I-3} - B_1 y_{1I-1} - B_2 y_{1I-2} - B_3 y_{1I-3}$   
 $y_{2I} = A_0 Z_{2I} + A_1 Z_{2I-1} + A_2 Z_{2I-2} + A_3 Z_{2I-3} - B_1 y_{2I-1} - B_2 y_{2I-2} - B_3 y_{2I-3}$

END DO

DO J = 1,N

$Z_{1J} = y_{1J}$

$Z_{2J} = y_{2J}$

END DO

RETURN

END

Subroutine ELLIPSE 2 (1FILTER,Z,N)

REAL Z(2,N), y(2,8192)

REAL XK(4)

$$A_0 = 1$$

$$A_1 = -(1+XK(1))$$

$$A_2 = (1+XK(1))$$

$$A_3 = -1$$

$$B_0 = 1$$

$$B_1 = XK(2)+XK(4)$$

$$B_2 = XK(3)+XK(2)*XK(4)$$

$$B_3 = -XK(3)*XK(4)$$

$$y_{11} = A_0 Z_{11}$$

$$y_{21} = A_0 Z_{21}$$

$$y_{12} = A_0 Z_{12} + A_1 Z_{11} - B_1 y_{11}$$

$$y_{22} = A_0 Z_{22} + A_1 Z_{21} - B_1 y_{21}$$

$$y_{13} = A_0 Z_{13} + A_1 Z_{12} + A_2 Z_{11} - B_1 y_{12} - B_2 y_{11}$$

$$y_{23} = A_0 Z_{23} + A_1 Z_{22} + A_2 Z_{21} - B_1 y_{22} - B_2 y_{21}$$

DO I = 4,N

$$y_{1I} = A_0 Z_{1I} + A_1 Z_{1I-1} + A_2 Z_{1I-2} + A_3 Z_{1I-3} - B_1 y_{1I-1} - B_2 y_{1I-2} - B_3 y_{1I-3}$$

$$y_{2I} = A_0 Z_{2I} + A_1 Z_{2I-1} + A_2 Z_{2I-2} + A_3 Z_{2I-3} - B_1 y_{2I-1} - B_2 y_{2I-2} - B_3 y_{2I-3}$$

END DO

DO I = 1,N

$$Z_{1I} = y_{1I}$$

$$Z_{2I} = y_{2I}$$

END DO

RETURN

END

## REFERENCES

- Fletcher, H. R., and D. Burlage, 1972: An initialization technique for improved MTI performance in phased array radars. Proc. of the IEEE, 60, (12), Dec., 1551-1552.
- Groginsky, H. L., and K. Glover, 1980: Weather radar canceller design. Preprints, 19th Conf. on Radar Meteor., Apr., Am. Meteor. Soc., Boston, Mass., 192-201.
- Krehbiel, P. R., and M. Brook, 1979: A broad-band noise technique for fast-scanning radar observations of clouds and clutter targets. IEEE Trans. on Geosci. Elec., GE-17, (4), Oct., 196-204.
- Nathanson, F. E., 1969: Radar Design Principles. McGraw Hill, New York, N.Y.
- Rabiner, L. R., J. F. Kaiser, O. Herrmann, and M. T. Dolan, 1974. Some comparisons between FIR and IIR digital filters. Bell Syst. Tech. J., Vol. 53, Feb., 305-331.
- Zrnich, D. S., 1975: Simulation of weatherlike Doppler spectra and signals. J. Appl. Meteor., 14, (4), 619-620.
- \_\_\_\_\_, 1979: Estimation of spectral moments for weather echoes. IEEE Trans. on Geosci. Elec., GE-17, (4), Oct., 113-128.
- \_\_\_\_\_ and R. J. Doviak, 1976: Effective antenna pattern of scanning radars. IEEE Trans. on Aerosp. Elec. Syst., AES-12, (5), 551-555.